Simulating Ductile Fracture in Steel using the Finite Element Method: Comparison of Two Models For Describing Local Instability due to Ductile Fracture.

by

Henning Levanger

THESIS

for the degree of

MASTER OF SCIENCE

(Master i Anvendt matematikk og mekanikk)

Faculty of Mathematics and Natural Sciences
University of Oslo

May 2012

Det matematisk- naturvitenskapelige fakultet
Universitetet i Oslo

Foreword

This thesis is written for the degree of Master of Science at the University of Oslo, Department of Mathematics, Mechanics division. The work has been done in collaboration with Det Norske Veritas, in the Ship Structure and Concepts section of the Maritime Advisory department, and has been carried out at their main office at Høvik, Oslo.

The topic of the thesis originates from the desire of group leader Eivind Steen to investigate the field of fracture mechanics and related theory and methods. Its main goal is to develop a better understanding of how to use the finite element method to simulate collision events and damage caused by dropped objects, and how to compute a structure's resistance and the amount of damage inflicted by such an events. The focus of the thesis has been on the event of ductile fracture of metal, particularly steel, and the use of two different models for simulating ductile fracture behavior using the finite element method. During the work on the thesis I have learned a lot about the subject of fracture mechanics, a subject I did not have any insight into before I began this work. I have also learned a great deal from fiddling with the FE-analysis software ABAQUS, and spent many hours learning and understanding how to use the finite element method in the context of my work.

I would like to thank Lars Brubak and Eivind Steen for giving me the opportunity to collaborate with their section while working on the thesis, and especially Lars Brubak for helping me as my supervisor both at DNV and at the university. I would also like to thank Gabriele Notaro, for sharing his experience on using the finite element method and ABAQUS to simulate collision events, and for the many hours of guidance and discussions of the different results and choices that have been made during the last year. I would also like to thank Tom Klungseth Øsvold for sharing his opinions on some of the problems that I have encountered during this year. Thanks to Helene Lo Casico Sætrefor proofreading, and last, but definitely not least, a great thank you to my girl-friend Ingrid Senje Rasmussen for great moral support and for the help with proofreading the thesis.

Abstract

In the shipping industry, there is an increase in the requirement of determining a ship's strength when it comes to collision events. This involves ship-against-ship collisions, but also strength against damage caused by dropped objects, grounding events and collision with rigid objects. There are many methods of determining the damage inflicted to the structure when two objects collide. The most advanced ones make use of numerical methods and particularly the finite element method.

This thesis gives an overview of the theory involved in a ductile failure of an isotropic ductile material such as steel, and explains two different methods of modeling the material behavior related to ductile fracture for use in the finite element method. One model uses the material's true stress/true strain relationship to simulate the structural response due to reduced load-bearing capacity form ductile fracture. The other is a complete fracture model that reduces the load bearing capacity by inflicting damage to the elements used, and is based on the assumed amount of energy it takes to create a crack. The theory behind the two models is explained in this thesis, and material models are developed using a tensile test model in the finite element software package ABAQUS. Then the material models developed are used on a model simulating a steel plate being penetrated by a cone shaped object. The results are compared to earlier material tests done on the same type of structures. Both fracture models are capable of simulating the ductile fracture of a tensile specimen, and no significant differences can be found when monitoring the energy output. When the same material-definition models are used in an analysis of a plate being penetrated, it is however evident that there are differences that are caused by the difference in the way the ductile fracture is simulated. Particularly the effect of reduced stiffness in the elements when using the energy-based fracture model leads to the conclusion that the two methods make the FE-model behave differently when high values of in-plane tensile strain is present.

Contents

List of Notations

A	Cross-section area
A_0	Initial cross-section area
D	Damage parameter
E	Young modulus
E_{AE}	"Artificial" strain energy
E_{DM}	Damage dissipated energy
E_{Fric}	Energy dissipated by friction effects
E_{Int}	Internal energy
E_{KE}	Kinetic energy
E_{PD}	Plastic deformation energy
E_{SE}	Elastic strain energy
E_{UB}	Unbalanced energy
F	Force
G	Shear modulus
G_f	Energy dissipated to damage per unit area of crack
K	Stress intensity factor
L_σ	Lode parameter
S_1, S_1, S_3	Principle deviatoric stresses.
V_V	Void volume
W_{Ext}	External work
W_{PW}	Work done by the penalty contact definition
$[\boldsymbol{C}]$	Dampening matrix
$[\boldsymbol{M}]$	Mass matrix
$\bar{\varepsilon}^{pl}$	Equivalent plastic strain
$\bar{\varepsilon}^{pl}_D$	Equivalent plastic strain at the point of damage initiation
$\bar{u}^{pl}$	Fracture displacement
$\bar{u}^{pl}_f$	Fracture displacement at fracture.

$\boldsymbol{S}$	Deviatoric stress tensor
$\ddot{u}$	Second derivative of displacement
$\dot{\bar{\varepsilon}}^{pl}$	Equivalent plastic strain rate
$\dot{\varepsilon}_i$	Strain rate
$\dot{u}$	First derivative of displacement
η	Deviatoric stress component
η	Stress triaxiality
$\gamma_{xy}, \gamma_{yz}, \gamma_{zx}$	Shear strain components
ν	Poisson's ratio
ω_{max}	Maximum natural frequency
ρ	Material density
σ	Stress
$\acute{\sigma_1}, \acute{\sigma_2}, \acute{\sigma_3}$	Deviatoric components of the principle stress
$\sigma_1, \sigma_2, \sigma_3$	Principle stress ($\sigma_1 \geq \sigma_2 \geq \sigma_3$)
σ_c	Interfacial stress. Stress acting across the interface of two different particles
σ_e	von Mises equivalent stress
σ_e	von Mises equivalent stress
σ_m	Hydrostatic stress
σ_u	Ultimate strength stress
$\sigma_x, \sigma_y, \sigma_z$	Stress components
σ_y	Yield stress
$\sigma_{Y,lower}$	Stress value at the lower yield point
$\sigma_{Y,upper}$	Stress value at the upper yield point
σ_{eng}	The "engineering" stress ($\frac{F}{A}$)
σ_{ij}	Stress acting on the i plane in the direction of j.
σ_{true}	The true stress in the material
$\tau_{xy}, \tau_{yz}, \tau_{zx}$	Shear stress components
θ	Lode angle
ε	Strain
ε^{el}	Elastic strain
ε^{pl}	elastic strain
$\varepsilon_x, \varepsilon_y, \varepsilon_z$	Strain components
ε_{eng}	Engineering strain
ε_{tot}	Total strain ($\varepsilon_{tot} = \varepsilon^{el} + \varepsilon^{pl}$)
ε_{true}	True/logarithmic strain
ξ_{max}	The dampening ratio for the ω_{max} mode
$\{\boldsymbol{R^{ext}}\}_n$	External load vector

$\{\boldsymbol{R}^{\boldsymbol{int}}\}_n$	Internal load vector
$\{\ddot{\boldsymbol{u}}\}$	Second derivative of displacement (acceleration)
$\{\dot{\boldsymbol{u}}\}$	First derivative of displacement (velocity)
c_d	Speed of sound in the material
l	Initial length
l	Length
l^c	charateristic element length
l^e	Element length
l^e_{min}	Smallest dimension of a element
p	Equivalent hydrostatic pressure
t	time
u	Displacement

Chapter 1

Introduction to the thesis

1.1 Introduction

In shipping, the forces involved when a collision takes place are enormous, and will produce permanent deformations, cracks, local buckling, collapse and tearing of the ship structure. These damages may lead to flooding of the hull, stability problems and possible progressive collapse of the ship's structure. With smaller damages, the ship's stability may not be affected, but leakage of oil and fuel may occur, threatening the environment. The amount of damage caused by the collision is crucial when the remaining strength of the hull is to be determined.

To better determine the amount of damage caused by a collision or grounding of a ship, it is important to use a reliable deterministic analysis models. The most advanced models are making use of the finite element method and non-linear analysis in computer assisted analysis, using software packages such as ABAQUS, ANSYS and LS-DYNA. However, the quality of the solutions produced in these programs when preforming an analysis is no better than the information inputted into the model, and is dependent on a large number of parameters, particularly when trying to simulate fracture and the development of cracks in the material. These parameters are essential for understanding, and having control over the results, when computing the extent of damage and the energy absorbed by the structure.

Det Norske Veritas has for the past few years been working to develop new and

more accurate methods and models to determine the energy and deformation caused by collision forces. This has been done by evaluating different scenarios, including different hull designs, and using simplified methods of accidental limit state analysis. DNV has developed the computer analysis program SIDECOLL/ BOWCOLL which makes use of simplified methods. A more detailed approach is desirable in order to calibrate and improve these simplified models against non-linear FE-analyses.

1.2 Specification of the thesis

The objective of this thesis is to find and validate the properties of a specified material to be used when performing a FE-analysis considering large deformation and ductile fracture of the material. The main objective is to identify different parameters that may have an impact on a model's ability to absorb energy during a simulated collision, and to make simplifications to the input data in order to simplify the modelling procedure. The materials that will be used are homogeneous isotropic ductile metals, as this is the material most used in ship structures of today.

The main focus of the thesis will be the material properties, and determining the fracture criteria related to the mesh size of the FE-model. It will also be perform a comparison of two different approaches to model the materials fracture behavior, and applicate them in the finite element method. A tensile test experiment will be performed using the finite elements software package ABAQUS, in order to develop material models for two different theories to model fracture. These material models will then be used to simulate a plate being penetrated by an object at low speed. The goal is to determine the different material models' ability to simulate the fracturing of the material, and to compare the models against each other. The thesis is limited to ductile fracturing of isotropic homogeneous ductile materials.

The theory regarding the topics above will be studied and presented as an introduction into the science of material fracture, and how these theories are implemented into the finite element method.

1.3 Organization of the thesis

The thesis is divided into nine chapters. The first chapter is an introduction to the thesis and the work done to prepare it. Chapter 2 contains theory about material behavior for mechanical loads and in the third the material theory of fracture for ductile fracturing is presented. The fourth chapter explains some of the material parameters that are of interest when ductile fracturing is studied. Chapter 5 introduces the two material models to be used in the experiments carried out during the work of the thesis. The sixth chapter explaines the explicit time integration method used in the finite element analysis in the subsequent chapters. In Chapter 7 a tensile experiment performed using the finite element software analysis program ABAQUS is presented, and the results are discussed. The main goal of this experiment is to develop material models in to be used in ABAQUS for dynamic analysis of a forced penetration of a steel plate specimen. The penetration experiment is presented in Chapter 8, and the results regarding the use of the two material models developed as well as the results related to the fracturing of the plate are discussed. In Chapter 9 the results and findings are discussed, and a conclusion is made.

Chapter 2

Material Theory

2.1 The stress-strain curve

The stress and strain relationship for a material is one way to define how a material will react mechanically to an applied loading condition. In a finite element analysis, the properties of a material is inputted as the relationship between true stress and true strain for the plastic straining, and the Young's-modulus and the Poisson's ration define the linear-elastic behavior leading to the plasticity (see section 2.3). In this section, an introduction to the different parts of the stress-strain-curve is outlined, based on the publication of R. Hill [14]. A general description of the true stress/true strain curve compared to the global force/displacement curve is shown in Fig. 2.1.

The figure shows the global engineering stress/strain curve (A) and the true stress/true strain curve (B). The stress value at 1 is the ultimate strength of the material, while the stress at point 2 is the yield point of which the material starts to deform plastically. At point 3 the material fails and the structure fractures. Zone 4 is the plastic deformation zone where plastic strain-hardening occurs. Zone 5 is the instable zone where the material loses load-bearing capacity. During this deformation the elongation of the structure is concentrated in a small area, creating a necking zone (See Section 3.1).

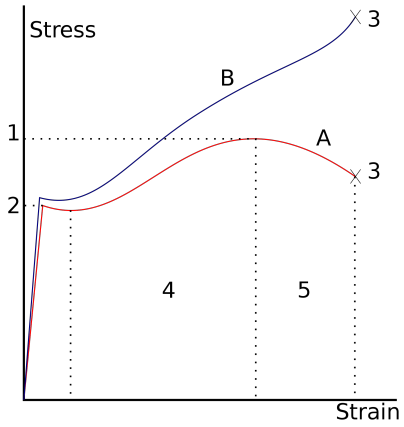

Figure 2.1: *Global responce of the material (A) and the local true stress/true strain relationship (B) for the same material.*

In order to determine a material's mechanical properties, it is usually put through mechanical tests where different parameters are measured. Normal test methods are tensile tests of flat-bars or rods, compression of a short cylindrical block or twisting of a thin-walled tube. The force applied and the deformation that is produced can be used to calculate the internal stress in the material and the total straining of the material. The internal stress σ, and the true strain ε_{true} and the engineering strain ε_{eng} of the material can be calculated as

$$\sigma = \frac{F}{A} \tag{2.1}$$

$$\varepsilon_{true} = ln(\frac{l}{l_0}) = ln(1 + \varepsilon_{eng}) \tag{2.2}$$

$$\varepsilon_{eng} = \frac{l - l_0}{l_0} \tag{2.3}$$

.

A is the deformed cross-section area, F is the external applied force, ε_{true} is the *logarithmic strain* or *true strain*, and ε_{eng} is the *engineering strain* or *conventional strain*. For small values of strain, the two different strain measurements are approximately equal, but for higher strain values ε_{true} develops significantly higher strain values because of the logarithmic development, while ϵ_{eng} develops in a linearly manner. The relative difference in strain value can be seen in Fig. 2.2. This

way of measuring the strain in a structure depending on the global elongation of the material, is only valid as long as there are no local instabilities present in the material.

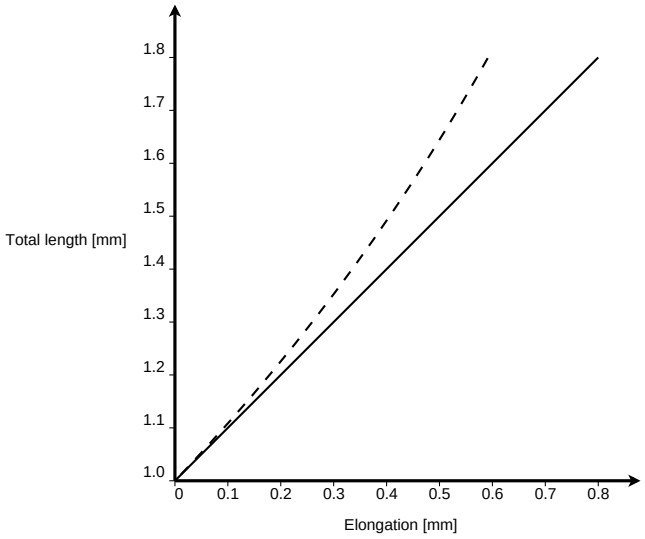

Figure 2.2: *The difference between logarithmic strain ε_{true} (dashed curve) and engineering strain ε_{eng} (solid line). For small values of strain, the two different strains are as good as equal, but for strain values above 2-3 % the difference may become significant depending on the case studied.*

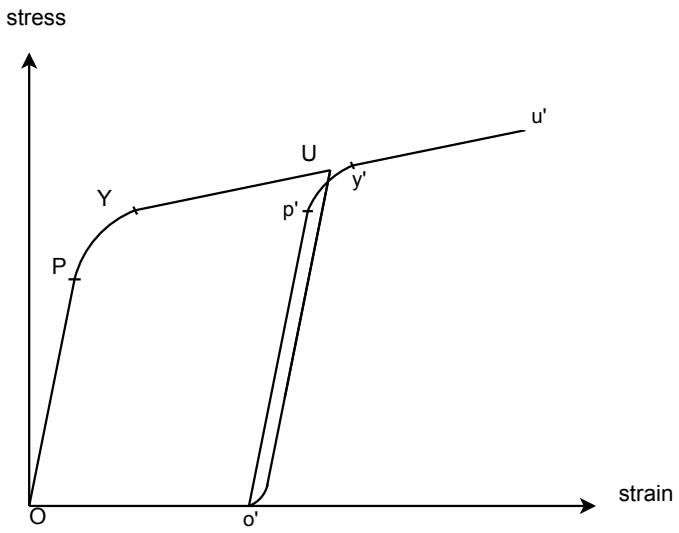

Figure 2.3: *The loading path of a material is plotted as stress against strain. P and p′ mark the proportional point for initial loading and reloading respectively. Y and y′ are the initial loading yield point and reloaded yield point, the limit between elastic and elasto-plastic material behavior. O is the initial state, while o′ is the state after the material has be loaded up to point U. The distance Oo′ is the plastic deformation obtained by this load cycle. The small curve in the unloading path towards o′.*

When a tensile specimen is subjected to an increasing load, it will respond by elongating. At first, the material will elongate in a linearly-elastic manner, following Hooke's law (Section 2.2). The stress and strain will increase linearly dependent on each other, up to the proportional point P, in Fig. 2.3. At this point, the stress-strain relation stops being linearly dependent according to Hooke's law, but in most cases the strain is still elastic up to point Y. At the point of yielding Y, the maximum elastic strain ε^{el}_{max} is reached. Any further straining of the material will result in plastic deformation and energy dissipated to permanent deformation of the material.

After the yielding point, the stress-strain curve starts to flatten out. For most ductile materials, an incremental increase in stress $\delta\sigma$ will produce a progressively larger increase in strain $\delta\varepsilon$, meaning that the slope of the curve is decreasing. This is the effect of strain-hardening in the material making it tougher as the strain increases. If the specimen at some random point U (Fig. 2.3) during the plastic deformation is being unloaded until the internal stress is zero, the strain response will drop following the slope defined by the Young's modulus. A perfect material will follow this path down to a value of zero stress. At the end of unloading, the

curve may however bend off right before the stress reaches zero (in Fig. 2.3 the bend is highly exaggerated). This effect is due to some grains in the material being orientated in such a way that they produce a very small amount of plastic strain. This small amount of strain energy is released some time after the external load is removed, and the result is that the material is not fully contracted before the load has been removed for some time [14]. The difference in strain value between O and o' in the figure is the plastic elongation caused by the plastic straining of the material.

When the load is applied once more, the material will elongate in an elastic manner once more, following Hooke's law from point o' up to the new proportional point p', and the yield at point y'. The yield point y is reached at a higher value of stress than the first yield point Y, because of the pre-straining of the material before the load is applied for a second time. The yield point y can be considered as the yield point for a material specimen that is pre-strained to a value of ε_{pre}^{pl} equal to the strain value defined by the distance between O and o'.

During the plastic deformation of the material, the material increases its load bearing capacity per unit cross-section area, as a result of the strain hardening effect. At the same time, the effective cross-section is reduced due to transverse contraction as the material is stretched. The stress/strain curve will rise as long as the strain-hardening is increasing faster than the cross-section area is decreasing, meaning that $\delta\sigma/\delta\varepsilon < \sigma$, where σ is the true stress in the material. The decreasing slope in the stress/strain curve is caused by the $\delta\sigma$ getting smaller compared to $\delta\varepsilon$. At some point during the plastic straining of the material, the increase in strain-hardening will be overcome by the cross-section area reduction. At this point the maximum load that the structure can carry is applied. The point is defined to be when [24]

$$\frac{d\sigma}{d\varepsilon} = \sigma \tag{2.4}$$

where σ is the current true stress value. Any further straining of a material will introduce a local instability in the material, leading to an even more reduced load bearing capacity and eventually fracture. This is explained in more detail in Sec. 3.1.

2.2 Elasticity

A material will behave elastically if the strain energy that is built up in the material is recoverable when the material is unloaded. When a force F is acting on a piece of material giving a displacement Δl, it will exert an external work which equals $W_E = F\Delta l$. It is assumed that all of the external energy is used to produce the deformation Δl, and that the kinetic energy and energy lost to friction forces are negligible. If so, the external energy will be matched by the internal energy, and the internal energy is equal to the elastic strain energy in the volume.

$$W_{Ext} = E_{Int} = E_{SE} \tag{2.5}$$

W_E is the external work, E_{Int} is the internal energy and E_{SE} is the elastic strain energy in the material.

Many materials, steel included, are linear-elastic, meaning that the displacement produced by the applied force is linearly dependent on the force. For a material that is linearly elastic and isotropic, the elastic behavior of the material can be represented by the Young modulus E and Poisson's ratio ν. These materials will follow Hooke's law. This law states that the relation between the force applied and the deformation is governed by E and ν. For axial forces the law yields ([13] page 20)

$$\boldsymbol{\varepsilon} = \boldsymbol{E}^T\boldsymbol{\sigma} = \begin{Bmatrix} \varepsilon_x \\ \varepsilon_y \\ \varepsilon_z \end{Bmatrix} = \frac{1}{E}\begin{bmatrix} 1 & -\nu & -\nu \\ -\nu & 1 & -\nu \\ -\nu & -\nu & 1 \end{bmatrix}\begin{Bmatrix} \sigma_x \\ \sigma_y \\ \sigma_z \end{Bmatrix} \tag{2.6}$$

and for shear

$$\boldsymbol{\gamma} = \boldsymbol{G}^T\boldsymbol{\tau} = \begin{Bmatrix} \gamma_{xy} \\ \gamma_{yz} \\ \gamma_{zx} \end{Bmatrix} = \frac{1}{E}\begin{bmatrix} 2(1+\nu) & 0 & 0 \\ 0 & 2(1+\nu) & 0 \\ 0 & 0 & 2(1+\nu) \end{bmatrix}\begin{Bmatrix} \tau_{xy} \\ \tau_{yz} \\ \tau_{zx} \end{Bmatrix} \tag{2.7}$$

The shear modulus G is defined by E and ν, $G = E/(2(1+\nu))$. This is called the

full Hooke's law for 3D-space.

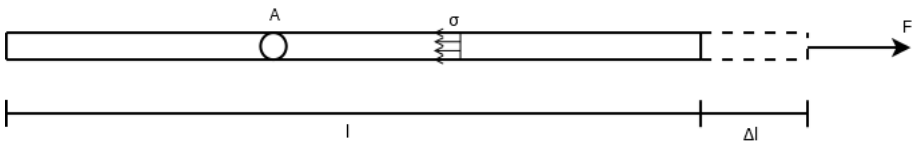

Figure 2.4: *A beam with an applied force F resulting in a internal stress of* $\sigma = F/A$ *and a elongation* Δl*.*

Considering a simple structure like the rod in Fig. 2.4, the relation between elongation and strain, and applied force F and internal stress σ becomes apparent.

$$\sigma = \frac{F}{A} \tag{2.8}$$

The strain value in the material is determined as

$$\varepsilon_{eng} = \frac{l_0 + \Delta l}{l_0} \tag{2.9}$$

where l_0 is the initial length and δl is the elongation of the material.

As long as the material is acting elastically, all of the strain energy is recoverable and the material will obtain its original shape and size if the force F is removed. In a real structure, some of the energy applied to the structure may be lost through e.g. heat. These effects are often neglected when studying structures loaded in the elastic region, because the amount of energy lost through them is small. In a high speed impact, there will also be a significant amount of energy dissipated to dynamic damping and the inertia of mass. These kinds of scenarios usually bring the material into high levels of plastic strain deformation, and the dynamic effects are small during the time the material is acting in an elastic manner.

For cases where ductile fracture of a material is studied, the elastic behavior of the material is of less importance during loading because the fracture strains are much larger than the elastic yield strain of the material. Normally, the maximum elastic strain value for steel is about $2 - 3$ ‰, while the fracture strain is around $20 - 24$ % defined in engineering strain ε_{eng}. In an analysis where fracture is studied, the deformation of the material is much larger than what the elastic strain can produce,

and therefore it is not of great importance how the material behaves in the elastic area when the deformation is increasing. For unloading of a structure that has been loaded beyond the point of ultimate strength (referring to Fig. 2.1) the elastic properties of the material are important. These are discussed in more detail in section 2.3.

2.3 Plasticity

When the material deforms according to its elastic properties, the strain energy applied is recoverable. When the stress in the material reaches the yield point, the maximum elastic strain ε^{el}_{max} is obtained, and applying a higher load will produce strain that will be permanent. This permanent strain is called plastic strain ε^{pl} and the energy gone into creating the plastic strain is not recoverable, and the deformation caused by the plastic straining will become permanent. The total strain value in the structure is the sum of elastic and plastic strain.

$$\varepsilon_{tot} = \varepsilon^{el} + \varepsilon^{pl} \tag{2.10}$$

In Fig. 2.5 the true stress/true strain relationship for a perfect plastic material is shown. The material will behave elastically up to the point of σ_y, which is the yield point. As the material is deformed further, the elongation is caused by the plastic straining of the material. The reduction of load bearing capacity (the decreasing slope of the curve) between σ_y and σ_u is caused by the ratio of strain hardening to effective cross-section area is reduced, as explained in Section 2.1. This part of the curve defines the plastic behavior of the material, and differs significantly in shape for different materials. At some point the material can not take any more load, and the strain will continue to grow if the loading is left at this value. The maximum load a material can take, is defined as the ultimate load the material can take, and is at the point of the materials ultimate capacity. For a perfect plastic material the true stress/true strain curve will continue horizontally. For most materials, the stress value needed to increase the load after the point of ultimate strength will decrease, leading to a negative slope on the true stress/true strain curve.

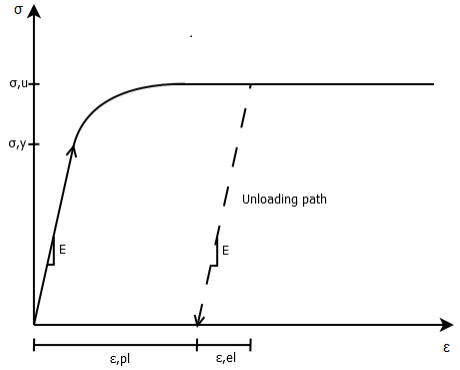

Figure 2.5: *The stress-strain relationship for a perfect plastic material. When the material reaches its ultimate loading at σ_u it will continue to deform plastically without the load increasing.*

The plastic properties and the stress/strain relationship for a material deforming plastically is often determined by performing tensile tests on the material. In [11], several test pieces of steel were stretched until fracture occurred in order to find the correct plastic behavior of the material. The result is a force-displacement relationship that uses the global elongation of the test piece and the total force required to produce this elongation. In a finite element analysis, the input must be in the form of a true stress/true strain relationship, meaning the stress and strain that each element experience in order to produce the same global response as the tensile test. One way of converting force and displacement into stress and strain is presented in the Abaqus User's Manual ([9] section 10.2).

The global strain, called the engineering strain ε_{eng} is calculated as shown i Eq. (2.1). This is the global strain of the test piece, measured over the total length of the tensile test specimen in the direction of elongation. It is related to the true strain in the material as

$$\varepsilon_{true} = ln(1 + \varepsilon_{eng}) \tag{2.11}$$

The true strain is the same as the logarithmic strain defined in Section 2.1. The force that produces this strain can be converted into true stress by dividing the force F by the current cross section area of the test piece. The current cross-section area A is related to the initial cross-section area A_0 as

$$A = A_0 \frac{l_0}{l} \tag{2.12}$$

and inserting this into the force-stress relation $\sigma = F/A$ gives

$$\sigma_{true} = \frac{F}{A} = \frac{Fl}{A_0 l_0} = \sigma_{eng} \frac{l}{l_0} \tag{2.13}$$

The relationship between force and stress, and displacement and strain shown here, is independent of the mesh size, but only valid up to the point of ultimate strength, the point at which local instabilities start to develop and eventually result in necking of the tensile specimen. The material behavior after the point of ultimate strength is explained in Section 3.1.

2.4 Yield criterion

When a material deforms, a transition from elastic to plastic behavior will occur if the loading is large enough to provoke plastic strain. This yielding point is explained physically in Sec. 2.1. In order to predict the onset of plastic deformation, the yield point must be determined mathematically. Through history, many different approaches have been proposed in order to solve this problem, but only two have been proven solid enough to last. These are the only ones that take into account the hydrostatic stress that is present in the material [14]. These two are *the Tresca yield criterion* and *the von Mises yield criterion*.

Of the two yield criteria, the von Mises yield criterion is the most used. It defines the plastic yielding of a material to be initiated when ([14] pg. 15)

$$f(J_1, J_2, J_3) = 0 \tag{2.14}$$

where J_1, J_2 and J_3 are calculated based on the three principle stresses.

$$J_1 = \sigma_1 + \sigma_2 + \sigma_3 \tag{2.15}$$
$$J_2 = -(\sigma_1\sigma_2 + \sigma_2\sigma_3 + \sigma_3\sigma_1) \tag{2.16}$$
$$J_3 = \sigma_1\sigma_2\sigma_3 \tag{2.17}$$

f is a characteristic value for the state of the material regarding plastic yielding.

In order to reduce the complexity of the yield criterion, it is assumed that the yield of a material is unaffected by moderate- hydrostatic pressure and tension. An other simplification is to eliminate the *Bauschinger effect*[1]so that the yield criterion is the same for compression- and tension stress states. By making these assumptions, it has been shown [14] that the yield criterion only depends on the principal components of the deviatoric stress tensor[2]($\acute{\sigma_1}, \acute{\sigma_2}, \acute{\sigma_3}$), and that the yield criterion is reduced to

$$F(J_2) = 0 \tag{2.18}$$

The J_2 is called the second deviatoric stress invariant, and is defined as

$$J_2 = \frac{1}{2} S_{ij} S_{ji} \tag{2.19a}$$
$$= \frac{1}{6}\left[(\sigma_x - \sigma_y)^2 + (\sigma_y - \sigma_z)^2 + (\sigma_z - \sigma_x)^2\right] + \sigma_{xy}^2 + \sigma_{yz}^2 + \sigma_{xz}^2 \tag{2.19b}$$
$$= \frac{1}{6}\left[(\sigma_1 - \sigma_2)^2 + (\sigma_2 - \sigma_3)^2 + (\sigma_3 - \sigma_1)^2\right] \tag{2.19c}$$

The deviator stress tensor S_{ij} is defined in Section 4.2.3.

[1]The Bauschinger effect is an effect occurring in some materials, which link the maximum yield stress for tensile loading to the yield stress for compressive loading. If e.g. the tensile yield stress limit is increased, the compressive yield stress limit is equally reduced.

[2]Deviatoric stress is the stress that acts on a body giving changes only in the shape of the solid volume, and not in the volume. The hydrostatic stress is the stress forces responsible for changing the volume of the body. The real stress state is the sum of the hydrostatic and the deviatoric stress states in the body ([6] pg. 609).

In practical use, the von Mises yield criterion is said to be fulfilled when the equivalent von Mises stress σ_e (defined in Section 4.2.1) is equal to the set yield stress σ_Y ([2] pg. 67) defined by

$$\sigma_Y = \frac{\sqrt{2}}{\sqrt{\frac{2}{3}}}k \tag{2.20}$$

The value of k must be determined for each material by material testing, and is dependent on the amount of prestraining in the material. In most cases the value of the parameter k is chosen so that the von Mises circle passes through the corners of the Tresca hexagon (from the Tresca yield criterion), as seen in Fig. 2.6, giving the von Mises yield criterion the same σ_Y for axial loading conditions as the Tresca yield criterion, and letting the shear stress yielding differ with a factor of $\frac{2}{\sqrt{3}}$, with the Tresca criterion being the most conservative criterion.

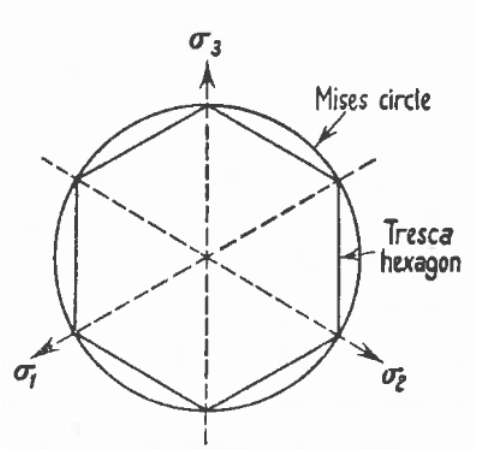

Figure 2.6: *The Tresca hexagon and the von Mises circle plotted in the space defined by* $(\sigma_1, \sigma_2, \sigma_3)$*[14]*

Chapter 3

Fracture mechanics

3.1 Introduction to ductile fracture

In section 2.1 the definition of the point of ultimate strength is explained. When the material reaches this point, an increase in loading will make the true (plastic) strain increase drastically, and even if the load is reduced, the strain will increase. This phenomenon can be explained by the ratio of strain hardening not increasing the strength of the material sufficiently to overcome the loss of load carrying capacity because of the decreasing cross-section area. After the point of ultimate strength for the material, the ratio of change in true stress to change in true strain is

$$\frac{\delta\sigma_{true}}{\delta\varepsilon_{true}} < \sigma_{true} \tag{3.1}$$

When the material deforms plastically, the true strain in the material is approximately equal through the specimen. As the ultimate strength is reached, all parts of the material are strained to the material's maximum tensile strength. Some place in the material there will be a weak zone, that will not be able to carry the loading applied. In this zone, the ductile fracture will start to develop. The loading will cause the weaker area to strain further than the rest of the model, even if the load is not increased. The increased straining in the small part of the specimen makes the material weaker in this area, which reduces the load bearing capacity of the speci-

men. This means that the rest of the material will reduce its strain value, since the external force and the internal true stress in the material decreases ([14] pg. 12). A schematic description of this behavior are given in Fig. 3.1. The zone of weakened material is defined as the instability zone, or the necking zone, because the effect causes the material to form a local "neck" in the structure, as seen in Fig. 3.2.

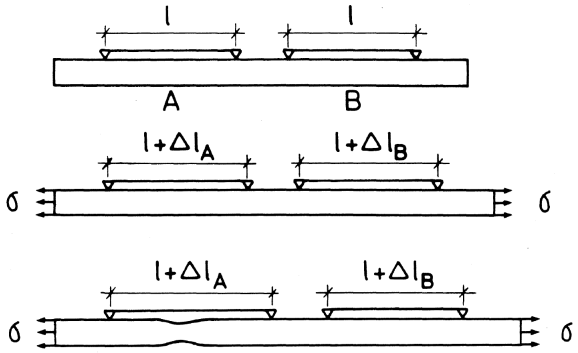

Figure 3.1: *In the unloaded position (top) two gauge length have the same length. As the material is loaded and the strain increases, the two gauge lengths are strained the same amount and* $\Delta l_A = \Delta l_B$*. When the ultimate strength of the material is reached, a local instability will occur somewhere in the material. Increasing the load beyond the ultimate strength will only increase the strain in the unstable zone, increasing* Δl_A *while* Δl_B *is reduces since the material in this section recovers elastically. [15]*

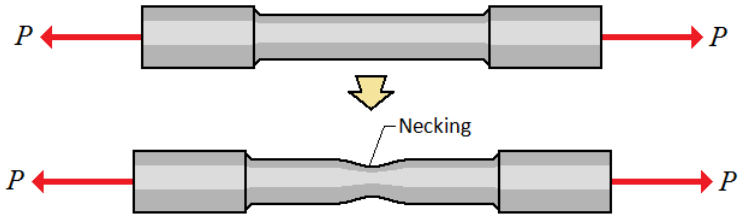

Figure 3.2: *The local instability that arises in the material due to ductile fracturing, is visible as a "neck" when the phenomenon is observed on a tensile test piece. Picture courtesy of engineeringarchives.com*

The "neck" appears because only the material inside the instable zone reduces its cross-section area. The material outside the unstable zone is experiencing the same stress values, but since it never crossed over from plastic behavior into fracture, it will instead recover elastically as the stress is reduced. All the deformation is now taken by the material inside the unstable zone since this part has been weakened in comparison to the rest of the material in the specimen.

3.2 Ductile Fracture

3.2.1 Creation of voids

According to [2], there are four common mechanisms in metals and metal alloys that may impose failure in a material. Three of them are cleavage fracture, intergranular fracture and fatigue. This thesis focuses on the fourth mechanism, ductile fracture. A general description of three of the mechanisms is seen in figure 3.3.

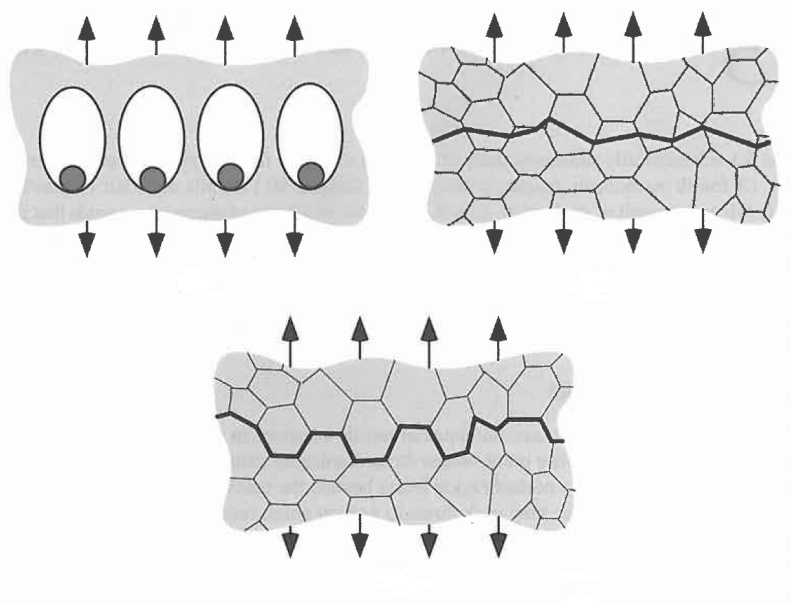

Figure 3.3: *Three of the most common fracture mechanisms in metals and alloys. Upper left: ductile fracture, Upper right: cleavage, lower: intergranular fracture [2].*

When a ductile material is loaded and strained towards the ultimate capacity of the material, the strain hardening in the material evens out the capacity lost due to reduction of cross section area. At one point the material will reaches its ultimate strength. Further straining will result in local instabilities in the material. After the point of the ultimate strength, all the elongation of the material is localized in a small region where the material is rapidly losing its load carrying capacity. This region is the necking region, and after the creation of this region, all further deformation will be localized inside it. Metals containing minimal amounts of impurities will have a more sudden failure after necking, while materials containing larger amounts of impurities will have a smoother behavior when approaching

failure, but start to fail at lower values of strain. The mechanisms related to ductile fracture can generally be summed up into three stages ([2] page 219):

1. The formation of free surfaces around a particle inside the material, either by interfacial decohesion or fracture in the particle itself.
2. Growth of the voids created around particles, due to plastic straining and hydrostatic stress.
3. Coalescence of the growing voids that eventually leads to failure of the material.

Some materials have strong bonds between the particles in the material, and these material's properties regarding ductile fracture is controlled by the development of voids around the particle. The strong bonds are usually caused by the material having particles that are relatively uniform in size. When the voids first start to appear, the stress inside the material is so great that the growth and coalescence of voids happens quickly. This gives a material that is identified by a small amount of straining from the point of ultimate strength and to fracture. Other materials where the bonding between particles is weaker, usually because of larger differences in size between particles, the voids easily develops around the large particle. The development of fracture is controlled by the growing and coalescence of the voids around the larger particles that are evenly spread, but have a great distances between them. This gives a material with a softer fracture behavior, but with large fracture straining, from ultimate strength to fracture.

Voids tend to appear around inclusions and so-called second-face particles that may be in the material. What happens is that the stress between the material matrix and the surface of the particle increases until the interfacial surface starts to slip and a void is created between the particle and the material matrix. It may also occur that the stress is so great that the particle itself fractures, splitting into parts and creating voids when it is pulled apart by the surrounding material.

Several models have been presented in order to define the stress causing the formation of voids. A widely used model presented in [2] and developed by A.S. Argon et al., states that the stress between the surface of a cylindrical particle and the material matrix is approximately the sum of the equivalent von Mises stress and the hydrostatic stress in the material. This gives

$$\sigma_c = \sigma_e + \sigma_m \tag{3.2}$$

where σ_c is the stress acting across the interface between a particle and the material matrix surrounding it, σ_e is the von Mises equivalent stress, and σ_m is the hydrostatic stress.

Later, this model has been redefined by The Beremin research group ([2] page 221) in order to make it better at predicting the right stress value when the production of the material may lead to different directional properties due to rolling direction:

$$\sigma_c = \sigma_m + C(\sigma_e - \sigma_Y) \tag{3.3}$$

C is a parameter that is 0.6 for loading transverse to the rolling direction of the material, and 1.6 when loaded parallel to it. σ_Y is the yield stress of the material.

Both these models use the equivalent von Mises stress and the hydrostatic stress in order to define the stress responsible for the creation of material voids.

A third model is developed by Goods and Brown ([2] page 221). They argue that small dislocations near the surface of the particle will increase the stress value around the particle by

$$\Delta\sigma_d = 5.4\alpha G\sqrt{\frac{\varepsilon_1 b}{r}} \tag{3.4}$$

α is a constant ranging from 0.14 to 0.33, G is the shear modulus, ε_1 is the maximum remote normal strain, b is the magnitude of Burger's vector and r is the radius of the particle. They then define the interfacial stress σ_c to be

$$\sigma_c = \Delta\sigma_d + \sigma_1 = \Delta\sigma_d + S_1 + \sigma_m \tag{3.5}$$

where σ_1 is the maximum principle stress in the material and S_1 is the maximum deviatoric stress.

This latest model states that a material containing large particles will have a lower decohesion stress value because the larger radius of the particle means a lower value of $\Delta\sigma_d$. Later studies have shown that the opposite is more likely to be true. Larger particles have an increased probability of having faults in them, making them more prone to fracture and therefore more likely to fail at a lower stress loading [1].

3.2.2 Void growth and coalescence

After the creation of voids in a material, these voids start to grow and coalesce as the load on the material increases. Before the voids are created, the stress in the material is carried by the cross-section area of the specimen. As voids are created, the effective cross-section that can carry the load is reduced, since only the material between the voids is available to carry it. The plastic straining resulting from the increasing elongation is concentrated in the walls between the voids. It is this effect that causes the necking phenomenon of the material. In Fig. 3.4 a schematic description of the void growth and coalescence are shown.

The growth of voids is governed by the increasing plastic strain and the hydrostatic stress that acts on the material. In a specimen exposed to straining, the volume at the center of the cross-section area carrying the load will experience a higher amount of hydrostatic stress than the volume closer to the edge. This higher hydrostatic stress results in a higher state of stress triaxiality (Hydrostatic stress and stress triaxiality are explained in Chapter 4) in the center of the cross-section area. This will increase the speed at which the voids around the larger particles grow, and make the center of the loaded cross-section area fail before the edges ([2] pg. 223). The shape of the center fracture caused by the growth of voids around the larger particles, is often circular shaped. (In a flat-bar specimen the circular shape is compromised by the shape of the specimens cross-section area)

Outside the center fracture zone, the stress triaxiality has a lower value because the hydrostatic stress is smaller. This has promoted the growth of smaller voids around the smaller particles, resulting in a lower maximum amount of strain from ultimate strength to fracture. When suddenly all of the loading is put onto this area

[1] In a short article by Jay R. Lund and Joseph P. Bryne [19] the theory behind the fact that larger bodies of mass are more prone to material weakness is pointed out based on an experiment performed by Leonardo da Vinci.

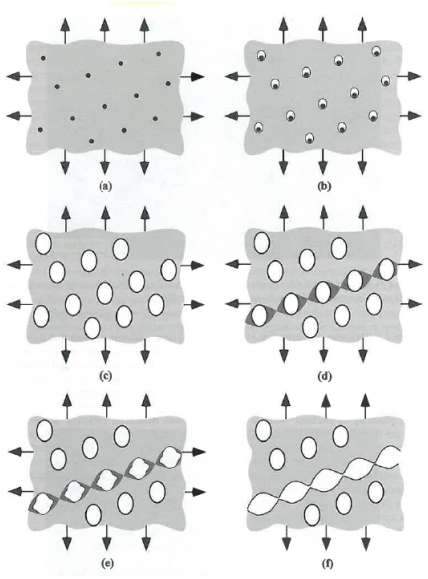

Figure 3.4: *The growth of voids is for the most part concentrated around the larger particles in the material. A state of high stress triaxiality caused by high values of hydrostatic stress encourages the growth of voids around the larger particles, giving large voids that are sparsely spread. A state of lower stress triaxiality will in addition give void growth around the medium sized particles, giving a higher number of small voids evenly spread in the material. [2].*

because of the failure of the center region, the void growth will happen quickly and failure will occur fast.

The fracture of the outer ring happens at an angle of about 45 ° on the direction of loading, creating the characteristic cup and cone fracture surface, as seen in Fig. 3.5. This, and the fact that the voids are so small that they are almost invisible, even by microscope, makes it look like a shear fracture. The angle of 45 ° is created because the maximum plastic strain occurs in this direction. The growth of voids along these bands is enhanced and the coalescence of voids will happen at a faster rate along this path, creating the angled fracture.

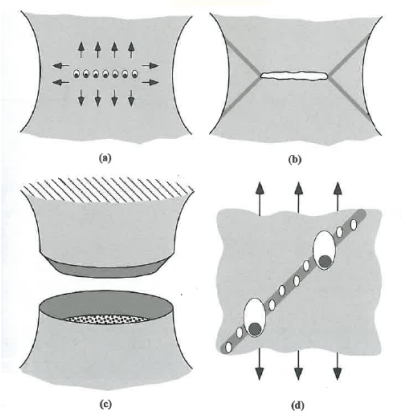

Figure 3.5: *The figure shows how the cone and cup shape fracture developed in a round-bar tensile specimen. In the center of the cross-section area in the necking area the high value of stress triaxiality causes voids to appear and grow around the larger particles in the material. When they coalescence, the circular shaped center fracture creates bands of high plastic strain at an angle 45 ° on the direction of tensile loading. This encourages the growth of voids along this bands creating a fracture surface at an angle of 45 °. [2].*

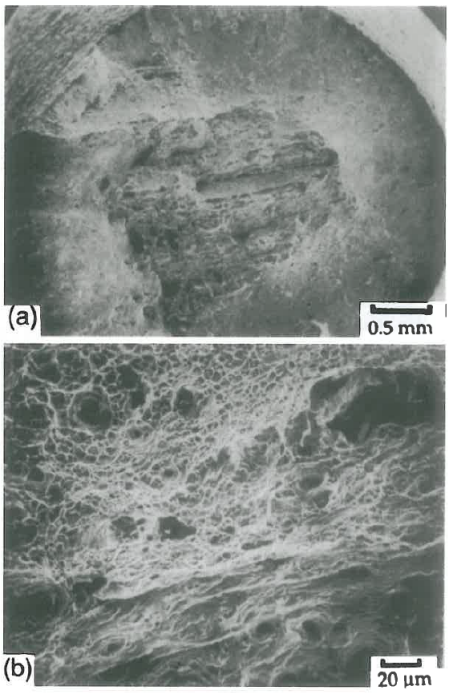

Figure 3.6: *Microscopic images of the fracture zone of a ductile material. In picture (a) the rough surface of the center fracture can be seen surrounded by the smooth surface of the angle fracture. In picture (b) close up on the rough surface of the center fracture area. [2].*

3.2.3 Mathematic models for predicting the growth of voids and onset of fracture.

Several models have been made in order to describe the behavior of void growth leading to failure of the material. One is made by Rice and Tracey [21] and describes the growth of one single void in an infinite solid subjected to remote principle stresses ($\sigma_1, \sigma_2, \sigma_3$) and remote strain rates ($\dot{\varepsilon}_1, \dot{\varepsilon}_2, \dot{\varepsilon}_3$). The void is assumed to be spherical in its initial state, but deforms into an ellipsoidal shape. Rice and Tracey concluded that the growth of one void representing the voids in the material can be approximated as the ratio of radial size of the assumed void to the initial radius of the undeformed void.

This model has the weakness of not being able to account for the coalescence of voids as they grow ever larger, since only one void is present in the material model. The model is also unable to predict the failure of the material. A failure criterion can be introduced by saying that the material is assumed to fail once a preset void radius size has been reached.

Another model is presented by Gurson [12] and later modified by Tvergaard [22, 23]. It assumes that the voids are homogeneously distributed in a continuous material. It differs from classical plastic theory by being dependent on the hydrostatic stress in the material in order to define the yield surface, and thereby introduces a strain-softening effect to the plastic material. The model assumes that the growth of voids results in a yield surface defined as a function of void volume, the equivalent stress, the hydrostatic stress and the flow stress in the matrix material, as seen in Eq. (3.6) ([2] pg. 229).

$$g(\sigma_e, \sigma_m, \bar{\sigma}, V_V) = 0 \tag{3.6}$$

The model given by Gurson and Tvergaard assumes that the failure of the material occurs when the plastic strain causes a local instability in the form of localized strain bands. Because the voids are assumed to be a homogeneous part of a continuous material, the onset of local instability from necking of the void sidewalls can not be predicted. Thomason ("Ductile fracture of metals" 1990) introduces a simple model to determined when this instability takes place. He assumes that in a plane loading state ($\varepsilon_3 = 0$) the fracture due to local instability in the sidewalls between

voids (coalescence of voids) takes place when the stress in the section between the voids σ_n reaches a critical value $\sigma_{n(c)}$. If a is the length of a void in the direction of σ_1, b is the width of the void, and d is the distance between two voids (the thickness of the side wall dividing two voids) then fracture is predicted to occur when

$$\sigma_{n(c)} \frac{0.5d}{0.5(d+b)} = \sigma_1 \tag{3.7}$$

All of these models are assumptions made in order to best predict the onset of fracture due to coalescence of voids. In most material the fracture will occur due to minimal increase in the nominal strain when the void volume fraction is over about 10-15 % ([2] pg. 231)

Chapter 4

Fracture mechanic parameters

4.1 Introduction

In this chapter, different parameters that have an influence on the behavior of ductile materials, particularly when it comes to fracture, are presented. In a real structure, the onset of damage can be expected to occur around weaknesses in the material, as explained in chapter 3. In a finite element based numerical analysis, the material are assumed to be homogeneous, and there is no weak part of the material where the fracture can start to develop. To overcome this problem, it is common to introduce some form of an initiation criterion, based on measurable values of stress, strain or energy parameters. To be sure that the material behaves equally in every direction, parameters that are independent on the coordinate system they are calculated from must be used. This means that for a given state of e.g. stress, there will be equivalent scalar value of stress that is independent of the coordinate system that the stress components it are calculated from are defined in. This ensures that the coordinate system used in the analysis does not influence the result regarding fracture.

The term equivalent points to this ability to be independent of the directions, and always giving the same result regardless of th coordinate system its components are calculated in. At the same time the equivalent value of a parameter does not display the whole truth, and its value is in most cases somewhat smaller than the maximum of its components.

The following section gives an explanation of the most used parameters related to fracture initiation and development.

4.2 Stress parameters

4.2.1 the von Mises equivalent stress

The *von Mises equivalent stress* comes from the *von Mises criterion* which is a yielding criterion used when simulating yielding of isotropic ductile materials such as metals, as explained in section 3.2. For anisotropic ductile yielding, the Hill yield surface criterion can be used. The von Mises criterion suggests that the yielding of the material starts when the equivalent stress σ_e is equal to a critical value defined as the uniaxial yield stress σ_Y ([2] page 66). The *von Mises stress* for principal stresses is defined as ([6] pg. 117)

$$\sigma_e = \frac{1}{\sqrt{2}}\left[(\sigma_1-\sigma_2)^2+(\sigma_1-\sigma_3)^2+(\sigma_2-\sigma_3)^2\right]^{1/2}, \quad (\sigma_1>\sigma_2>\sigma_3) \tag{4.1}$$

and defined from general stress components

$$\sigma_e = \frac{1}{\sqrt{2}}\left[(\sigma_{xx}-\sigma_{yy})^2+(\sigma_{yy}-\sigma_{zz})^2+(\sigma_{zz}-\sigma_{xx})^2+6\left(\tau_{xy}^2+\tau_{yz}^2+\tau_{zx}^2\right)\right]^{1/2}. \tag{4.2}$$

The σ_1, σ_2 and σ_3 are the three principal stresses, σ_{xx}, σ_{yy} and σ_{zz} is the stress and τ_{xy}, τ_{yz} and τ_{xz} is the shear stress. σ_e is a scalar stress value representing an effective stress occurring in the body. Equation (4.1) defines a cylindrical surface in the space defined by the three principal stresses, around the hydrostatic axis defined as $\sigma_1 = \sigma_2 = \sigma_3$, see figure (4.1).

A material is assumed to change from purely elastic behavior into elasto-plastic behavior when the equivalent stress exceeds a limit set as the yield stress σ_Y.

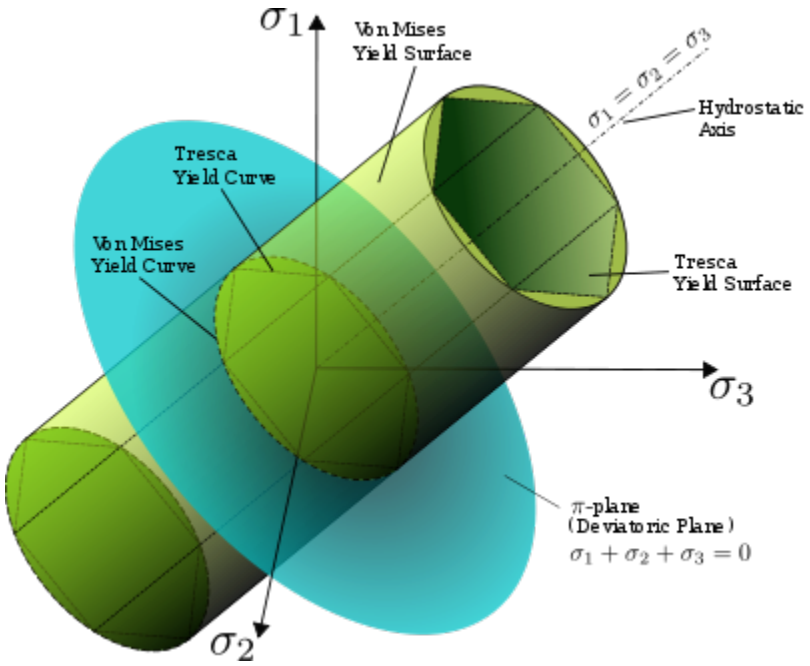

Figure 4.1: *The figure shows the von Mises yield surface in the space defined by the three principal stresses σ_1, σ_2 and σ_3. The criterion defines a cylindrical surface around the hydrostatic axis defined as $\sigma_1 = \sigma_2 = \sigma_3$. The Tresca-yield surface (hexagonal shaped) is also shown in comparison to the von Mises yield.*

In ABAQUS this limit is defined by the first line in the plastic properties, where an equivalent stress value is defined as the point of zero equivalent plastic strain (when using isotropic hardening). The material will behave purely elastically as long as the equivalent von Mises stress is lower than this limit.

The von Mises stress is independent of the coordinate system in which it is calculated, and will display the same numerical regardless of the coordinate system in which the stress components are calculated, provided that the loading conditions are the same. It is also always positive ([6] pg. 117). This makes it most useful as a general criterion for yielding.

The benefit with the von Mises stress is that it is a scalar measure for the entire stress state for the point in which it is calculated for ([6] pg. 117). The stress components may give the same information as the von Mises stress for some parts of the model, but they are dependent on the direction in which they are calculated, and only measure parts of the true stress state at a given point.

4.2.2 Hydrostatic stress/Pressure stress

The hydrostatic stress σ_m is also known as the pressure stress. It is an average of the three principle stresses in a body, and is often used as a parameter for the stress state of the material. The hydrostatic stress is defined as the stress that causes volumetric changes to a volume of solid, and does not alter the shape of the volume (just resizing it). The shape is being influence by the deviatoric stress state, and the total stress state is the sum of the hydrostatic state and the deviatoric state ([6] pg. 609). Hydrostatic stress is defined as [10]

$$\sigma_m = -p = \frac{1}{3}(\sigma_1 + \sigma_2 + \sigma_3) \tag{4.3}$$

p is the equivalent hydrostatic pressure, and is related to the hydrostatic stress σ_m as seen above. The negative sign in front of p comes from the definition of that compression is normally denoted as negative and tensile positive, but since p is a measure for the pressure state of a volume it is defined as positive when in compression.

The hydrostatic stress is defined by the three principle stresses alone, it contains no form of shear deformation, since the principle stresses are defined by principle planes elimination the shear stresses. The hydrostatic stress is the stress components that are responsible for changing the volume of a predefined volume of a solid. From Eq. (4.4) it can been seen that the hydrostatic stress is $\boldsymbol{\sigma_m = -p = \sigma' - \sigma}$.

In the space defined by the three principle stresses the hydrostatic stress is a vector lying in the von Mises surface, parallel with the hydrostatic axis ($\sigma_1 = \sigma_2 = \sigma_3$), starting in the deviatoric plane (π plane) as seen in Fig. 4.1.

Hydrostatic stress is greatly influencing the material behavior when voids are developing and growing in materials exposed for ductile fracture, since the stress triaxiality discussed below is dependent on the hydrostatic stress and the von Mises equivalent stress. In a localized necking zone, the equivalent stress may have about the same value all over, but the center region of the volume is experiencing a higher hydrostatic pressure stress than the outer parts of the volume, and therefore it has a higher value of stress triaxiality.

4.2.3 Deviatoric stress

While the hydrostatic stress changes the volume of a solid, the deviatoric stress components are responsible for altering the e shape, i.e. changing the angles between the sides in a predefined volume of a solid. Summed up with the hydrostatic pressure it defines the stress state in the material as

$$\boldsymbol{\sigma} = \boldsymbol{\sigma}' + \boldsymbol{p} = \underbrace{\begin{bmatrix} \sigma_{xx} & \sigma_{xy} & \sigma_{xz} \\ \sigma_{yx} & \sigma_{yy} & \sigma_{zy} \\ \sigma_{zx} & \sigma_{zy} & \sigma_{zz} \end{bmatrix}}_{\text{True stress}} = \underbrace{\begin{bmatrix} S_{xx} & S_{xy} & S_{xz} \\ S_{yx} & S_{yy} & S_{zy} \\ S_{zx} & S_{zy} & S_{zz} \end{bmatrix}}_{\text{Deviatoric stress tensor}} + \underbrace{\begin{bmatrix} \sigma_m & 0 & 0 \\ 0 & \sigma_m & 0 \\ 0 & 0 & \sigma_m \end{bmatrix}}_{\text{Hydrostatic stress}} \tag{4.4}$$

where σ_{ij} is the true stress in the material.

As seen in Eq. (4.4) the shear stress is only related to the deviatoric stress components, since pure shear stress does not change the volume of a solid, ut only alters the shape of it.

In the space of principle stresses, the deviatoric stress is a vector starting in origo and lying in the deviatoric plane (π plane) seen in Fig. 4.1.

4.2.4 Stress Triaxiality

Stress triaxiality is defined as

$$\eta = \frac{\sigma_m}{\sigma_e} = \frac{\frac{1}{3}(\sigma_1 + \sigma_2 + \sigma_2)}{\sigma_e} \tag{4.5}$$

It is used as a parameter to determine the state of stress in a body based on the hydrostatic stress and the von Mises equivalent stress. In materials that are subjected to ductile fracture, the stress triaxiality is an important parameter. The equivalent strain at which a material starts to fail (damage initiation) is highly dependent on

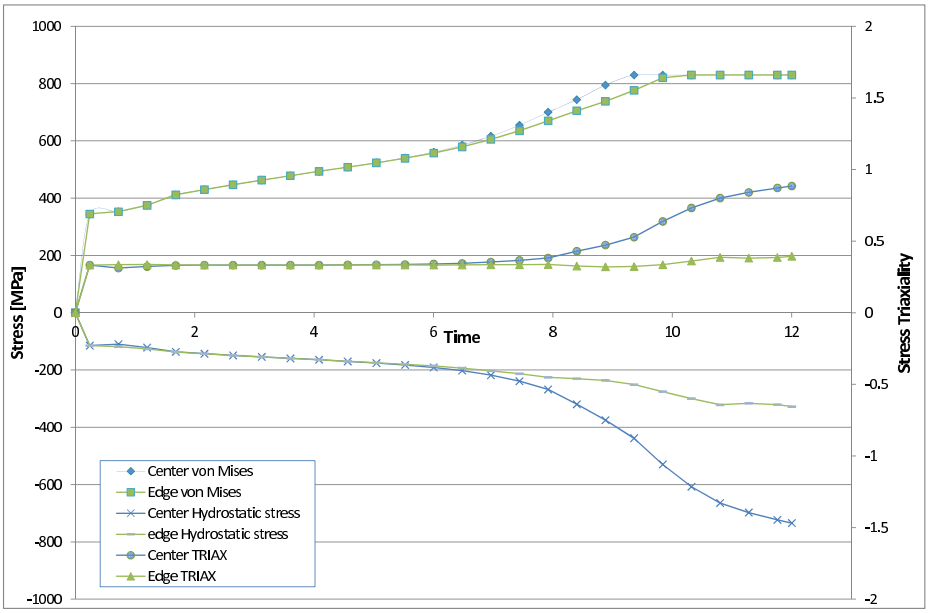

Figure 4.2: *The figure shows the development of equivalent stress, stress triaxiality and hydrostatic stress for two elements in a tensile test simulation performed using the ABAQUS software package. The center element is experiencing higher hydrostatic stress than the element on the edge of the plate after the initiation of necking, at the point of 5.5 sec. This increases the amount of stress triaxiality in the element.*

the stress state of the material, hence the stress triaxiality.

In a fracture zone of a material, the equivalent stress may be about the same value all over. Experiments have shown that ductile fracture due to growth and coalescence of voids is initiated in the center of the volume. When a material is necking, a volume inside the necking zone is strained in tension in the direction of the main principle stress σ_1, and compressed in the two transverse directions because the thickness and width of the specimen is reduced by the necking phenomenon. This creates a state of high hydrostatic stress leading to a higher state of triaxial stress in the volume. A volume which is located nearer the edge of the specimen will not have the same amount of hydrostatic stress because the straining of this element is more of a shape altering strain than a volume changing one.

The influence of the stress triaxiality on the behavior of a material in post necking state can be seen in Fig. 4.2. Two elements in a tensile test simulation performed with the ABAQUS software package are compared. The center-element is located at the center of the plate, inside the necking area, and the edge-element is located at the edge of the model. Both elements are at the mid span of the model. Up to the

point of necking, the stress states of the two elements are equal, but after around six seconds the hydrostatic pressure of the center element starts to rise. This causes the hydrostatic pressure to increase. It can be seen that the von Mises stress in both elements is similar. In this model, the center element will fail before the element on the edge, because of the increasing value of the stress triaxiality caused by the high value of compression stress.

Studies have shown that the effect of stress triaxiality in a material is a parameter that is not possible to avoid, and that the best way to cope with its effect is to be aware of it and try to use materials that can withstand its effects on the structure [5].

4.3 Strain parameters

4.3.1 Equivalent plastic strain

The *equivalent plastic strain* is often used together with the *von Mises equivalent stress* to determine the state of the material. Like the von Mises equivalent stress, it is a scalar value representing the plastic strain state of the material. It is derived from the plastic strain rate as shown in Eq. (4.6) ([7] section 22.2.1).

$$\bar{\varepsilon}^{pl} = \bar{\varepsilon}^{pl}|_0 + \int_0^t \sqrt{\frac{2}{3}\sum_{i=1}^{n} \dot{\varepsilon}_i^{pl}\dot{\varepsilon}_i^{pl}}\,dt \tag{4.6}$$

where $\bar{\varepsilon}^{pl}$ is the equivalent plastic strain, $\bar{\varepsilon}^{pl}|_0$ is the equivalent plastic strain at $t = 0$ and $\dot{\varepsilon}_i^{pl}$ is the plastic strain rate during the time increment t.

The rate of the equivalent plastic strain $\dot{\bar{\varepsilon}}^{pl}$ can be calculated as ([7] section 20.1.2.)

$$\dot{\bar{\varepsilon}}^{pl}|_{t+\Delta t} = \omega\frac{\Delta\bar{\varepsilon}^{pl}}{\Delta t} + (1-\omega)\dot{\bar{\varepsilon}}^{pl}|_t \tag{4.7}$$

where $\Delta\bar{\varepsilon}^{pl}$ is the change in equivalent plastic strain during the time increment Δt. ω is a factor that dampens out high-frequency oscillations occurring in strain-rate-dependent materials.

Like the von Mises equivalent stress, the equivalent plastic strain is a simplification of a more complex state in the material. The benefit of the equivalent plastic strain is that it is a simpler way to describe the strain state in the material than looking at each strain component for themselves.

4.4 Other parameters related to yielding and fracture of ductile materials

4.4.1 Lode parameter and lode angle

For decades, the stress triaxiality has been the only parameter associated with fracture due to void growth and coalescence in ductile materials. Recently, it has been discovered that there is a second parameter involved in characterizing the stress state of the material [4]. The lode parameter gives information of the state of stress in the material for a given von Mises equivalent stress by implying that the main stress is caused by axial or shear stress components. The lode parameter is defined as ([14] pg. 18)

$$L_\sigma = \frac{2\sigma_3 - \sigma_1 - \sigma_2}{\sigma_1 - \sigma_2}, \quad L_\sigma \in < -1, 0 > \tag{4.8}$$

$$L_\sigma = -\sqrt{3} tan\theta \tag{4.9}$$

The lode parameter is always in the range of -1 to 0, representing uniaxial stress state and pure shear stress state respectively. (uniaxial stress state: $\sigma_1 \neq 0, \sigma_2 = \sigma_3 = 0$, pure shear stress state: $\sigma_3 = \frac{1}{2}(\sigma_1 + \sigma_2)$ giving $\frac{1}{2}(\sigma_1 - \sigma_2, \sigma_2 - \sigma_1, 0)$)

In [3], Bai and Wierzbicki presents a new plasticity model taking into account the influence of both the hydrostatic stress state and the lode parameter for the material stress state. They define the parameter known as the lode angle to be the angle

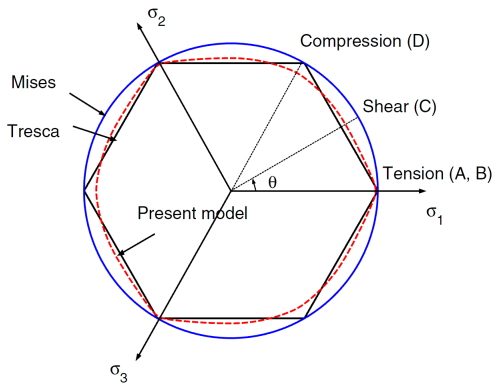

Figure 4.3: *The deviatoric stress plane with the von Mises yield curve, Tresca yield curve and the yield criterion presented by Bai and Wierzbicki in [3]. The lode angle is defined as the angle between the path of pure tension (along the σ_1-axis) and the vector representing the equivalent stress state in the material (in this case the line from origo towards C) [3].*

in a polar coordinate system with the equivalent stress as the radial coordinate and the lode angle as the circumferential coordinate.

The lode parameter and lode angle are not used in ABAQUS up to the present version (v.6.11-1), and for this reason they will not be evaluated in the simulations carried out in the work of this thesis.

4.4.2 Characteristic Element Length

In order to reduce the computational cost of running a computer assisted FE-analysis, element properties are often related to one single size measurement of the dimensions of each element. In earlier fracture simulation studies done by A. Hillerborg [15, 16] and Hillerborg et al. [17] they introduced a parameter $\bar{u}^{pl}$ that was used to describe the behavior of a material when fracturing. This parameter is influenced by the size of the structure, or in a FE-model the element size it is related to (see 5.3.2). This introduces a need for a characteristic element length l_c that can be used to determine the energy released when a fracture develops in an element. In [17] the relation between the element elongation and the energy dissipation during necking and failure is defined as

$$G_f = \int_0^{\bar{u}_f^{pl}} \sigma d\bar{u}^{pl} \tag{4.10}$$

G_f is the energy dissipated per unit area by the fracturing of the material, and can be considered a material constant [16], and $\bar{u}_f^{pl}$ is the total elongation of the element from damage initiation to failure.

From the work of A. Hillerborg the definition of the characteristic element length is the dimension of the element in the direction of the elongation. Since this work was carried out on simple bar elements with only two nodes, this must be generalized some more. ABAQUS has adopted much of the theory presented by A. Hillerborg el. al. [17] and presents a definition that is generalized to apply for all types of elements:

> The definition of the characteristic length depends on the element geometry and formulation: it is a typical length of a line across an element for a first-order element; it is half of the same typical length for a second-order element. For beams and trusses it is a characteristic length along the element axis. For membranes and shells it is a characteristic length in the reference surface. For axisymmetric elements it is a characteristic length in the $r - z$ plane only. For cohesive element it is equal to the constitutive thickness ([7] section 20.2.3.).

An elements can have different side lengths in the different directions. It is recommended to use elements with side lengths as equal as possible, thus giving the elements the same properties in every direction when it comes to fracture modulating. This reduces, but does not eliminate, the dependency of the element mesh.

The characteristic element length presented here can be related to the strain reference length used by Ehlers and Varsta in [11], and that is descussed in section 5.2.

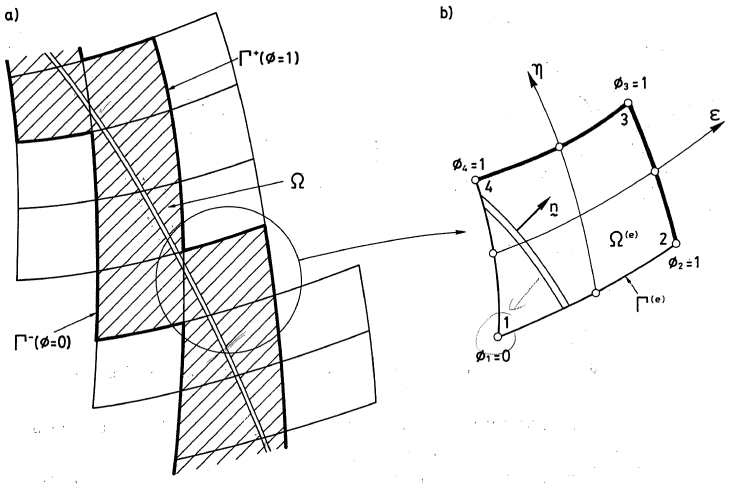

Figure 4.4: *a) The path of a crack through a plate modeled with shell elements. b) The path of the crack through one of the elements, with the normal vector n defining the direction of the elongation of the crack [20].*

A model for calculation the element length for shell elements

In recent times there have been presented models that try to eliminate the mesh dependency altogether. An article written by J. Oliver [20] presents a method for shell elements that uses the dissipated fracture energy, assumed to be a material parameter and therefore constant throughout the material, and relates it to a crack angle in order to find a characteristic element length.

In a plate modeled by quadratic shell elements, a crack will take a random path through the plate and randomly through the elements making up the plate. Such a random path can be seen going through the element in Fig. 4.4. For each element, the energy that must be dissipated is a function of the elements base functions, the angle of the crack path through the element and which edges of the element the crack path goes through. Using these parameters a characteristic length for the element can be calculated as

$$l^c = \left(\frac{\partial \phi(\xi_j, \eta_j)}{\partial x'} \right)^{-1} = \left(\sum_{i=1}^{n_e} \left[\frac{\partial N_i(xi_j, \eta_j)}{\partial x} cos\theta_j + \frac{\partial N_i(\xi_j, \eta_j)}{\partial y} sin\theta_j \right] \phi_i \right)^{-1} \quad (4.11)$$

Here, N_i is the base functions for the element j node i, defined in the coordinate system (ξ, η) with origo of the coordinate system in the middle of the shell element. x' is the x-axis of the coordinate system defined by having the y' parallel to the crack going through the element, and the the x'-axis in the direction of the elongation of the crack. θ_j is the angle of rotation between the two coordinate systems for element j. ϕ_i is either zero or one depending on which side of the crack the node i is located, see Fig. 4.4.

This method can be used to remove the mesh dependency of the fracture criterion in a finite element analysis. But the computational resources needed to calculate the characteristic element length for each element is high, and software programs like ABAQUS uses less demanding definitions that will give sufficiently precise results of equivalent element lengths.

Chapter 5

Fracture models in the finite element method

5.1 Introduction

In the finite element method, the structure has to be simplified into a finite numbers of elements that have more or less the same properties all over. The ideal approach is to have uniform elements all over, of the same size and with the same properties regarding stiffness, mass and other material related properties. The behavior of the structure is dependent on the inputted data regarding how each element is supposed to respond to load cases and straining. For the elastic behavior of the element the deformation is small and evenly spread out through the structure. For the plastic behavior the same applies as long as the straining of the material is smaller than the combination of strain and stress values that will bring the material up to its point of ultimate strength.

In the FE-method, the model's behavior are independent of the element size used in the mesh of the model, within certain limits. Two models shearing the same material input will behave more or less in the same way for a specific load case, even if the element sizes used are different. Some effects may arise due to poorly chosen mesh, where some element may be deformed in a manner that produces effects that are not realistic. This includes shear locking in shell elements, major distortion of elements due to unfortunate deformation of elements or the solution

may not converge because there are too few elements being used.

As long as the mesh is capable of representing the structure under the loading conditions applied, the size of the element in the mesh should not influence the result up to the point of ultimate loading. For ductile materials, the effect of passing the point of ultimate strength is explained in section 3.1. In a FE-model, whats happens is that the continued elongation of the model is being concentrated into straining of a few elements, representing the instability zone. During this deformation, the element size is crucial. Since the elongation is produced through straining of perhaps as little as one element, the properties of this element alone now govern the behavior of the whole model.

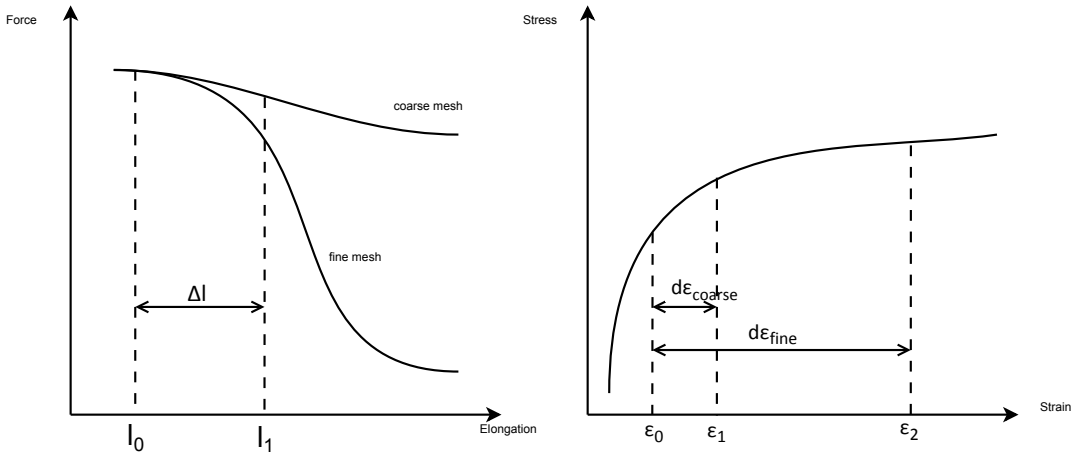

Figure 5.1: *The figure illustrates the relationship between the true strain in the element of a FE-analysis, and the global elongation of the model. For models containing smaller elements, the true strain increases by a higher value than for a corresponding model with larger elements. This makes the fine meshed model behave more soft than the model with larger elements in a post-ultimate strength state.*

If the same model is meshed using two different element sizes, but the material properties are kept the same, the global response after the point of ultimate strength for the coarser meshed model will be stiffer than for the finer meshed model. This is a result of the effect of the global elongation being dependent on true stress/true strain relationship in only one element, as the elongation continues beyond the point of ultimate strength. At the point of ultimate strength the elongation l_0 of the model is

$$l_0 = l^e n_{elem}\, \varepsilon \tag{5.1}$$

where l^e is the element length, n_{elem} is the numbers of elements and ε is the strain in the elements. The elongation of the model is spread out evenly as strain in the elements. If both models are supposed to elongate the same amount Δl from the point of ultimate strength (Fig. 5.1), the true strain in the element being strained in the fine meshed model must be

$$\Delta l = \delta\varepsilon_{fine}\, l^e_{fine} \; = (\varepsilon_2 - \varepsilon_0) l^e_{fine} \tag{5.2}$$

where ε_0 is the true strain at the point of ultimate strength and ε_2 is the true strain at the point of elongation l_1 for the fine meshed model. L^e_{fine} is the element length. The same relationship for the coarser meshed model will be

$$\Delta l = \delta\varepsilon_{coarse}\, l^e_{coarse} \; = (\varepsilon_1 - \varepsilon_0) l^e_{coarse} \tag{5.3}$$

where ε_1 is the true strain in the element for the coarse meshed model when elongated to l_1.

Δl are equal in Eq. (5.3) and Eq. (5.3), so substituting the two equation into each other yield

$$\delta\varepsilon_{fine}\, l^e_{fine} \; = \delta\varepsilon_{coarse}\, l^e_{coarse} \tag{5.4}$$

Since l^e_{coarse} is larger than l^e_{fine}, then $\delta\varepsilon_{fine}$ must be larger than $\delta\varepsilon_{coarse}$, hence $\varepsilon_2 > \varepsilon_1$.

The coarse meshed model has a higher stiffness (the slope of the true stress/true strain curve lies higher) while elongating from l_0 to l_1 than the fine meshed model does. This makes the finer mesh model act more softly, giving a steeper drop in the force-displacement curve after the point of ultimate strength.

Since the post-ultimate strength behavior is dependent on the mesh, the plastic

properties, calculated as the engineeering strain cannot be used directly to model the material during this part of deformation. This calls for the introduction of fracture models, since this behavior is due to ductile fracturing of the material. Two different approaches to model the post-ultimate strength behavior follows in this chapter.

5.2 A fracture model using the true stress/true strain relationship

5.2.1 Introduction

In the scientific journal Thin-Walled Structures Sören Ehlers and Petri Varsta from the Helsinki University of Technology present a method for modeling the local instability up to the point of fracture, causing necking in a material under tensile loading by tuning the plastic properties for the material in the FE-model [11]. The idea is to get around the limit of validity for the true stress/true strain relationship obtained from the engineering strain measured in a material test, as explained in Section 2.1. The data used for the stress and strain relationship is related to an element's length, called the strain reference length, and is obtained from tensile tests of the material where the strain is optically measured at the surface of the material in the necking zone. The related stress is obtained independently of the strain, from calculating the cross-section area by measuring the contraction of the material in the width and thickness of the tensile specimen, and dividing the load on this calculated cross-section area. The tensile tests are done on three flat-bar dog-bone shaped tensile specimens with different length to width rations, The thickness was 5.87 mm for two of the specimens (referred to as 6 mm) and the third being 4.04 mm thick (4 mm). The surface strain in the necking zone of the material is measured using stereoscopic cameras that could trace the relative movements of a stochastic pattern of black and white pixels painted on the surface of the specimen.

When a relationship for the stress and strain for the material was established for different strain reference lengths, this data was used as input for the material properties when simulating the tensile test using the FE-analysis program LS-DYNA. The element size used in the FE-analysis was the same as the strain reference length

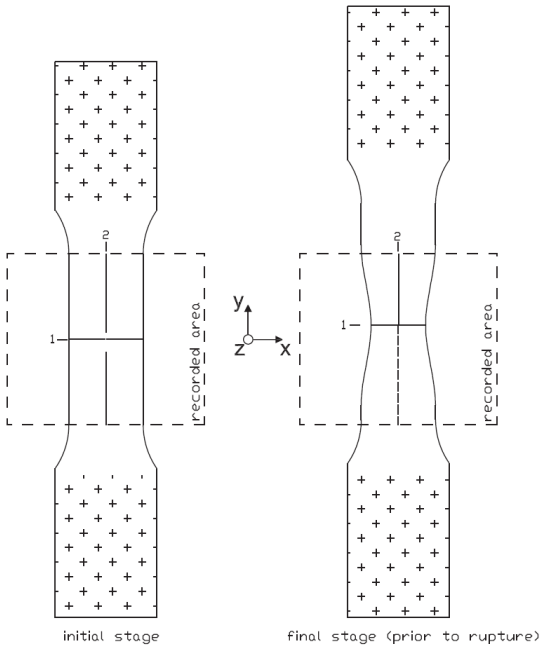

Figure 5.2: *The test specimen's initial shape and its shape right before failure. The area inside the dashed box is recorded by the cameras in order to measure the strain on the surface of the material. The marks at the end symbolizes the part being clamped by the test-rig machine.[11]*

related to the stress/strain relationship.

Ehlers and Varsta conclude, that this method of obtaining the stress/strain relationship and using it to simulate the local instability experiments with ductile fracture causing necking of a tensile specimen, could improve non-linear numerical simulations.

5.2.2 Ehlers and Varsta plasticity model

True strain measurement

What separates this method from the conventional method of obtaining the stress-strain relationship is that the strain is measured as a true value over a small gauge length, and thus contains the true value of the local strain in the material as the zone of instability develops. Conventional methods measure the strain as a mean value of the ratio of the elongated length and the initial length. Such conventional

methods of calculating the strain do not isolate the effect that the local instability has on the elongation, but evens its effects out over the whole specimen. This makes the stress/strain relationship obtained from measuring the global elongation not valid after the point of ultimate strength, since the straining of the specimen after this point is concentrated in the necking zone, while the material outside of this zone recovers elastically ([14] pg. 12).

Ehlers and Varsta used cameras taking stereo pictures of the surface of the necking zone of the tensile specimen when the load was increased from zero through ultimate strength and to fracture. These cameras were able to trace facets of pixels painted on the surface of the specimen, and the strain was measured as the relative elongation of a distance between two facets. The initial distance between the facets was uses as the gauge length and referred to as the strain reference length.

The strain reference length was used to relate the obtained stress/strain relationship to an element size in the FE-model when the data was used in a FE-analysis. As for a FE-model where the smallest length which the strain in the model can be measured over are the distance between the nodes (i.e. the element length for first order elements and half the element length for second order elements), the smallest distance the strain could be measured over was the strain reference length determined by the facet size.

The facet sizes used ranged from 10x10 pixels to 50x50 pixels, giving a strain reference length ranging from 0.88 mm to 4.4 mm. A total of seven different strain reference lengths were used to measure the true strain for seven different mesh sizes in the following FE-analysis. The true strain was measured as

$$\varepsilon_{true} = ln\frac{l + \delta l}{l} \tag{5.5}$$

where l is the strain reference length and δl is the change in the length of l.

Determination of true stress

The true stress related to the true strain measurement explained above, was calculated on the basis of the transverse displacement of the edges in the necking zone

and the out-of-plane (the z-direction in Fig. 5.2) displacement measured by the stereoscopic cameras. The cross section area at each stage was calculated as

$$A(y) = \int [t + 2u_z(x, y)]dx \tag{5.6}$$

where y is the position of the cross-section in the direction of deformation, t is the initial thickness of the flat-bar and u_z is the out-of-plane displacement of the section at each stage. The measured cross-section area is seen in Fig. 5.3.

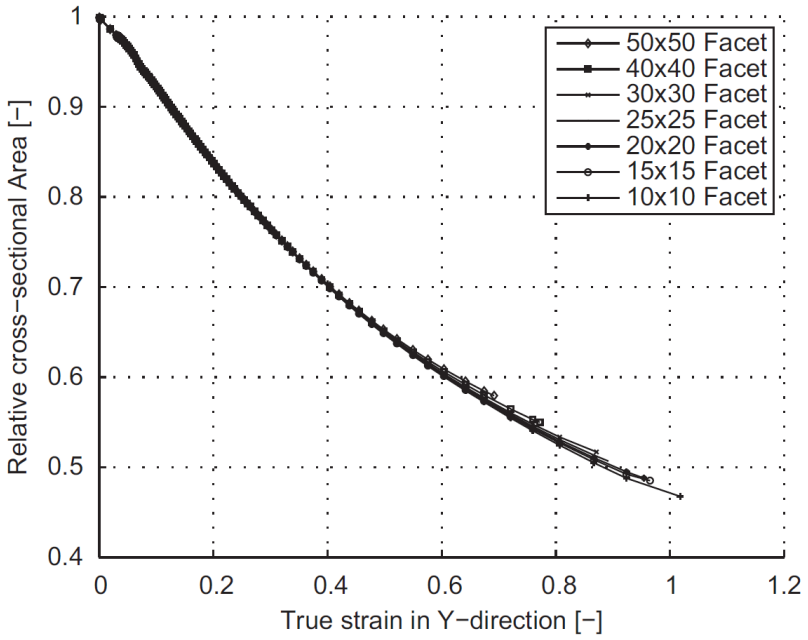

Figure 5.3: *The reduction of the cross section area as a function of the true strain measured. [11]*

At each stage during the deformation, the true stress in acting across the cross-section area in the position defined by y is

$$\sigma_{true} = \frac{F}{A} \tag{5.7}$$

where F is the force applied onto the structure, and A is the current cross-section area.

Table 5.1: *The strain reference length, the corresponding facet size used when optically measuring the local strain at the surface of the material of the tensile specimen, and the element size used when reproducing the results in LS-DYNA [11].*

Strain reference length [mm]	Facet size [pixes]	Element side length [mm]
0.88	10x10	0.88
1.32	15x15	1.32
1.76	20x20	1.76
2.2	25x25	2.2
2.64	30x30	2.64
3.52	40x40	3.52
4.4	50x50	4.4

Implementation of the true stress-true strain relationship into the FE-model

The true stress/true strain relationships that were measured using a different gauge length on the different tensile test specimens were used to recreate the tests in the FE-analysis software LS-DYNA. The element type used were four nodded quadrilateral Belytschko-Lin-Tsay shell elements, and the analysis was performed using the explicit time integration solver in LS-DYNA. Each of the three different tensile specimens was meshed with seven different element sizes (see table 5.1)

The stress and strain relationship obtained for the corresponding tensile specimen measured using a strain reference length equal to the element side length was inputted as the plastic properties for the material. Then the tensile experiments were reproduced using the FE-method and LS-DYNA. The force-displacement curve from the finite element analysis was compared against the force-displacement curve recorded during the tensile testing of the specimens. They show good agreement between the recorded results and the results from the finite element method.

The method of obtaining the stress and strain relationship proposed by Ehlers and Varsta in [11] does not include any fracture criterion, and the FE-models behavior is only controlled through its plastic material properties.

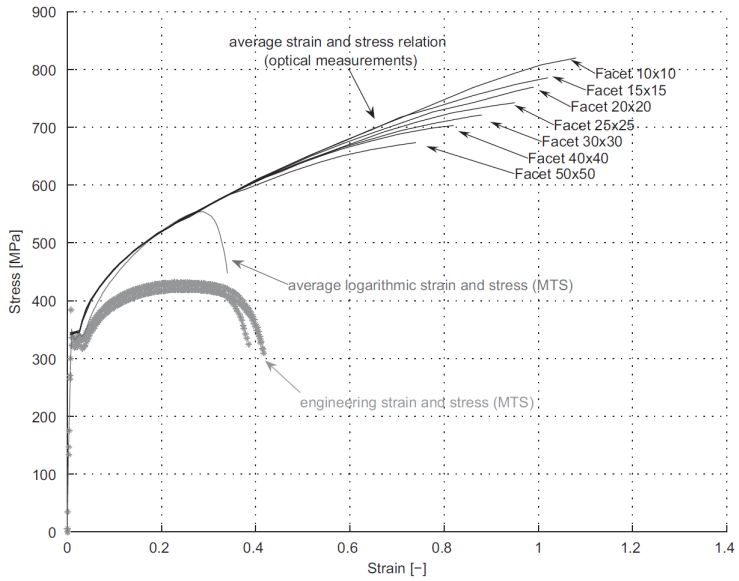

Figure 5.4: *The stress and strain relationship that is measured from one of the tensile test specimen. The engineering strain and stress relationship and the logarithmic strain and stress relationship are calculated from the overall elongation of the tensile specimen. [11]*

5.3 Fracture model defining the fracture energy dissipated

5.3.1 Introduction

In the 1970s, Arne Hillerborg published a number of articles [17, 15, 16] regarding a fracture model based on the fracture energy dissipated during failure of concrete. His goal was to create a fracture model for use in FE-analysis that would explain the creation and propagation of cracks without depending on a very fine mesh in the area of the fracture, to be able to analyse complicated models using FEM by using less computer processing power than earlier models did.

Earlier there had been methods using a stress intensity factor in order to explain the prorogation of a crack due to high values of stress at the end of the crack. The stress was assumed to approach infinity at the crack, and decreasing towards the general stress state in the material following the relation

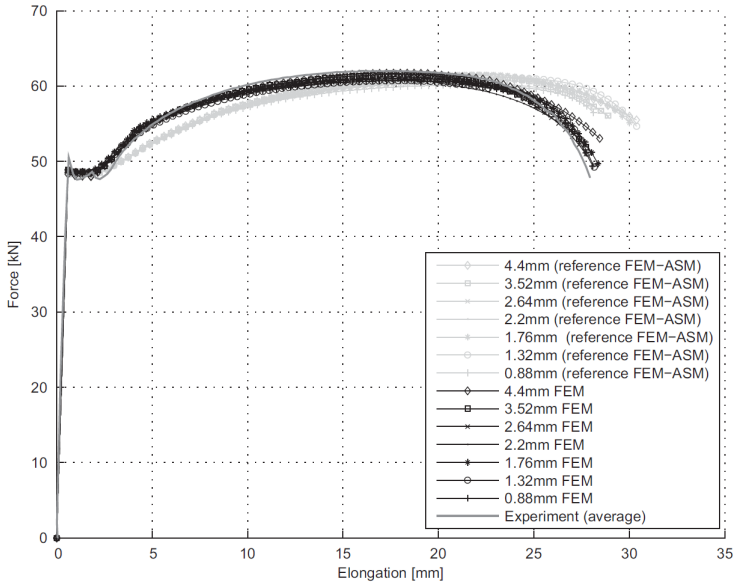

Figure 5.5: *The force-displacement curve for the FE-analysis, compared to the force-displacement results of the tensile test. This shows good agreement between the proposed method of obtaining the stress and strain relationship and the results of the tensile test of the material. [11]*

$$\sigma = \frac{K}{2\pi r} \tag{5.8}$$

where r is the distance from the crack tip and K is a stress intensity factor [17]. The crack is assumed to propagate when the value of $K = K_c$. The drawback of this model is the need of relatively small elements near the crack that is modeled, and the model cannot be used to explain the creation of cracks in an undamaged material.

An energy balance model had also been used in FE-analysis, where a crack is assumed to propagate when the release of energy is equal or greater than the amount of energy absorbed by the model. The yield stress σ_Y is assumed to act across the crack in a zone of plastic strain. Only when the crack opens to a certain width, the stress will stop acting across the crack. The model enables the use of relatively large elements, but the creation of the crack is not explained.

5.3.2 Fracture model by Hillerborg et al.

Hillerborg et al. proposed in [17] that the energy balance method could be modified in order to create a fracture model that was related to the energy dissipated because of fracturing, and retaining a realistic approach for describing the stress state near the crack tip. They assumed that at the crack tip, seen in Fig. 5.6, the stress is equal to the tensile strength σ_Y ($\sigma = \sigma_Y$).

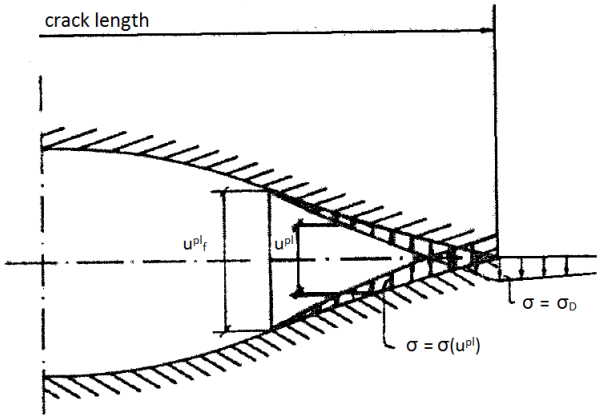

Figure 5.6: *The visualization of a crack in a homogeneously isotropic material. The stress is assumed to act across the crack as long as the crack width is less than $\bar{u}^{pl}_f$, and decreasing from σ_D at the crack tip to zero at where the crack has widened to $\bar{u}^{pl}_f$. [17]*

The part of the crack where the crack width is less than a value u^{pl}_f the stress is assumed to decrease with the width of the crack ($\sigma = \sigma(u^{pl})$). At the point of which the crack has widened to u^{pl}_f the stress is zero. This implies that as long as the crack width is less than u^{pl}_f, there will be stresses acting over the crack. Because of this stress reduction, the opening of a unit area of crack from zero to a width of u^{pl}_f dissipated a certain amount of energy that can be calculated as

$$G_f = \int_0^{u^{pl}_f} \sigma du^{pl} \tag{5.9}$$

G_F is the dissipated fracture energy per unit area of crack created, and is a material parameter that can be found from testing the material by means of tensile tests.

The energy dissipated per unit area crack is the area beneath the $\sigma - \varepsilon$-curve, and the total energy dissipated inside the fracture zone is the area beneath the $\sigma - u^{pl}$-curve [16].

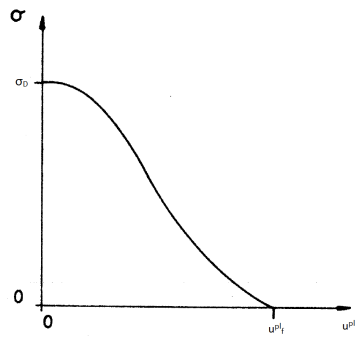

Figure 5.7: *As the crack propagates, the stress will decrease as the width of the crack increases. The energy dissipated in the fracture zone by fracture is equal to the area beneath the $\sigma - u^{pl}$-curve. [17]*

The shape of the curve in Fig. 5.7 determines the behavior of the material if it is loaded beyond the ultimate strength of the material. Different shaped $\sigma - u^{pl}$-curves may give the same value of G_f, and therefore will dissipate the same amount of energy due to fracturing, but they will behave differently because of the difference in shape.

An advantage with to this model is that it is a general model that can be used to predict the failure of materials subjected to different kinds of loadings. It can also predict the creation of cracks in an element from the value of true strain or true stress in the element. The onset of damage is then said to be when the true strain reaches a critical value $\varepsilon = \bar{\varepsilon}_D$ or when the true stress is $\sigma = \sigma_D$. Often, the equivalent stress and strain values are used as initiation criterion because they measure the strain and stress independently of the directions of the stress and strain components, see 4.2.1 and 4.3.1. The model also well adapted to be used in numerical calculations, because the stress values are finite, and stress, deformation and dissipated energy are logically related.

When using the model proposed by Hillerborg et al., it must be clear that the *model laws* does not apply to the structure after the initiation of failure. The model law states that two specimens with the same material, geometry and loading, but with different size will behave equally by obtaining the same value of stress and strain at a corresponding point. If this is done using FEM and the fracture model proposed by Hillerborg et al., inputting the same data regarding σ and u^{pl}, the stress values

will be the same at corresponding point, but the value of u^{pl} will be proportional with the size of the specimen [15]. Said differently, the σ-u^{pl}-curve for a specimen must be in relation to its size. If data developed for testing a small specimen is applied in order to model fracture of a larger specimen, the larger specimen will fail at a lower value of strain ε than it should. (Both models should fail at the same global strain value ε_f, but with different values of elongation after the point of ultimate strength u^{pl}).

Chapter 6

Explicit dynamic analysis in FEM

6.1 Introduction

One choice that has to made when planning an analysis is which method should be used to solve the problem numerically. In dynamic analysis, the explicit time integration is favorable when solving problems containing high speed deformations within a short amount of time, because the method can calculate a high number of incremental points close together in time, at a low computational cost. It is preferred in cases where contact definitions between different part of a structure model is present [7]. The element size and the time used to run an explicit analysis are directly linked together through the critical time increment size Δt_{cr}, as defined in Section 6.3.2.

6.2 Dynamic analysis using direct integration methods

When performing a FE-analysis there are many different methods offered to perform dynamic analysis, each of them with advantages and disadvantages depending on the problem you are trying to solve. One method that is often used for dynamic nonlinear analysis is the "explicit dynamic analysis method". For linear

dynamic analysis, it will in most cases be more effective to use analysis methods based on modal methods. They depend on calculating the eigenvalues of the system and then calculating the response of the model using these eigenvalues. The calculations performed in order to find the eigenvalue are costly, particularly since the number of eigenvalues that is needed for complicated structures is not known before starting the analysis. The explicit dynamic analysis method uses direct-integration and integrates the global equation of motion through time. For linear analysis this is not very effective, but for non-linear analysis, as collision events often are, this direct-integration method is often more effective.

Direct integration is used to calculate the response history step-by-step in time. Each data point is calculated as a time increment Δt after the previous calculations. For non-linear problem the equation of motion can be generalized as ([6] pg. 407)

$$[\boldsymbol{M}]\{\ddot{\boldsymbol{u}}\}_n + [\boldsymbol{C}]\{\dot{\boldsymbol{u}}\}_n + \{\boldsymbol{R}^{\boldsymbol{int}}\}_n = \{\boldsymbol{R}^{\boldsymbol{ext}}\}_n \tag{6.1}$$

where $[\boldsymbol{M}]$ is the mass matrix of the system, $[\boldsymbol{C}]$ is the systems dampening matrix, $\{\boldsymbol{R}^{\boldsymbol{int}}\}$ is the internal load vector and $\{\boldsymbol{R}^{\boldsymbol{ext}}\}$ is the external load vector. The equation is calculated at the time increment n. The time factor is discretized using a finite difference approximation of the time derivatives. This can be done in many ways, but for application to dynamic collision events, the explicit time integration is best suited.

6.3 Explicit analysis

In the explicit analysis, the displacement and the velocity at the beginning of each increment are known. This means that the global mass and stiffness matrix need not be formed and inverted for each increment, saving much computational work. The size of the time increments however, have to be smaller than a critical time increment Δt_{cr}, see Section 6.3.2. This makes the method conditionally stable, and the increments must be kept small enough to preserve the stability of the result. Since the incremental steps are small, the incremental result will never greatly deviate from the exact solution, and any inaccuracy will most likely be corrected when calculating the next increment. Because of this there is often no need to con-

trol the accuracy as with the implicit method.

The stability of the method is related to the time it takes for a stress wave to move through an element. If the element is relatively small, or the wave is moving through the element at a high speed, the time increment must be small. Usually the increment must be smaller than the time it take a stress wave to get cross an element, traveling the distance between to nodes. This makes the method good for analysis where the total analyzing time is only a few orders of magnitude larger than the stability limit. But also for some quasi-static processes where the use of mass scaling is appropriate, which reduce the wave speed and therefore increases the length of the critical time increment in the analysis.

The explicit procedure is well suited for high-speed dynamic events, and slower quasi-static analysis. In the case of high speed events, the small increments mean that more detailed calculations are made and large deformation occurring over a short time can be captured. For quasi-static analysis, the deformation is assumed to be to slow too cause dynamic response in the structure. The dynamic effect can be neglected. The treatment of contact is also simplified, making it a good choice for dynamic or quasi-static analysis containing contact between surfaces. The total time needed to run the analysis is linearly dependent on the size of the model and the total time simulated, assumed that the mesh size is kept constant. A increase of any of the two factors, will result in an equal increase in calculation time.

The explicit method is preferred before the implicit method because of the ability to convert the mass matrix to a diagonal matrix, often referred to as lumped mass. This reduces the number of calculation needed for each time increment with up to 4000 times for a three dimensional FE-analysis [6]. Also the amount of data storage needed for each increment calculation is much smaller for the explicit method.

6.3.1 Central Difference Method

The explicit analysis method makes use of the central difference method to calculate the state of the next increment. The equilibrium equations are satisfied at the beginning of each increment (t_i). The acceleration at t_i is used to find the velocity at $t_{i+\frac{1}{2}}$ and the displacement at t_{i+1}. Each calculation is relatively inexpensive, and is done using "lumped" element mass matrices. The velocity ($\dot{u}^N_{i+\frac{1}{2}}$) and the

displacement (u^N_{i+1}) is calculated as

$$\begin{aligned} \dot{u}^N_{i+\frac{1}{2}} &= \dot{u}^N_{i-\frac{1}{2}} + \frac{\Delta t_{i+1} + \Delta t_i}{2} \ddot{u}^N_i \\ u^N_{i+1} &= u^N_i + \Delta t_{i+1} \dot{u}^N_{i+\frac{1}{2}} \end{aligned} \tag{6.2}$$

where u^N is a degree of freedom, and the subscript i is the increment number in the analysis.

The efficiency of the procedure comes from the use of lumped stiffness matrices, which are diagonal. This makes it easier to calculate the acceleration at the beginning of each increment (Equ. (6.3), as the matrices are easy to invert and the vector multiplication only demands one operation for each degree of freedom. The acceleration is the calculated as

$$\ddot{u}^N_i = ([\boldsymbol{M}]^{NJ})^{-1}(\{\boldsymbol{R^{ext}}\}^J_i - \{\boldsymbol{R^{int}}\}^J_i) \tag{6.3}$$

where $[\boldsymbol{M}]^{NJ}$ is the mass matrix, $\{\boldsymbol{R^{ext}}\}^J_i$ is the applied load vector and $\{\boldsymbol{R^{int}}\}^J_i$ is the internal force vector. The internal force vector is assembled with contributions from individual elements in such a way that a global stiffness matrix is not needed.

6.3.2 Stability

The stability of the procedure is dependent on the highest frequency of the system. Equation (6.4a) shows the limit for a system with and without damping in the system, respectively.

$$\Delta t \leq \frac{2}{\omega_{max}} \left(\sqrt{1 + \xi^2_{max}} - \xi_{max} \right) \tag{6.4a}$$

$$\Delta t \leq \frac{2}{\omega_{max}} \tag{6.4b}$$

Here ω_{max} is the maximum natural frequency, and ξ_{max} it the corresponding dampening ratio.

In ABAQUS, a small amount of dampening in the form of bulk viscosity is introduced to the system in order to control the high frequency oscillations that can occur during an analysis. This effect is by default applied as a linear effect, but for solid continuum elements it can also be a quadratic effect that is used in compression state in order to prevent elements experiencing high velocity gradients when collapsing, and the volume is suddenly reduced to zero.

6.3.3 Estimation of the stable time increment size

The size of the stable time increment Δt is often estimated as being smaller than a critical time increment size Δt_c [6], that is

$$\Delta t \leq \Delta t_c = \frac{l^e_{min}}{c_d} \tag{6.5}$$

where L_{min} is the smallest element dimension on the model, and c_d is the speed of sound in the material [6] over the element. c_d is defined in equation (6.6). This is just an estimated value of the maximum stable time increment. In most cases, it is wise to use a shorter time increment for the analysis. For two-dimensional models ABAQUS uses a reduction factor between $\frac{1}{\sqrt{2}}$ and 1, and for three-dimensional models $\frac{1}{\sqrt{3}}$ and 1. The speed of which the stress wave travels through a material is dependent on the Young-modulus E and the density ρ of the material.

$$c_d = \sqrt{\frac{E}{\rho}} \tag{6.6}$$

From this it is clear that the critical time increment is increase if the material is softer (low Young-modulus) or has a high density. This can be used to manipulate the time needed to run the explicit analysis on a computer.

6.3.4 Time reduction

The time spent on performing an explicit analysis is dependent on the size of the element, the number of elements used and the time period being simulated. For a model with a given mesh size, the time period simulated is the decisive factor. To reduce the time it take to run the analysis, there are some tricks that can be applied. It is possible to speed up the simulation as compared to the time taken for the actual event. Speeding it up too much may however introduce unwanted kinetic effects in the form of increased inertia forces that may change the outcome of the simulation, or some rate dependent parameters may be triggered due to the higher rate of change in the structure. If there are rate dependent parameters in use, speeding up the simulation is not recommended because the rate of change is increased, and it may change the result without the user being aware of it.

Another way to save time is to use mass scaling, artificially increasing the density of the material ρ. This reduces the time period simulated as compared to the time taken for wave propagation through an element, in effect increasing the value of Δt_{cr}, making the simulation run faster. Rate dependent parameters will not be influenced by changing the density, but it has the same effect concerning inertia effects as speeding up the simulation.

A model with overall large elements, but with sections with smaller elements, will run slowly because the time increment length is set by the size of the smallest element in the model. If the number of small elements is significant smaller than the number of large element, a mixed time integration method can be applied. In ABAQUS, this method sets different time incremental length for different sized elements, meaning that the large elements are analysed by using fewer increments than the smaller elements. The same central-difference integration rule as shown in section 6.3.1 is used, but different lengths of time increments are used for different sets of nodes in the model.

6.3.5 Energy monitoring

In an explicit dynamic analysis, the energy in the model is important to monitor. The total energy in the model should be close to constant, and the artificial energies should be negligibly small compared to "real" energies as strain energy and kinetic

energy. For quasi-static analysis, the amount of kinetic energy should not exceed a certain fraction of the strain energy. For cases involving contact or constraints, it is wise to monitor the energy dissipated by constraint penalty and contact penalty. They should be close to zero in all cases. [7]

6.4 Single versus double precision

In the field of computer science, the terme single and double precision refer to the number of significant numbers used to store the computational data during a computer assisted FE-analysis [1]. For most cases single precision is sufficient to calculate the correct solution. This is not necessarily the case when using an explicit dynamic method. Since the time increments may become very small, the nodal displacement during a time increment may become so small that single precision accuracy does not calculate it precisely enough. The solution becomes affected by round-off errors that may propagate. Double precision is often recommended if the nodal displacement is anticipated to become to small, or if the numbers of time increments needed exceed a limit of 300 000 increments [7].

Running an analysis using double precision makes the round-off errors less likely to influence the result, but adds a significant amount of time needed to perform the analysis. 20-30 % additional computational time is not uncommon compared to running the same analysis using single precision. On the other hand, using double precision will always give a more accurate result.

Chapter 7

Tensile experiment in ABAQUS

7.1 Introduction

In the experiment done by Sören Ehlers and Petri Varsta in [11], the true stress/true strain relationship measured on tensile test specimens was used as the material input to reproduce the resulting force-displacement curve using numerical methods (FE-analysis). The aim was to use this new approach of using the plastic properties of the material to model the local instability effect of necking in a tensile specimen, as explained in 5.2. This method will in this chapter be compared to the use of the damage and failure model for ductile metals, explained in 5.3, to simulate the same fracture behavior of the material. In the experiment done by Ehlers and Varsta [11], their results showed good agreement between the results of the tensile test and the results of the FE-analysis when comparing the force-displacement curve for the tensile test and the analysis.

The damage model offered in ABAQUS is based on the energy release model presented in section 5.3.2. This is a complete model with a damage initiation criterion and a damage evolution model leading to failure. The method proposed by Ehlers and Varsta does not include a failure criterion, and will only simulate the material behavior up to right before the point of failure. In this thesis a failure criterion will be added to the method given by Ehlers and Varsta, to be simulate the final fracture when the model breaks into two part.

The experiment described in this chapter is based on the tensile test experiment presented in [11], in order to tune the input parameters in ABAQUS for both of the methods used, to give the same global force-displacement response in the tensile test. When the inputted material parameters produced the same results in terms of force-displacement in the tensile test, these inputs would be used in an FE-analysis where the penetration of a steel plate is simulated as in [10]. This application is presented in chapter 8.

The element sizes that are used ranged from 2.2 mm to 17.6 mm. This will result in a quite coarse mesh for the model using the largest elements, since the overall length of the tensile specimens used are 106.68 mm. The choice of using coarse meshed models derives from the desire to be able to recreate and analyses a impact scenario using the FE-method with as few elements as possible, but still being able to simulate the local phenomenon that is created when a material fractures in a ductile manner.

7.2 The FE model

The model is based up on the test pieces used by Ehlers and Varsta [11], and was modeled using ABAQUS. The geometry of the model is shown in Fig. 7.1.

Only the parts between the clamping wedges of the test rig are used to create the model, and this gives it a total length of 106.68 mm. In addition to the measurements provided in Fig. 7.1, the thickness is set to be 5.87 mm. A small narrowing of 0.02 mm is made to the width in order to make the model weaker at the midpoint. This would ensure that the instability zone always will appear at the same place. The models is meshed in the part module using an edge seed mesh control to get the right size of each element.

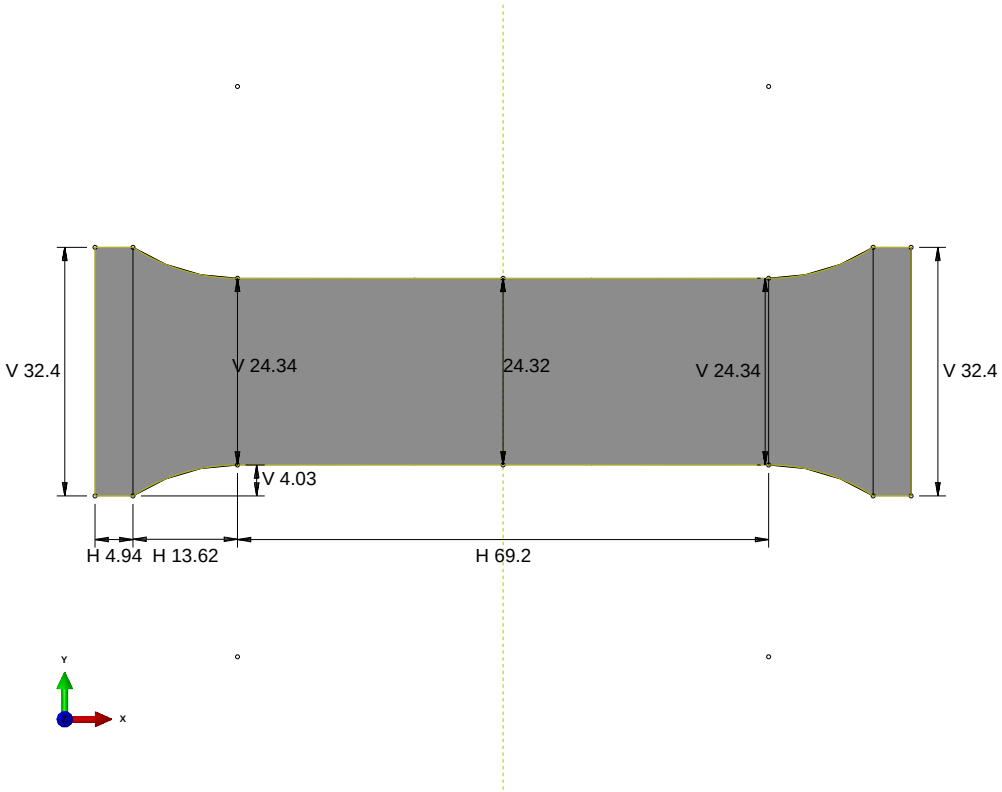

Figure 7.1: *The geometry of the model drawn in ABAQUS/CAE with the measurements used. The small narrowing of the width of the model in the middle is done in order to create a weaker point at which the local instability leading to necking will appear. All measurements are in millimeter.*

The different meshes can be viewed in Fig. 7.2. The model is meshed using the S4R element provided in ABAQUS. This element is a four-noded bilinear shell element using reduced integration, hourglass control and having finite membrane strains. Simpsons-integration rule is chosen as default with five integration points through the thickness of the element. It is also the only bilinear shell element with reduced integration that is available for three dimensional models solve using the explicit time integration solver.

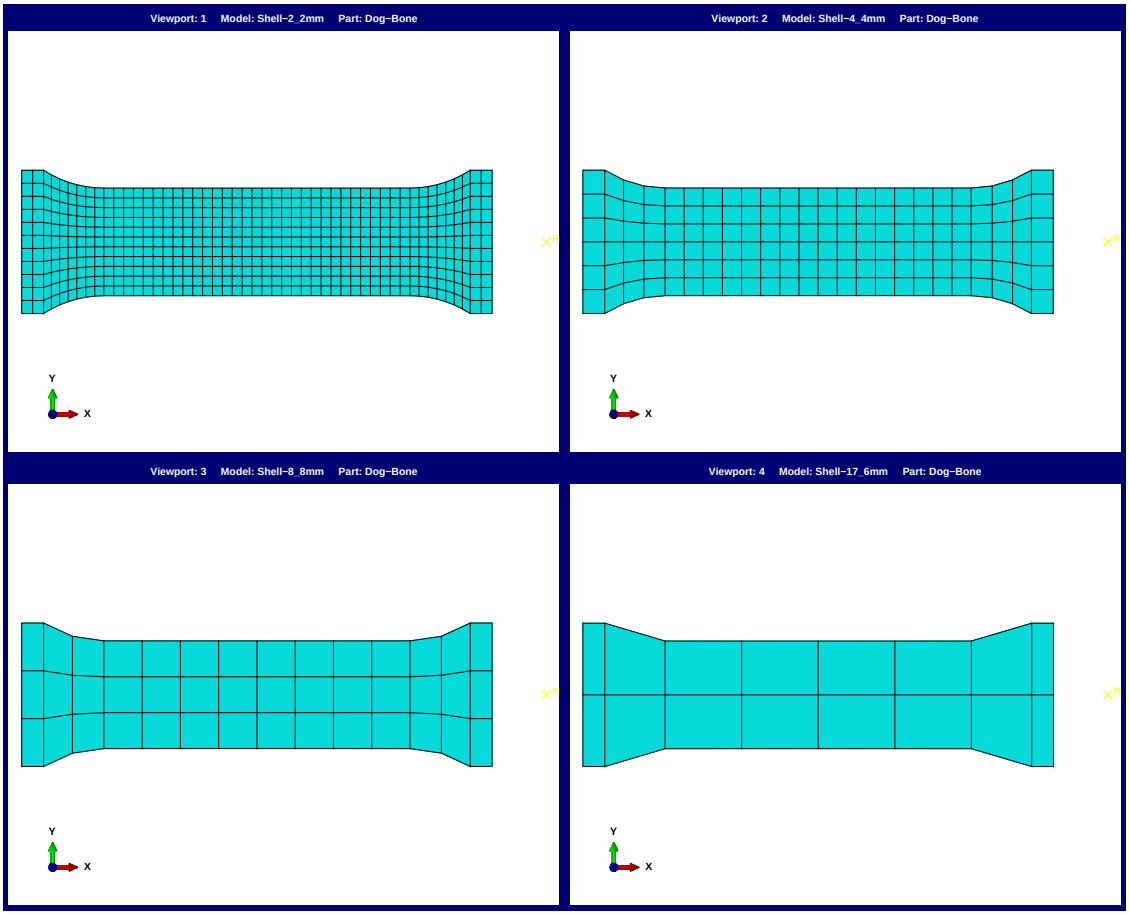

Figure 7.2: *The four different meshes used on the dog-bone model.(Top left: 2.2 mm, Top right: 4.4 mm, lower left: 8.8 mm, lower right: 17.6 mm) The model is meshed using edge seeds to define the side length of the elements in the middle part of the model, and the ends are seeded in order to keep a regular and well defined mesh.*

The material is defined by its elastic properties, plastic properties and density[1], an to be isotropic in its elastic properties, and to follow an isotropic strain-hardening rule in the plastic properties. No field variables are used and the material is defined as independent of the temperature and the strain rate. The whole model is defined as being homogeneous.

The boundary conditions are chosen to best simulate the clamped ends on the tensile test piece when it is was stretched. One end (the left edge in Fig. 7.2) is

[1]The density is needed since the analysis is performed using a dynamic time integration solver (ABAQUS/Explicit). This option requires that the model has a mass, that is provided by the density and the definition of a homogeneous material set in the Section module.

applied boundary conditions restraining all degrees of freedom, both translation and rotation, on all the nodes along the edge. In the other end (to the right in Fig. 7.2) all the nodes along the edge are restrained against all translation and rotations, except the translation in the x-direction. This is kept free to be able to strain the model. The elongation of the model is controlled by applying a constant velocity of $+3.33333$ mm/sec, in the x-direction, to the right side edge. This is the same velocity as used in the FE-analysis performed in [11]. The velocity is applied to the edge through a reference point, and a constrain forcing the edge of the model to move in unison with the reference point in the x-direction. All of the boundary conditions are applied to the geometry of the model, and not directly to the nodes. This makes it possible to change the mesh of the model without having to redefine the regions of the boundary conditions.

The main outputs asked for in the analysis include energy magnitudes in the whole model, like the internal energy of the model, external work, and their energy components. Also the reaction force in the reference point and the reference point's displacement. Each output is requested for 200 time steps, evenly spread out during the analysis.

The explicit dynamic analysis method is chosen when analyzing the models because this is the most appropriate analyzing method to use on impact scenarios and collision analysis of thin walled structures [11]. In this case, the analysis can be regarded as a quasi-static analysis. The ABAQUS documentation ([7] Sec. 6.3.3) recommend using the explicit analysis method for quasi-static analysis when there is a contact definition between elements in use, like in the analysis performed in chapter 8.

The analysis is set to last for a total time period of 9 seconds, leading to a total elongation of the model of 30 mm. Default values regarding incremental settings like how to estimate the maximum stable increment, maximum time increment allowed and time scaling are used. (For default values, please refer to the ABAQUS User's Manual ver. 6.11) Non-linear geometry is set to ON, allowing for geometric non-linear effects to be included.

All the analysis regarding the tensile experiment and tuning of the material properties is done using double precision. This means that the round of errors during the analysis is reduced because more significant numbers are used to calculate each incremental step. This influences the time used to run the analysis, increasing it

with up to 40 % as compared to running with single precision. The choice of using double precision is made because this reduced the vibrations that occurred in the model. Also, ABAQUS recommends that double precision is used when the total number of time increments is larger than 300.000, or if the nodal displacement per time increment is less than 10^{-6} times the corresponding nodel coordinate value ([7] Sec. 6.1.1). Using double precision will always give a more accurate result than using single precision, at the cost of higher computational cost.

7.3 Development of the material models

For each of the different mesh sizes there was developed a material model using the method of Ehlers and Varsta (Sec. 5.2), and another using the damage criterion provided in ABAQUS that is based on the method discussed in section 5.3. The first material model will be referred to as the *Plasticity material model* (PMM), and the later as the *Damage Evolution material model* (DEMM).

A total of eight FE-models are used to create the material models. Both the PMM and the DEMM were tuned using the dog-bone model presented in 7.2, with four different sized element meshes, using coarser meshes than used in [11]. This gives the following FE-models:

- Four models using the Plasticity Material Model and mesh with elements having side lengths of 2.2 mm, 4.4 mm, 8.8 mm and 17.6 mm.
- Four models using the Damage Evolution Material Model and mesh with elements having side lengths of 2.2 mm, 4.4 mm, 8.8 mm and 17.6 mm.

In order to know that the behavior of the material was physically possible, and can be related to the real world, the force-displacement curve produced in [11] was used as a reference and control. The curve is shown in Fig. 7.3. This result is based on the tensile test done on a 6 mm thick flat-bar dog-bone specimen made out of REAX S275 LASER steel. This specimen showed a behavior of having its ultimate strength after a global elongation of 17.5 mm. At the point of ultimate strength, the true strain in the elements, calculated as equivalent plastic strain, was 0.22.

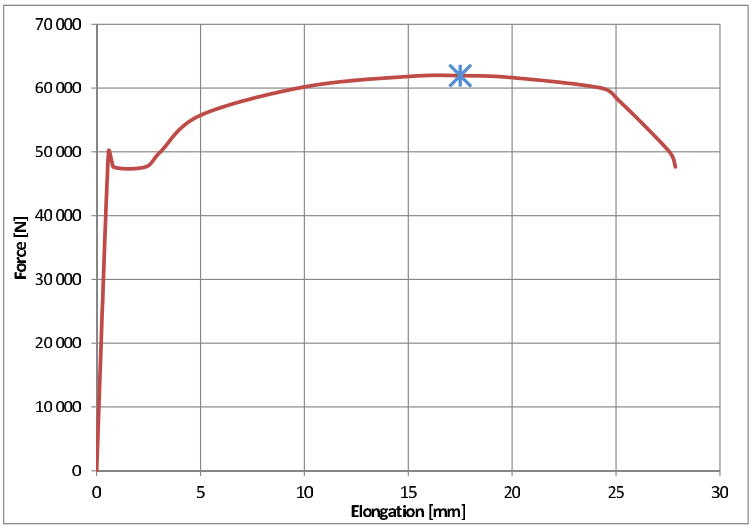

Figure 7.3: *The reference curve used to tune the tensile fracture model, taken from [11]. The cross marks the point of global ultimate strength, and the assumed point of elongation where the structure can support the maximum load.*

The only difference between the FE-models used to develop the material models are the material models used (PMM and DEMM), plastic properties and the use of the damage model provided in ABAQUS. The elastic properties, the density of the material and the plastic properties of inserted true stress/true strain up to the point of 0.22 equivalent plastic strain, are the same for both of them.

7.3.1 Plasticity-model (PMM)

For the Plasticity-Material-Model (PMM) the global response regarding the force-displacement curve is tuned by an iterative procedure, using the plastic properties of the material to tune the true stress/true strain relationship for each of the elements in the model until the FE-model gives the same global response as the reference curve in Fig. 7.3. This is done for each of the four meshes sizes shown in Fig. 7.2.

In order to achieve this global response, the plastic properties for the material had to be tuned in such a way that the behavior of the elements in the model when combined exerted the right stiffness in order to reproduce the global response. Up to the point of ultimate strength, when the true strain in the elements are about

0.22 all over, the plastic properties for each mesh size is equal. After the point of ultimate strength, when the true strain in the elements exceeds 0.22, the models differ depending on the mesh size. To get the right global response, the model was analyzed repeatedly, changing the plastic properties of the material in relation to the recorded output of the previous run. Since the response up to the point of ultimate strength were the same regardless of the element size, this part was tuned using the 2.2 mm meshed FE-model, since this ensured most accuracy, without interference from effects due to using large elements that could act stiffer than they should. The plastic behavior after the point of ultimate strength was tuned using the different meshed models, and point by point dialing in the right values of true stress and true strain in order to get the right global response.

The final fracture, the reduction of applied force from the end point of the reference curve in Fig. 7.2, was simulated using the Damage Initiation criterion and Damage Evolution for ductile materials, provided in ABAQUS, and was the same fracture model as used in the DEMM in section 7.3.2. The input data to the fracture model was obtained by running the model without this fracture criterion. Then the average value of the equivalent plastic strain for the elements that are supposed to be deleted, was measured at the point in time when the final fracture was supposed to happen. Then this strain value was used as the damage initiation criterion, and a linear damage evolution was defined. The fracture model data for the PMM are provided in Table 7.1 in the result section.

7.3.2 Damage Evolution Material Model (DEMM)

The DEMM used the method presented in Section 5.3 in order to model the response after the ultimate strength. How the damage initiation criterion and the following damage evolution works in ABAQUS is explained in Appendix A. This method was used on the same differently meshed models as the PMM.

The behavior up to the point of ultimate strength was also here controlled by the elastic and plastic properties of the material. Therefore, the same data for elasticity and the plastic true stress/true strain relationship up to this point (when the $\bar{\varepsilon}^{pl} = 0.22$) was used as for the PMM. Damage was initiated, using the *damage initiation criterion for ductile fracture* provided in ABABQUS, at an equivalent plastic strain value of 0.22. The point of damage initiation was set to be the same value

of equivalent strain for all of the different mesh sizes. After this point, the plastic properties for the material inputted was set to rise linearly following the same slope as right before damage was initiated, towards an equivalent plastic strain value of 1.1413 at an equivalent stress value of 1100 MPa. This was done because the DEMM needs a true stress/true strain path $\bar{\sigma}$ that the material would have followed if it had not been damaged, since the damage true stress/true strain path σ is defined by applying a damage parameter D so that $\sigma = (1 - D)\bar{\sigma}$. See Appendix A.3 for details about the damage parameter D. The data is inserted to the material model as a tabular relationship of the damage paramter D to the fracture displacement value $\bar{u}^{pl}$.

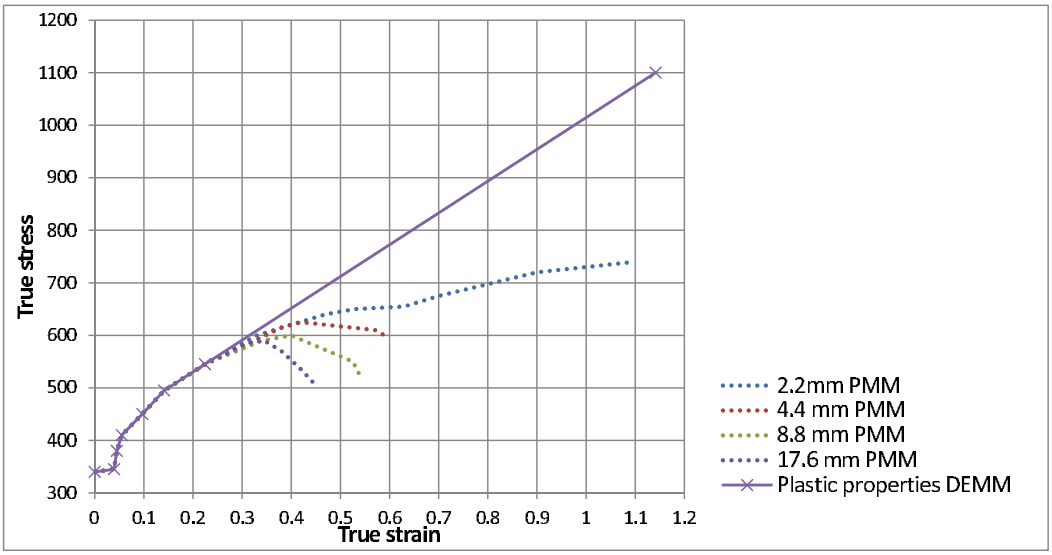

Figure 7.4: *The plastic properties used together with the DEMM. The plastic properties used the PMM for each of the four models in comparison.*

This unphysical material behavior will never be followed by the FE-model, because when the damage initiation criterion is breached by some of the elements i the model, the other are being unloaded because the reduced stiffness of the elements now following the damage evolution set by the fracture model is reducing the load carrying capacity of the model.

After damage was initiated the damage evolution for each of the different meshed models was tuned using an iterative procedure until the force-displacement curve for each of them matched the reference curve. The final tabular data used for the four differently meshed models can be viewed in table 7.3, and the same tabular

data are plotted in Fig. 7.7.

7.4 Results and discussion

7.4.1 The material models

The four different meshed models used together with the two different material models failed at a global elongation of of 27.75mm to 28 mm. In figure 7.5 the initial deformation state and three other states of deformation are shown for the 4.4 mm model.

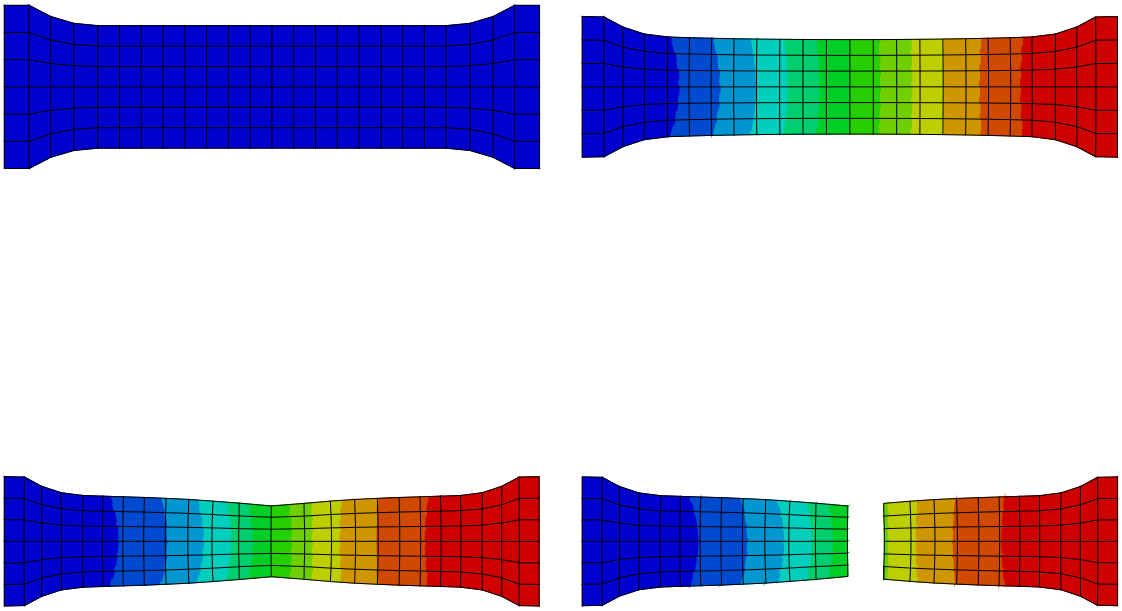

Figure 7.5: *Top left: The initial geometry of the dog-bone model. Top right: The deformation of the model when it has reached its ultimate strength. Bottom left: The deformation state right before the final fracture caused by the elements being deleted. Bottom right: The final deformation, when the element in the middle of the necking zone has been deleted.*

The tuning of the global force-displacement curve for each of the differently meshed models, resulted in the PMM presented in Table 7.1 and the DEMM presented in Table 7.3. The data from these two tables are shown as graphic plots of the true stress/true stress for the PMM in Fig. 7.6 and as the relation of the damage parameter D and the fracture displacement $\bar{u}^{pl}$ for the DEMM in Fig. 7.7. For all of the models, the same material data is used for the elastic behavior and the plastic behavior up to the point of ultimate strength, when the true strain in the elements is 0.22.

Table 7.1: *The inputed stress-strain relationship for the PMM.*

2.2 mm		4.4 mm		8.8 mm		17.6 mm	
Stress	Strain	Stress	Strain	Stress	Strain	Stress	Strain
340	0	340	0	340	0	340	0
345	0.0393	345	0.0393	345	0.0393	345	0.0393
380	0.0450	380	0.0450	380	0.0450	380	0.0450
410	0.0550	410	0.0550	410	0.0550	410	0.0550
450	0.0970	450	0.0970	450	0.0970	450	0.0970
495	0.1413	495	0.1413	495	0.1413	495	0.1413
545	0.2243	545	0.2243	545	0.2243	545	0.2243
600	0.3300	585	0.3143	565	0.2763	585	0.3100
640	0.4700	615	0.3800	590	0.3400	590	0.3450
650	0.5300	625	0.4200	600	0.4000	570	0.3800
655	0.6300	610	0.5700	550	0.5250	535	0.4200
675	0.7000	600	0.5900	515	0.5450	505	0.4500
720	0.9000						
740	1.1000						

Since the PMM origionally does not include any form of fracture criterion, it was chosen to use the fracture model for ductile fracture in ABAQUS to simulate the fracture causing the drop in force seen in Fig. 7.8. This is the same procedure that was used in [11] to make the model fracture, by deleting elements that hava reached a certain value of equivalent plastic strain. The data used to make the differently meshed models fracture are given in Table 7.2. This data contains a damage initiation criterion for each mesh size that defines the equivalent true strain value an element must obtain before being deleted. The value of $\bar{u}_f^{pl}$ was set to be equal for all the different mesh sizes because this defines the global displacement of the model during the time step when the element is deleted. The value of the equivalent strain at the point of damage initiation was collected by first tuning the plasticity-model and then finding the appropriate equivalent strain value for the damage initiation criterion. Then a damage evolution was set by defining a linear

path from the point of damage initiation to fracture. The elongation of the element during the damage evolution can be seen in Table. 7.2.

Table 7.2: *The input for the final fracture in the plasticity-model.*

	2.2 mm	4.4 mm	8.8 mm	17.6 mm
$\bar{\varepsilon}_D^{pl}$	0.85	0.66	0.54	0.445
$\bar{u}_f^{pl}$	0.175	0.175	0.175	0.175

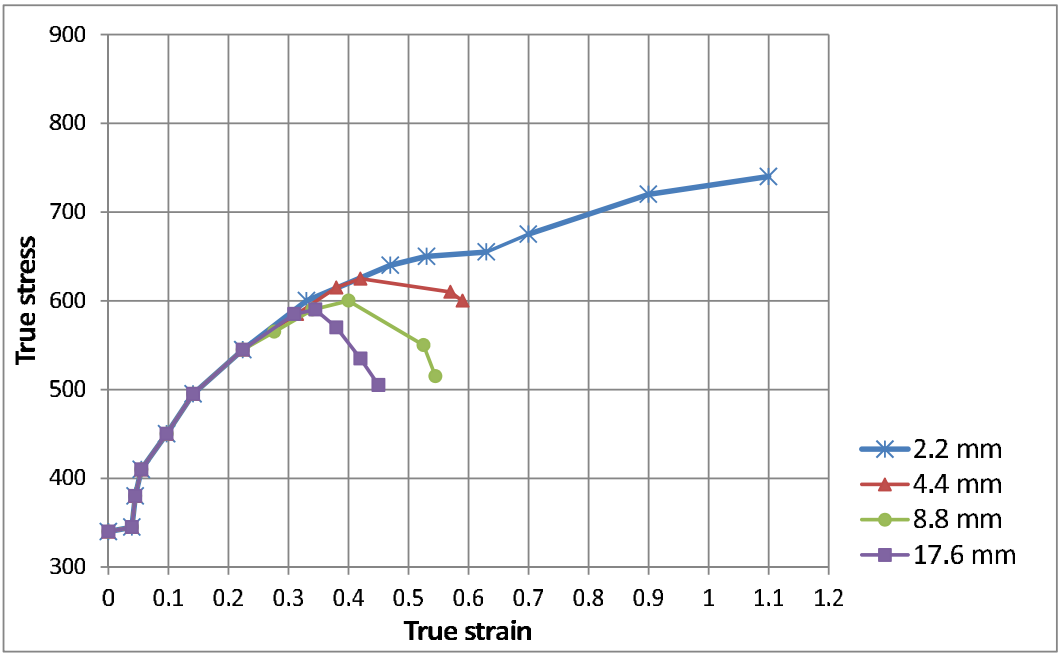

Figure 7.6: *The tabular data from table 7.1 plotted beside each other. Up to the point of ultimate strength, where the global elongation is 17.5 mm and the true strain in each element is 0.22, the plastic properties are the same. At higher strain values, the plastic behavior is dependent on the mesh size of the model.*

For the DEMM the fracture model for ductile material fracture in ABAQUS [7] was used to simulate the behavior of the material from the point of damage initiation at an equivalent plastic strain of 0.22 in the element, and until final fracture. The relationship between the fracture elongation $\bar{u}^{pl}$ and the damage parameter D developed for the four different meshed models are presented in Table. 7.3. This data is visualized in Fig. 7.7.

Table 7.3: *Tabular damage evolution data*

2.2 mm		4.4 mm		8.8 mm		17.6 mm	
D	$\bar{u}^{pl}$	D	$\bar{u}^{pl}$	D	$\bar{u}^{pl}$	D	$\bar{u}^{pl}$
0	0	0	0	0	0	0	0
0.070	0.700	0.059	1.000	0.0575	1.745	0.055	1.950
0.160	1.050	0.170	1.500	0.0850	1.945	0.075	2.350
0.215	1.450	0.250	1.900	0.1500	2.470	0.117	2.600
0.240	1.800	0.310	2.180	0.27	3.000	0.240	3.425
0.250	2.010	1	2.355	1	3.147	1	3.600
1	2.050						

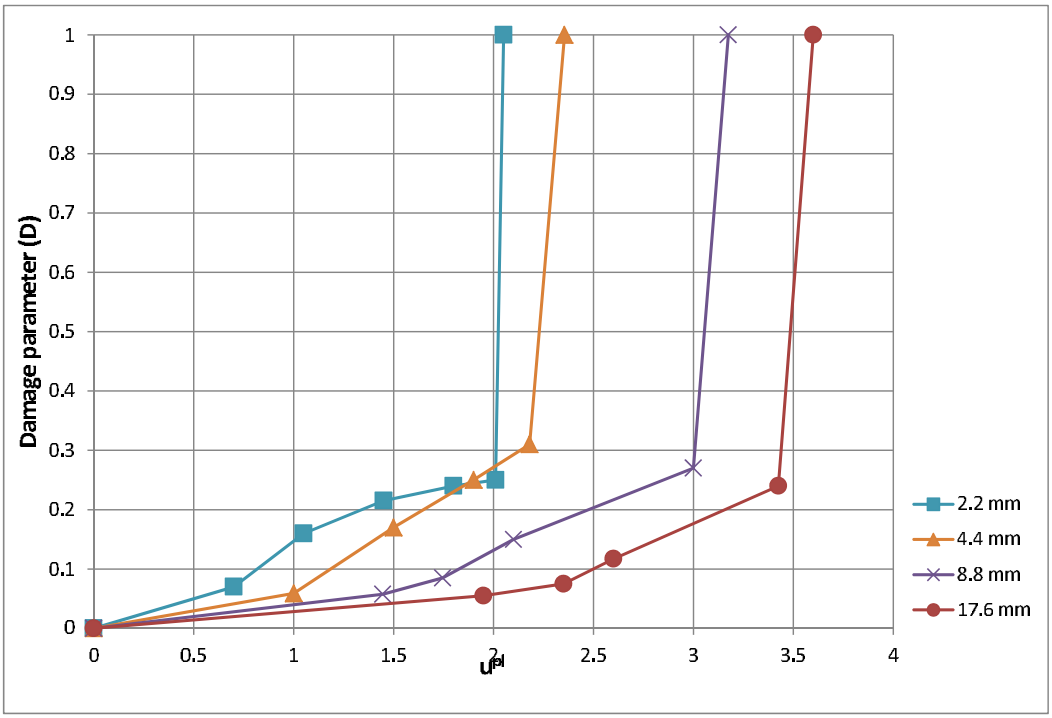

Figure 7.7: *Plot of the tabular damage evolution data*

At the point of ultimate strength, when the true strain in the elements are 0.22, the different meshed FE-models starts to behave different from each other. The models with the largest elements behave more stiffly than the models with smaller elements. For the PMM, the true stress/true strain relationship had to be tuned in accordence with this. The softer behavior of the fine meshed models is caused by the effect of the fine meshed FE-models obtaining a larger true strain in the elements than the coarser meshed models, when exposed to the same absolute elongation, as explained in Section 5.1.

The global force-displacement curve, produced by the FE-models using the material data provided in Table 7.1 and 7.2 for the PMM, and Table 7.3 for the DEMM, is seen i Fig. 7.8 and 7.9.

The 2.2 mm FE-model using the PMM shows a much softer behavior than the other FE-models, and the resulting true stress/true strain relationship is different in shape compared to the coarser meshed FE-models. This is caused by the 2.2 mm meshed FE-model actually being, to some degree, capable of simulating the instability caused by the $\delta\sigma/\delta\varepsilon$ ration becoming larger than the true stress in the elements, as explained in Section 3.1. This derives from the fact that the 2.2 mm FE-model is meshed with enough elements in the width of the model, giving it the capability to locally simulate the reduction in cross-section area responsible for causing the instability, as the strain hardening effect of the material becomes weaker. This is why the 2.2 mm meshed PMM FE-model develops a different true stress/true strain relationship, seen in Fig. 7.6 than the coarser meshed models. Only a small dent in the curve is needed to make the material behave in such a way that the global responce of the model follows the reference curve in Fig. 7.3. If we look back on the results from Ehlers and Varstas experiments in [11], shown in Fig. 5.4, the same effect can be recognized as applied to their simulation. They used much finer meshed models, and did not pass over the threshold where the small number of elements in the transverse direction prevented the FE-model from being able to simulate the reduction of the cross-section area. This meant that they did not have to create a drop in the materials' plastic stiffness in order to manipulate the model into following the global response seen from the tensile test they performed. The three other FE-models used in the experiments in this thesis are on the other hand more coarsely meshed, and this makes them lose the ability to simulate the necking just from the mesh alone. This effect was instead incorporated into the material definition itself, by letting the true stress/true strain curve for the PMM shown in Fig. 7.6 to drop. The larger the elements in the model are, the more stiffly it behaves. So the coarse mesh PMM FE-models must have a softer material behavior after the point of element ultitmate strength,in order to give the same global response regarding the force and deformation.

As for the PMM, the 2.2 mm mesh FE-model with the DEMM show a different behavior than the three other coarser meshed DEMM FE-models. Since this FE-model has the capability to simulate the effect of necking to some degree without altering the material, it already has a softer response than the other three FE-models using the DEMM. The models meshed with 4.4 mm to 17.6 mm element

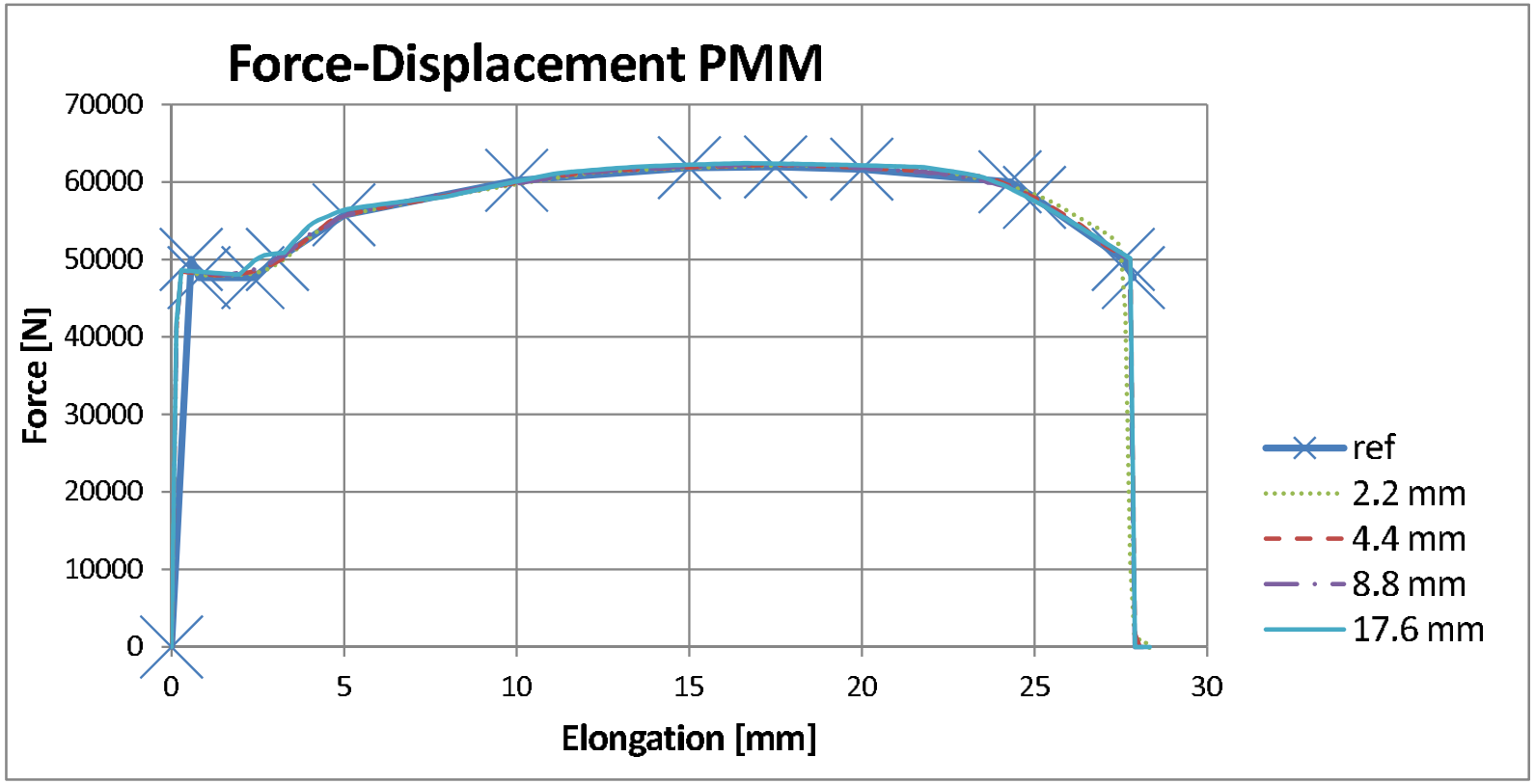

Figure 7.8: *The resulting force-displacement curves for the different mesh sizes when tuned against the force-displacement curve provided in [11]. The curve with the marks defines the reference curve. The point of ultimate strength is at the vertex of the curves, after an elongation of approximately 17.75 mm.*

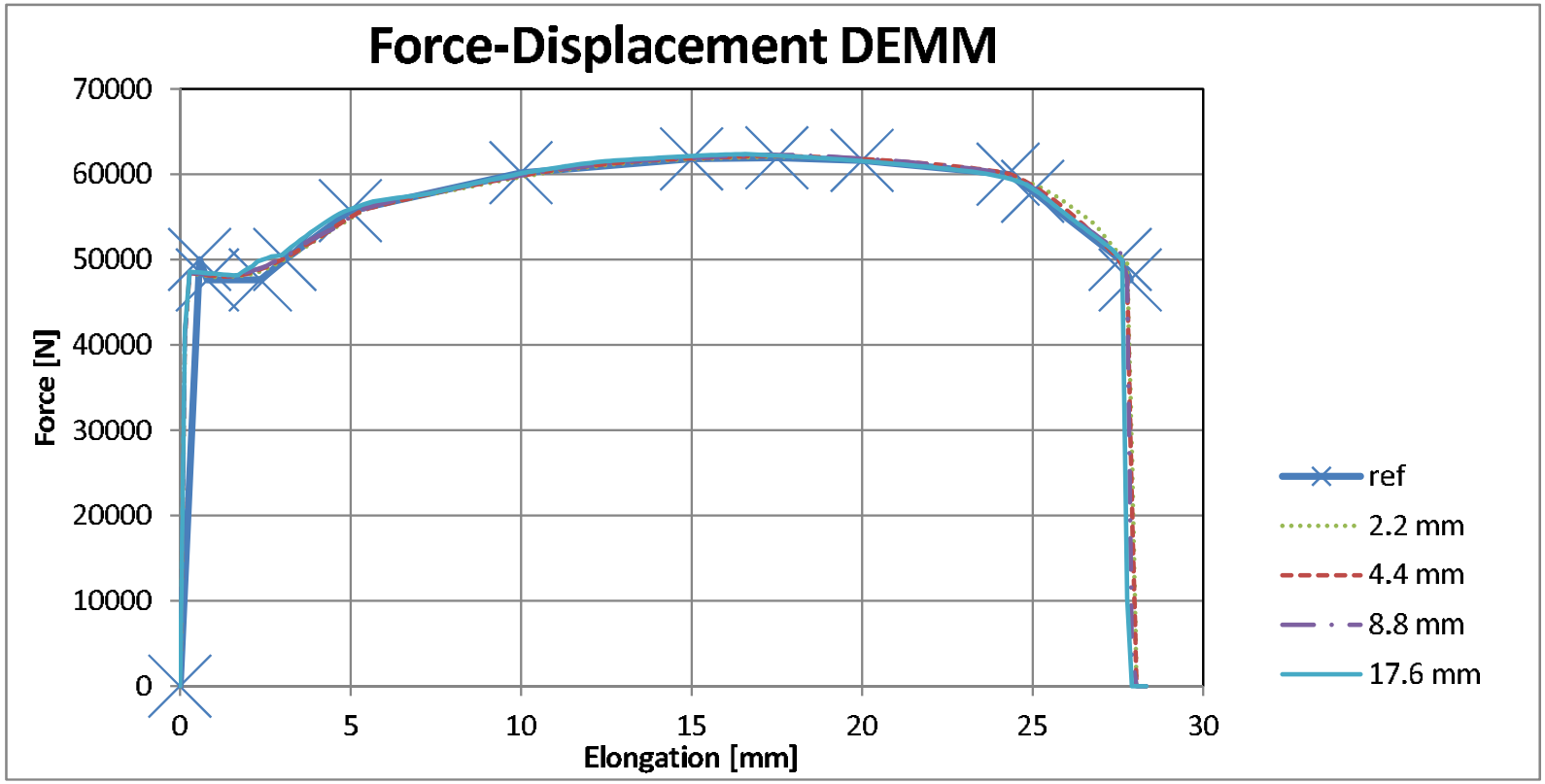

Figure 7.9: *The resulting force-displacement curves for the different mesh sizes when tuned against the force-displacement curve provided in [11]. The curve with the marks defines the reference curve. The point of ultimate strength is at the vertex of the curves, after an elongation of approxemently 17.75 mm.*

size are not capable of displaying the effect of the cross-section area being reduced enough to give necking as the true strain in the elements increase. This effect will come first at a higher strain value, giving it the wrong global response. As for the models using the PMM, the effect of instability is instead simulated by reducing the true stress value in the elements as the true strain increases.

For the DEMM, the reduction in strength in each element is not caused by lowering the true stress to true strain relationship. It is done by reducing the true stress values for a given true strain value in the plastic properties of the material with a factor called the damage parameter D. The inputted true stress/true strain defines a path $\bar{\sigma}$ (see Fig. 7.4) that the elements would follow if not influenced by the damage initiation criterion. If the elements trigger the damage initiation criterion the element will follow a true stress/true strain path where the true stress is defined as $\sigma = (1 - D)\bar{\sigma}$. At the same time, the elastic stiffness of the element is reduced with a factor $(1 - D)$, as the fracture elongation $\bar{u}^{pl}$ increases from 0 to $\bar{u}^{pl}_{f}$.

7.4.2 Comparing energy components

The two material models (PMM and DEMM) for the four different mesh sizes show good agreement between the global response of the FE-model and the global response of the tensile test performed in [11].

Since the FE-models are tuned to give the same amount of displacement for a given force using different mesh sizes and material input, the energies quantities in the material should be the same for all the different cases, they were monitored to make sure that no strange effects occur that may influence the result. The ABAQUS User's Manual recommends monitoring the energy quantities in the whole model to look for unexpected changes in the energy components of the model. A discussion of the different energy quantities follows.

The first check is that the internal energy should be matched by the external work applied to the model. In this analysis the external work is given as the force applied to the model multiplied by the elongation of the model in the direction of the force. Since the analysis is done using a constant speed giving a constantly growing elongation the external work is set to increase following a path defined by the elongation and the force needed to apply the deformation. Fig. 7.10 shows

the external work, comparing the PMM against the DEMM for the four different meshed models.

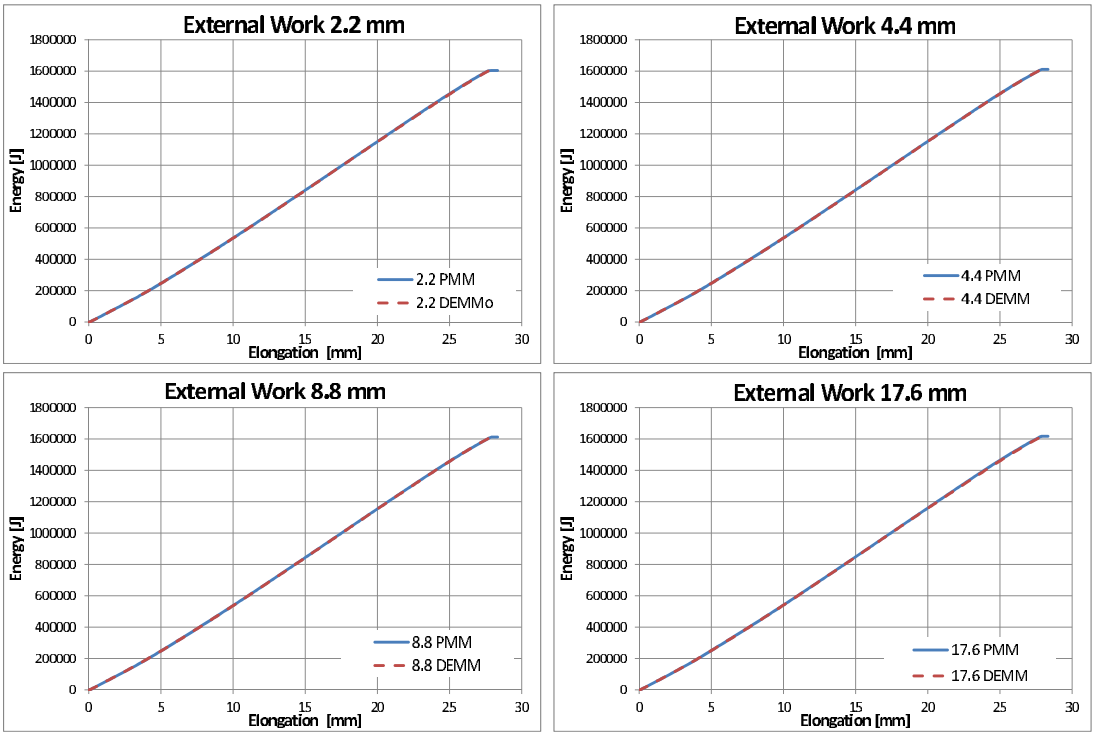

Figure 7.10: *The external work performed on the models.*

The internal energy should be the same as the external work, because there is no additional energy applied than the force giving the elongation, and there should not be any energy lost. Fig. 7.11 shows the internal energy, comparing the PMM against the DEMM for the four differently meshed models. The external work and the internal energy are in good agreement with each other, but the energy calculated by ABAQUS is not exactly equal, showing a difference of 0.1 % between the extrenal work and the interna energy. The energy missing in the internal energy is caused by the dissipation of energy to viscous damping and kinetic energy, caused by using a dynamic solver to solve the problem. Also, some energy is unaccounted for, and this amount of energy is added to the energy balance as a residual amount. Adding the energy lost to viscose dampening and the kinetic energy, and subtracting the residual energy from the given internal energy, produces the same result as the external work calculated by ABAQUS. This means that all of the energy added to the system is accounted for.

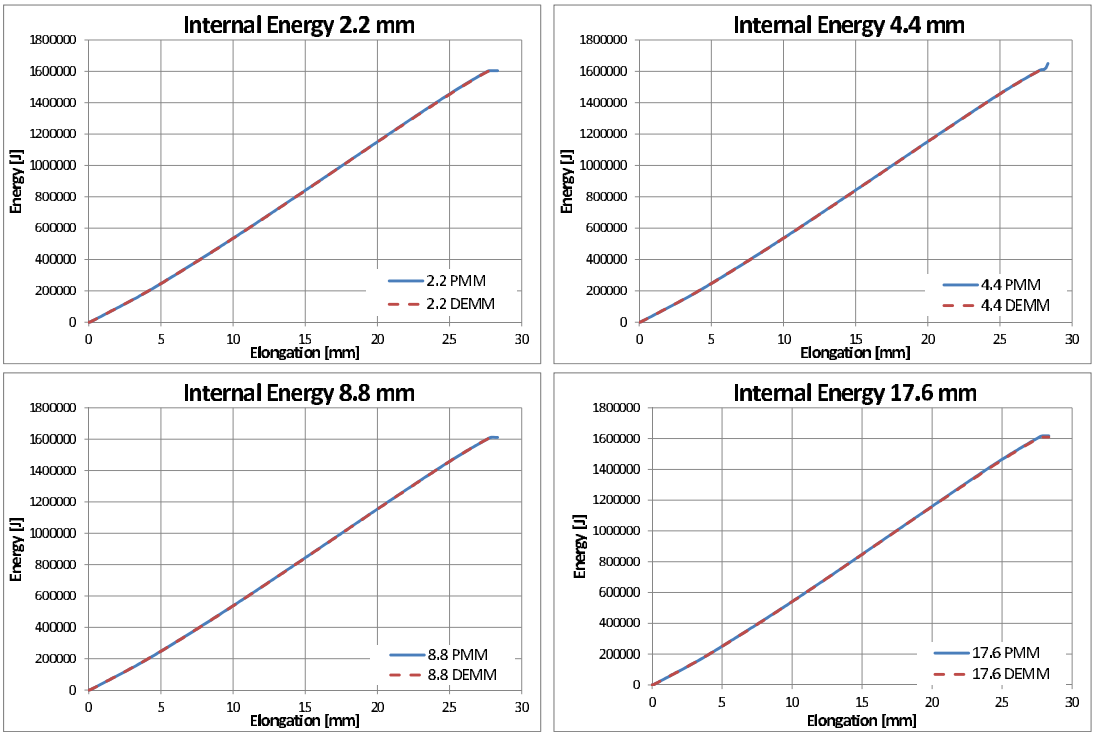

Figure 7.11: *The internal energy in the models.*

The difference between the two material models used, should be seen in the energy components, if there are any differences. From Fig. 7.11 we can see that the internal energy is the same for the two material models on each of the four meshed FE-models. The amount of internal energy is calculated as

$$E_{Int} = E_{SE} + E_{PD} + E_{AE} + E_{DM} \tag{7.1}$$

where E_{SE} is the recoverable strain energy, E_{PD} is the plastic displacement energy, E_{AE} is the artificial strain energy and E_{DM} is the energy dissipated through the use of damage models incorporated in the software. Artificial strain is the strain introduced to remove singular modes such as hourglass control in the elements [7].

Of the four components making up the internal energy the plastic displacement energy, seen in Fig. 7.12, is by fare the biggest one in the eight models used in this experiment. For the fine meshed 2.2 mm FE-model E_{PD} is responsible for 99.6 % of

the internal energy, and for the coarser meshed models with 17.6 mm elements it is 99.1 %. The rest is elastic strain energy seen in Fig. 7.14 that is for the most part recovered when the fracture occurs, except for the energy going into the fracture of the material.

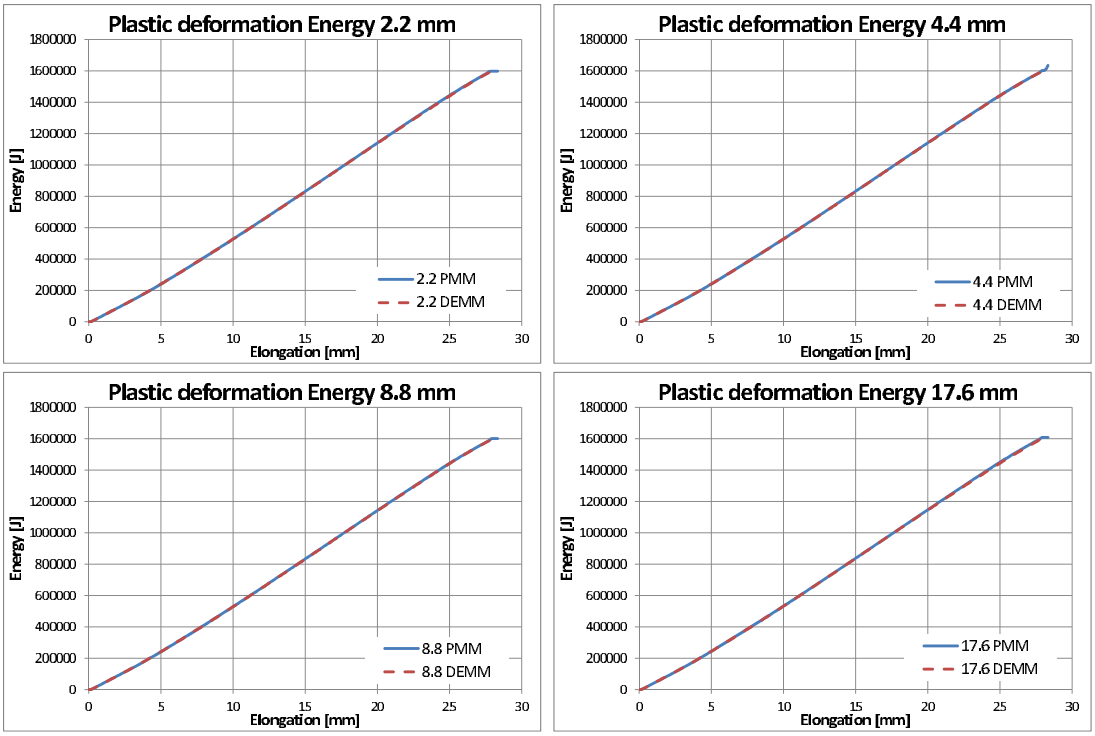

Figure 7.12: *The plastic deformation energy in the models.*

In Fig. 7.14 it can be seen that there are different elastic strain energy values for the two different material models. The DEMM displays a higher amount of elastic energy from the point of ultimate strength and until final fracture. This is caused by the damaging of the elements that has triggered the Damage Initiation Criterion for the material model, and has started to accumulate damage. The damage is quantified in the damage parameter D. As D increases from zero at the point of no damage to 1 when the elements stiffness is completely removed, the elements become softer because the elastic stiffness is reduced as shown in Eq. 7.2

$$\sigma = (1 - D)\bar{\sigma} \tag{7.2}$$

where σ is the true stress in the element, and $\bar{\sigma}$ is the true stress in the element if damage had not been present. The higher value of elastic strain derives from there being less elements in the DEMM accumulating damage, than there are elements in the PMM model that are stretched into high values of plastic strain, since their the stiffness is not reduces. The softer elements of th DEMM obtain a higher elastic strain value than the stiffer undamaged elements in the PMM. In Fig. 7.13 the elastic strain energy density for the PMM and the DEMM model is shown.

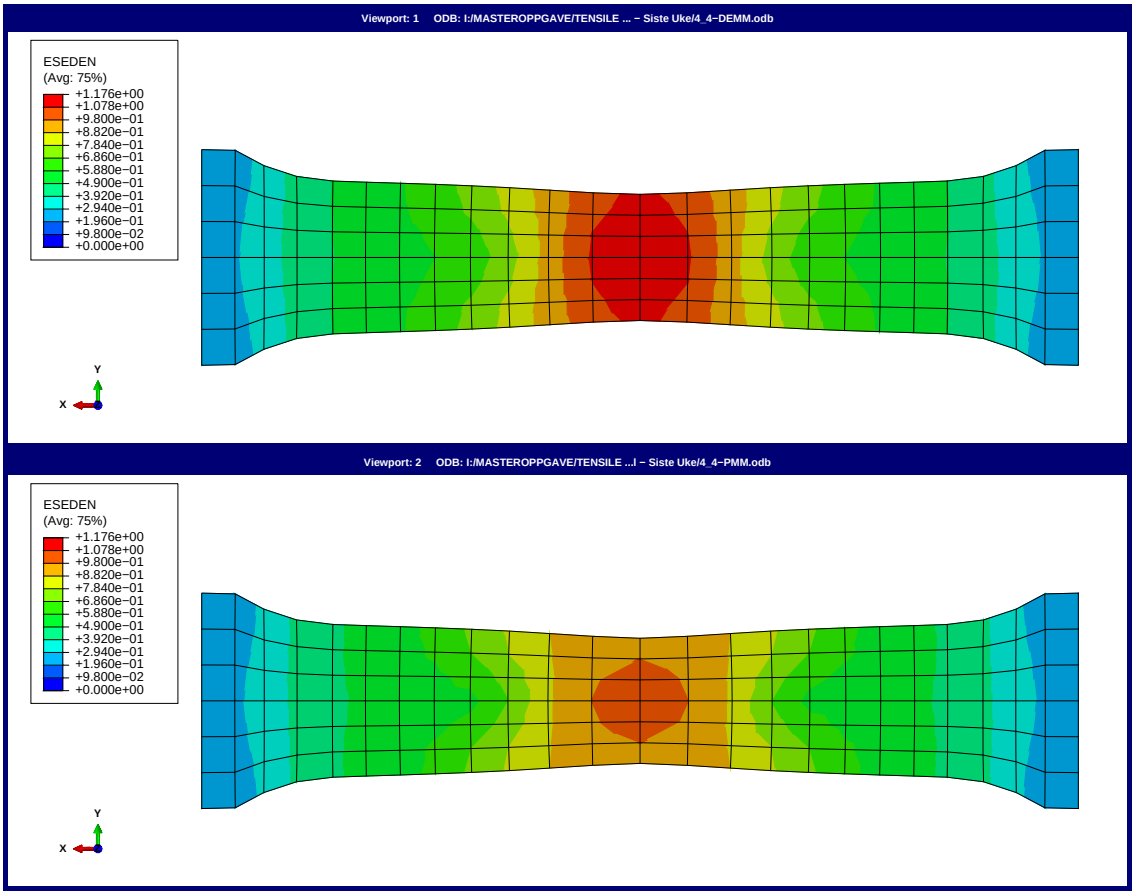

Figure 7.13: *The elastic strain energy density for the DEMM (top) and the PMM (bottom) at the same instance of time.*

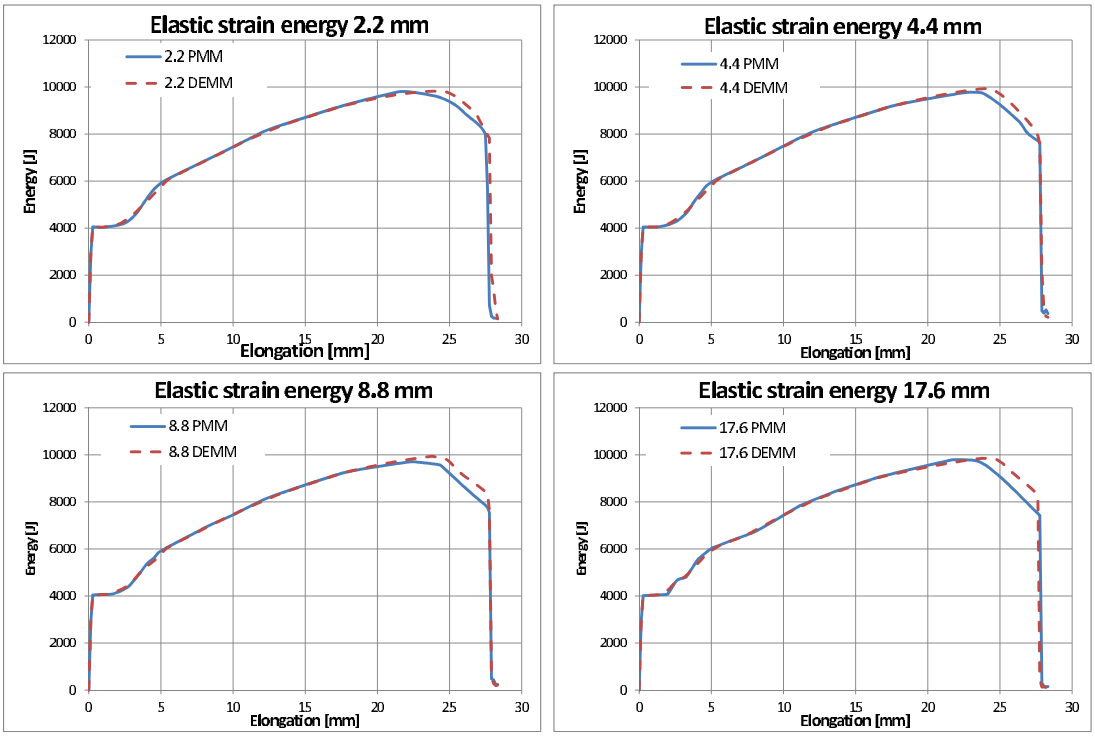

Figure 7.14: *The recoverable strain (elastic strain) energy in the models.*

The energy dissipated to damage, seen in Fig. 7.15 is the energy component that differs the most from the PMM and the DEMM. This is because the only energy dissipated by the damage models embedded into ABAQUS is recorded by this output. Since the DEMM uses a damage model in ABAQUS for the whole modeling of the reduced stiffness and final fracture, the energy dissipated by damage is higher than for the PMM, that only uses the damage model in ABAQUS to create the final fracture.

This makes a difference in the material after fracture. The FE-model using the PMM will consist of a stronger material near the fracture zone than the FE-model using the DEMM. This is because the DEMM model reduces the stiffness of the elements near the fracture as they are damaged from the simulated instability, causing them to accumulate damage quantified as the parameter D. The result of this difference will be discussed later on in this chapter.

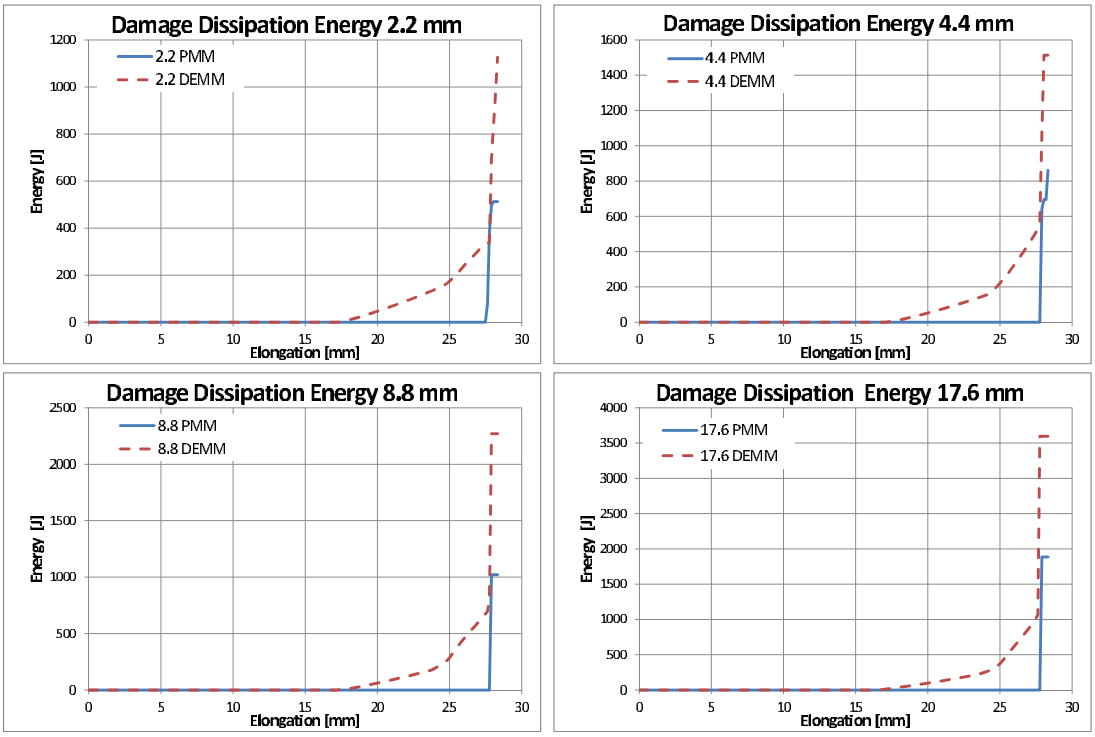

Figure 7.15: *The damage dissipation energy measured in the models.*

Some energy is dissipated through dampening in the system, but only a very small amount. At the point of fracture, the energy dissipated to dampening effects increases drastically, as the dynamic effect caused by the sudden removal of load occurs. The kinetic energy increases and the dampening energy follows. Also, the energy balance containing the energy that is not accounted for by ABAQUS is increased. This suggests that the solution may become unstable right after fracture has occurred, because high speed stress waves moves through the structure, lowering the critical time increment size Δt_{cr} to make the time increment Δt used by the FE-solver to large. These high speed stress waves are caused by the sudden removal of load, and will be dampened out through time as long as the system is stable and has a state of dynamic equilibrium.

During the analysis the kinetic energy in the models is more or less equal to zero. Since the analysis simulates the tensile test over such a long time, the method can be looked as as quasi-static. No dynamic effects are present during the elongation from initial length to fracture, as seen in Fig. 7.16. As the fracture occurs, energy is released from the recoverable strain built up in the model. This is released and some of it is take up as kinetic energy. The amount of energy is small, around 500 J

(while the total internal energy is 1.6 MJ), expect for the 4.4 mm model using PMM. Here the kinetic energy peaks at just short of 5000 J. This is probably caused by the form of the true stress/true strain inputted in the material data. The 17.6 mm and 8.8 mm PMM has a steeper drop in stiffness as the strain in the material closes in on the point of final failure. The 4.4 mm PMM has a more gently slop when reducing the stiffness as it nears the final failure, giving it little higher stress value in the material when i finally fractures. The higher stress value being removed introduces higher post-failure dynamics effects as kinetic energy and dampening in the system.

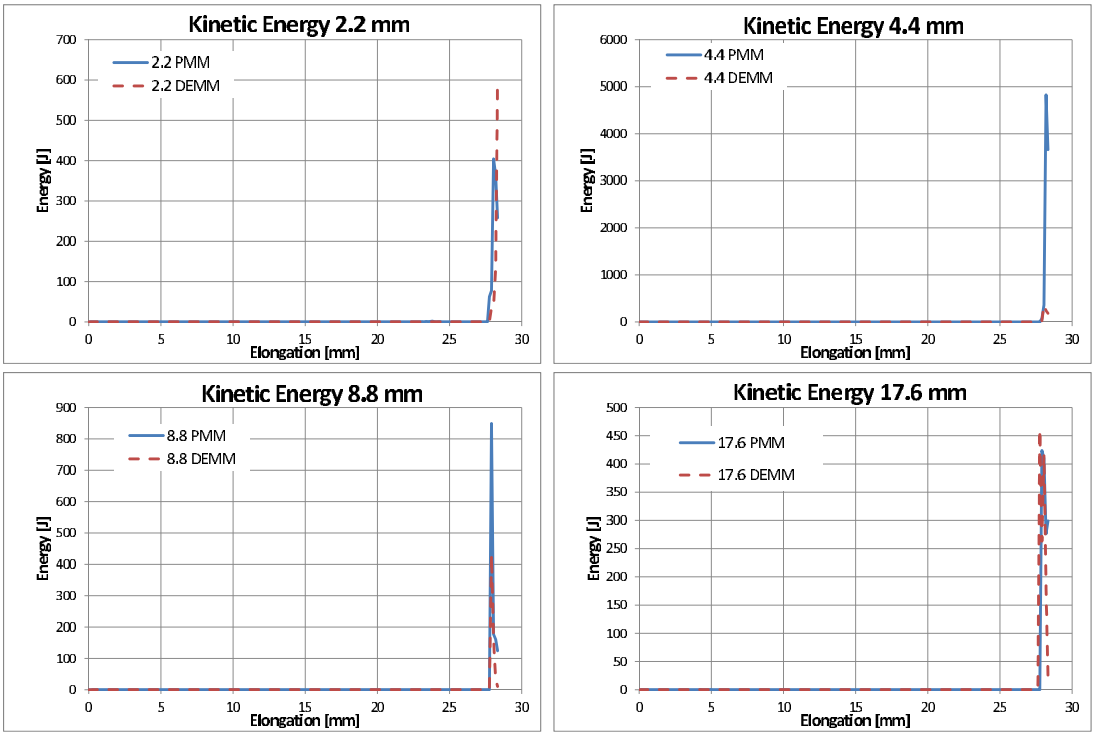

Figure 7.16: *The kinetic energy measured in the models*

From the discussion of the energy components there are only small difference between the two material models when used on the same mesh size. The material is tuned to give the same response regarding force and displacement, so a difference in the total energy would have been surprising, and does not happen. The only noticeable difference is the damage dissipation energy, and the elastic strain energy. These behave differently from the point of ultimate strength to final fracture. The PMM model has a lower value of recoverable strain than the DEMM. This derives from the reduction of strength in the elements exposed to damage in the DEMM

achieving a higher elastic strain value than the same elements in the model using the PMM model. The damage dissipation energy is different since the DEMM utilizes the damage model embedded in ABAQUS, and this energy is recorded into the damage energy output. The damage energy in the PMM is not recorded, but the energy dissipated by the fracturing is the same since the external work applied to the models is the same, regardless of the mesh.

7.4.3 Fracture displacement and reduced strength

According to the theory [17, 16] there should only be one band of elements going across the model starting to fail and getting damage by the damage evolution when the material reaches its ultimate strength. All the other elements should have elastically recovered without being individually influenced by the failure model. Since no other requirements than the minimum equivalent plastic strain were specified, all the elements in the instability zone reached a plastic strain of 0.22 and triggered the Damage Initiation criterion. This made it hard to calculate the fracture displacement $\bar{u}_f^{pl}$ for the material, according to the theory by Hillerborg et. al.

The value of $\bar{u}^{pl}$ and D should in theory be possible to calculate in forehand, instead of tuning them to the right value. The formula $\bar{u}_i^{pl} = (\bar{\varepsilon}_i^{pl} - \bar{\varepsilon}_D^{pl}) * l_c$, where i is the row number for the inputted data, was used to calculate the value to input as $\bar{u}^{pl}$. This did not give the right value for the failure displacement and the global elongation became too large. While the theory presented in Section 5.3 makes it seem fairly simple to calculate the amount of fracture displacement $\bar{u}^{pl}$ to apply to the element, the situation becomes more complicated when the method is used in ABAQUS. Since the instable zone (the necking zone) of the tensile specimen contains more than one element in the direction of elongation, the global elongation of the model is dependent on the fracture displacement of more than one element. All the elements inside the necking zone have an equivalent strain value above 0.22, will contribute to the global elongation with their fracture elongation $\bar{u}_i^{pl}$ This can be seen in Fig. 7.17, where the equivalent plastic strain is plotted at a time increment right before the final fracturing of the model. As a result of this, the total fracture displacement of the model becomes higher than the requested value.

A big difference between the two material models method used in these tensile tests, is the lack of capability for the PMM to accumulate damage in the material.

When using the DEMM, there is accumulated damage in the elements that has triggered the damage initiation criterion and therefore follows the fracture model of Hillersborg et. al. The damage to each element is quantified by the damage parameter D, and the load bearing capacity of the element is reduced by a factor $(1 - D)$. If the element according to the inputted true stress/true strain relationship for the plastic area should be able to carry a load $\bar{\sigma}$ when its equivalent plastic strain is ε, the damage element can only carry $\sigma = (1 - D)\bar{\sigma}$. Also, the elastic stiffness of the element is reduced by the same factor $(1 - D)$. This reduction of element stiffness is permanent, and can not be reversed. The PMM, as presented by Ehlers and Varsta in [11], does not include any damage parameter. In their model, the reduced stiffness is a result of the reduced value of true stress as the plastic strain increases (see Fig. 7.4), but this effect can be reversed by reversing the loading on the material, since there is no damage applied to the material of the elements when they pass their ultimate loading. In the tensile experiments, the damage inflicted to elements that were not deleted was up to 16 % reduction of elastic stiffness, in the DEMM. For the PMM no elements, except for the one that got deleted, were inflicted by any damage, and the elastic stiffness of the remaining material was preserved.

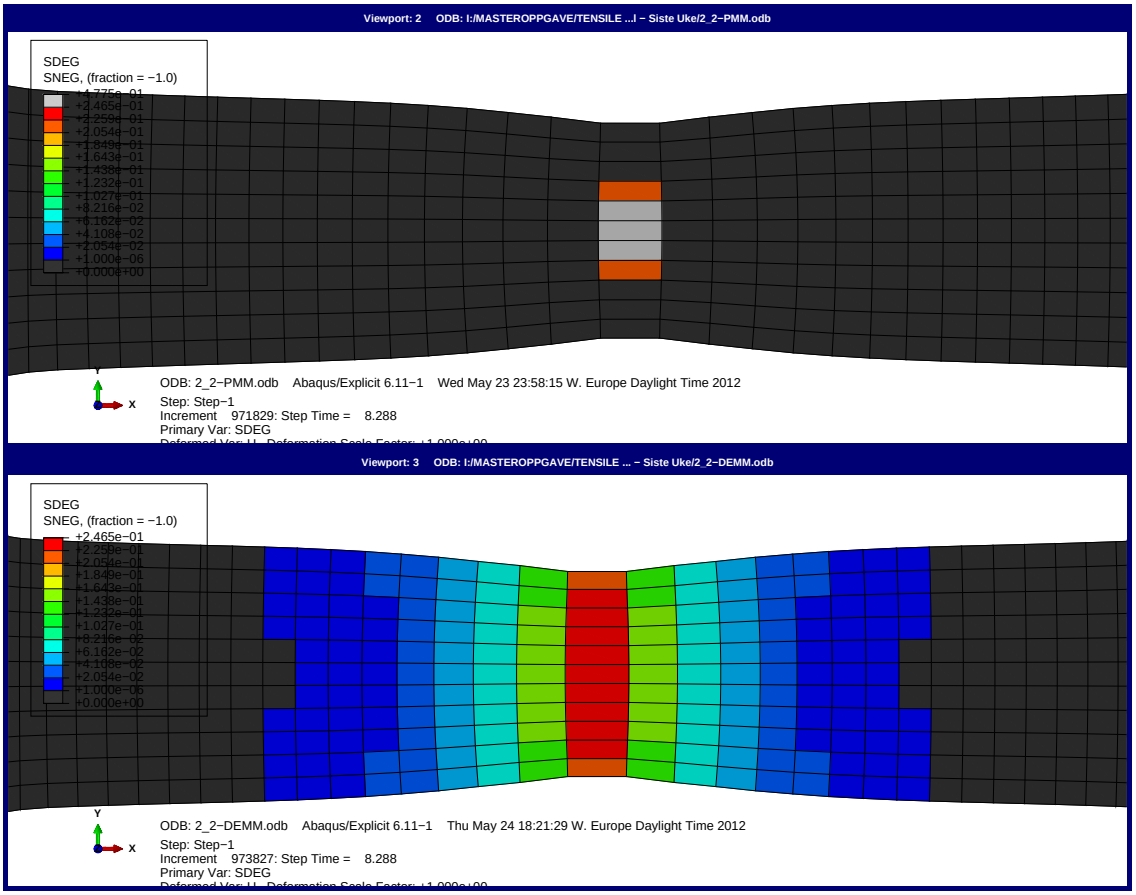

Figure 7.17: *Top: Only the elements that are being deleted are inflicted by damage in the PMM. Bottom: All the elements that have got an equivalent plastic strain above 0.22 are inflicted by damage. The damage accumulated in the elements that are not deleted are for the most part small, but the elements near the fracture zone have gotten their elastic stiffness reduced by about 16 %.*

The effect of this difference does not appear as long as the material is loaded in such a way that the strain is only increasing, and the material is not at any point unloaded. The difference will, on the other hand, be visible if the straining of the material is reversed, or the load removed, after the material has been strained beyond the point of ultimate strength. The Damage Evolution model will at this point have reduced the stiffness of some of the elements in the model, and the elastic recovery of these elements will change to a more soft behavior. Also, if the model is reloaded, the response to this new load will be different from that of the first time it was loaded, because of the reduced stiffness in some of the elements. The PMM does not accumulate any damage, and elastic recovery will follow the same elastic properties regardless of how much prestraining it has experienced

and the number of loading-unloading cycles it has gone through.

To prove this, a simple experiment was done to quantify the difference of having the element stiffness reduced or not.

The tensile test model used earlier in this chapter was modified so the elongation of the model was done in two stages, with a pause in between where the load was removed from the model, before it was applied once more. The first stage was similar to the test performed earlier, except that the elongation was stopped before the models reaches failure, but after the point of ultimate strength. Then the load was removed for a time period of one second, allowing the material to elastically recover, before the elongation continued until fracture occured. This was done using both the plasticity-model and the Damage Evolution model using the 2.2 mm mesh size model.

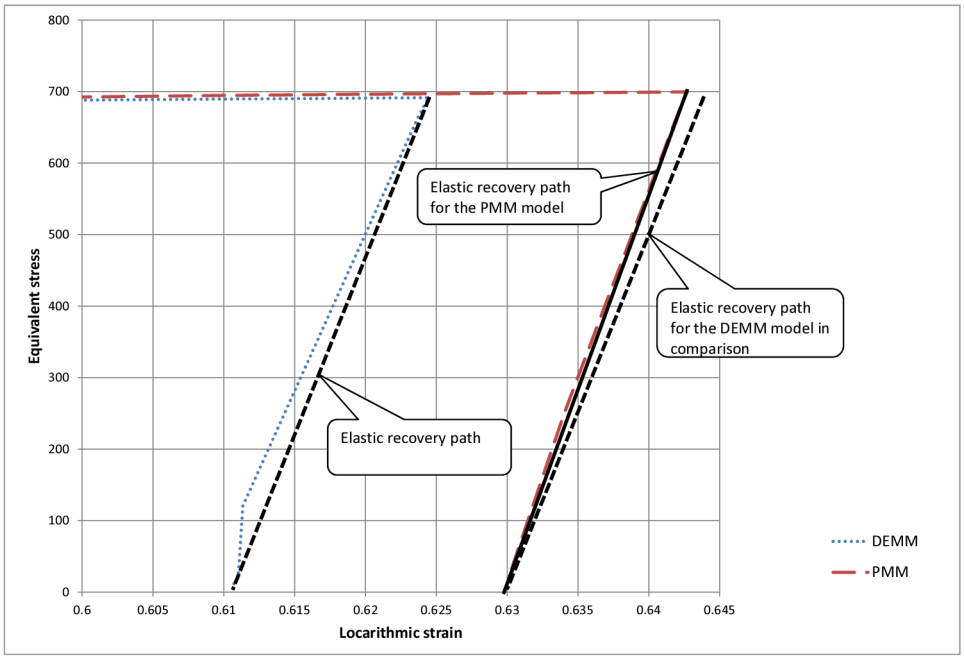

Figure 7.18: *The difference between the elements elastic recovery path in the plot of true stress and logarithmic strain in the element. The DEMM model (dashed line) has a recovery path with a lower slope than the PMM model (solid line), as they are being unloaded from a stress state of 700 MPa.*

By looking at the same element, located in the center of the necking zone, we can see in Fig. 7.18 that the element recover elastically differently in the two models. The element using the DEMM recover elastically using a lower elastic stiffness than the element using the PMM. The Young's-modulus that the elements use to recover elastically can be calculated as

$$E = \frac{\delta\sigma}{\delta\varepsilon} \tag{7.3}$$

where $\delta\sigma$ is the reduction in equivalent stress in the element when it is unloaded, and $\delta\varepsilon$ is the corresponding reduction in logarithmic strain.

This gives $E = 49700$MPa for the element using the DEMM, and $E = 57453$MPa for the element using the PMM. The initial Young's-modulus was 57500 MPa[2]. At the same time the damage parameter for the element using the DEMM was measured to be 0.1324. Since the element stiffness is reduced by the factor $(1 - D)$ this gives us a reduced elastic stiffness of

$$57500\text{MPa}(1 - 0.1324) = 49887\text{MPa} \tag{7.4}$$

for the DEMM, matching the elastic strain recovery stiffness measured in the plot in Fig. 7.18

7.4.4 Final comments to the results

The goal of this experiment was to understand and use the two different material models, the Plasticity-Material-Model (PMM) and the Damage Evolution-Material-Model (DEMM), to developed material models use in a fracture experiment on a plate. The material models develop to for the four different meshed FE-models will in the next chapter be used in a penetration experiment to get more data on the differences between the two approaches, in order to be able to simu-

[2]The Young's-modulus for this experiment was set to a lower value than normal because it would be easier to measure the difference in the slope of the unloading path with the material acting more softly than normal.

late the local instability that occurs during a ductile fracture, using as large finite elements as possible.

Chapter 8

Plate penetration experiment in ABAQUS

8.1 Introduction

In this chapter the analysis of a circular plate being penetrated by a cone-shaped puncher is presented. The aim of this experiment is to search for significant differences between using the two material models presented in the prior chapter on different meshed models using relatively large elements in order to save computation time. The material data to be used is the material models created for the different meshed FE-models in the tensile test experiment presented in chapter 7. The fracture of the steel plate is assumed to be governed by the ductile tensile fracture behavior of the steel material, as this is the type of fracture the material models are tuned for. Other types of fracture, if they should occur in such an experiment, are neglected.

This experiment is based on the experiment carried out by Sören Ehlers [10], but like in the tensile test experiment, the mesh size used here has larger elements. This is done, as explained earlier, because it is desirable to use as large elements as possible when modeling huge structures that are supposed to obtain damage in e.g. collision events. This is desirable because the analysis is solved using an explicit time integration solver, and the computation time is directly linked to the size of the smallest elements in the model.

This experiment will also make use of a contact definition that is used to model the interaction between different instants that are not connected to each other initially. It is recommended that the explicit time integration solver is to be used when the contact between different parts of the FE-model is expected to become complicated [7], as in a collision event. In this experiment, this is not expected to occur, but the explicit solver is used to create a quasi-static analysis of the impact scenario.

8.2 The model

The model used in the penetration simulation is based on the test specimen used by Sören Ehlers in [10]. The geometry given in the article is seen in Fig. 8.1.

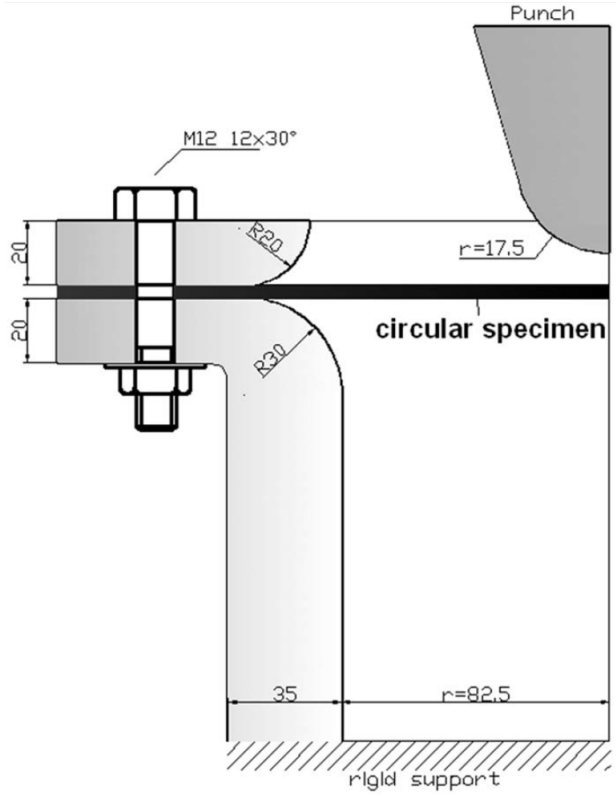

Figure 8.1: *The geometry of the plate penetration setup. [10]*

From this, the circular plate and the puncher were modeled. The rigid support structure was not included in the FE-model. The plate was modeled as a whole,

including the part being clamped by the test rig, but not the holes used to bolt the plate to the test rig model. The plate's dimensions can be seen in Fig. 8.2. The total radius is 170 mm, while the radius of the part of the plate inside the clamped rim is 112.5 mm. The squared region in the middle of the plate measures 114.55 by 114.55 mm, and is enclosed by a circle with a radius of 81 mm. The thickness of the plate is the same as in [10], 4.12 mm. The mesh of the model was supposed to be equal to the mesh of the tensile test models, in order to use the material models developed there. To get a quadratic mesh in the center of the plate where the contact between the puncher and the plate would be, a squared partition was made in order to give a quadratic mesh in the center. The squared middle section lies so that the corners are on the circle surrounding it. The circle segment in between is meshed in a way that gives it a mesh of S4R elements with the least possible distortion of the elements. For the 8.8 mm, 4.4 mm and 2.2 mm sized meshed element models, these segments had to be divided into two equal parts in order to keep the mesh symmetrical. The outer rim of the plate was meshed with the same element type, using a radial mesh control. According to Ehlers [10] this way of meshing the plate model secures the right dimensions of the element mainly responsible for simulating the deformation of the plate and the elements simulating the rim being clamped to the test rig.

Boundary conditions defining the clamped rim were applied to the outer section of the plate seen in Fig. 8.2, constraining all degrees of freedom in this part of the model. The boundary conditions were applied to the geometry of the plate, and not the mesh, as this made it possible to change the mesh of the model without having to redefine the boundary conditions.

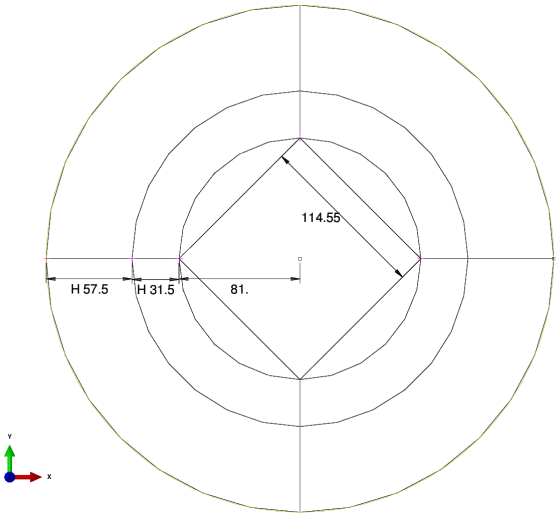

Figure 8.2: *The geometry of the circular plate used in the FE-model.*

The puncher was made as a discrete rigid surface. This means that the surface will not be able to deform, and will keep its initial shape throughout the analysis. The discrete rigid surface is defined by a mesh of undeformable elements. Having elements containing nodes is beneficial when the contact between the surfaces of the two parts are to be defined. This saves computation time when running the analysis. Alternatively, an analytical rigid surface could have been used. This is a rigid surface that is defined by the geometry, and not a mesh of rigid elements as the discrete rigid surface. This will make the computer analysis run more slowly, since the geometrically defined surface is more complicated to analyze than the meshed surface of the discrete rigid body. A test performed on the 4.4 mm meshed plate, using the DEMM, did not show any significant differences in the results of the plate being penetrated.

The dimensions of the puncher were only given in [10] by the radius of the rounded end. The figure clearly showed an angle side surface, but the details were not specified. The angle of this sloping surface and a horizontal plane was assumed to be $74°$, from measurements taken from Fig. 8.1. The spherical tip has a height of 12.7 mm, and a radius of 17.5 mm. The total height of the puncher was set to 49 mm. This ensured that the puncher did not pass all the way through the plate. In order to ensure that the puncher moved through the plate perpendicular to the plate's initial surface, the reference point of the puncher was restrained against all movements and rotations except for the translation in the global y-direction, perpendicular to the plane of the plate. A constant speed of -3.33333 mm/sec was

applied to the punchers reference point.

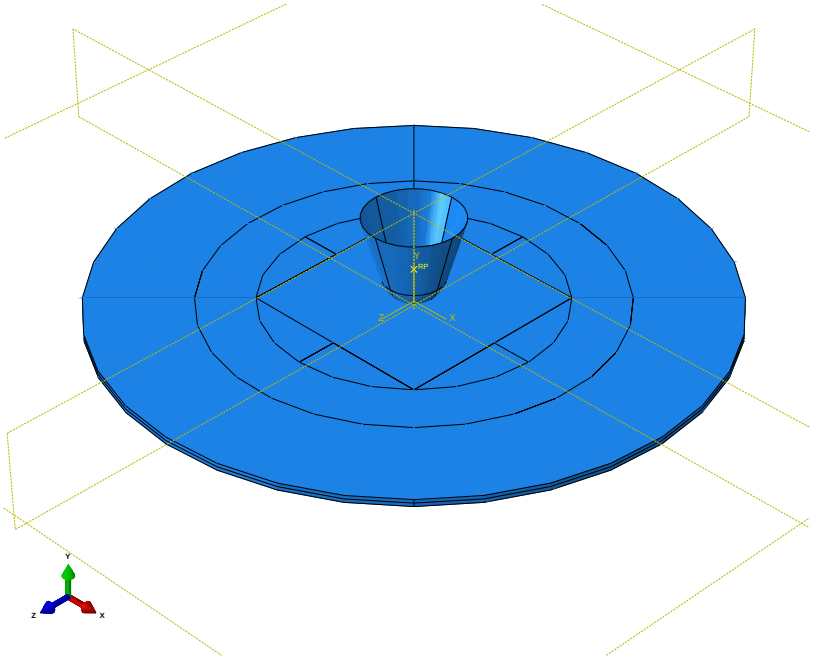

Figure 8.3: *The assembly of the two instants in the model.*

The two parts, the plate and the puncher, were assembled as seen in Fig. 8.3. The two parts were positioned so that the reference surface of the shell elements in the plate lies in the xz-plane where $y = 0$. Origo of the coordinate system is in the middle of the plate. The puncher was set to move in the negative direction of the y-axis. The initial distance between the puncher's surface and the top surface of the plate ($t/2$ from the reference plane of the shell element) was 0.01 mm. This ensured that there was no initial overlap of the two instances, but at the same time ensured that the contact would happen as early as possible during the analysis. An initial contact or overlap between surfaces that are defined as a contact pair is not favorable, and should be avoided if possible. The contact definition algorithm embedded in ABAQUS would usually solve this problem before the first increment is calculated, but it may cause some odd effects.

The contact between the outer surface of the puncher and the upper surface of the plate is defined using the General Contact model for the Explicit module in ABAQUS ([7] sec. 34.4.1) This is the most general and easiest to use contact definition that includes surface-to-surface- and edge-to-edge contact. The default setting is to include every surface and edge defined in the model, but for this model, the

Table 8.1: *Contact pairs used in the plate penetration experiment.*

Surface 1	Surface 2	Contact type
Plate - Upper surface	Plate - Upper surface	Self-contact
Plate - Upper surface	Puncher - Outer surface	Surface-to-surface
Pucher - Outer surface	Puncher - Outer surface	Self-contact

surfaces were picked manually, as they are clearly defined. This saves time when running the analysis because elements and nodes that are sure not to participate in the contact can be left out from the calculations. The surfaces included in the contact definition are defined as surfaces in the FE-model. Both surface-to-surface and self-contact were defined for the surface of the puncher and the top surface of the plate-elements.

In short terms, the contact between the surfaces is modeled by monitoring the nodes of both surfaces, and calculating if they are in contact or not. If a node on one surface is found to be penetrating the surface of the other object, a force just large enough to push the node back to the surface of the penetrated object is applied. This small force and displacement creates a small amount of work that is recorded as penalty contact work.

As for the tensile test experiment, double numerical precision was chosen, in order to reduce the vibrations that by experience can occur during such an analysis. Also, the number of increments used to calculate some of the finer meshed plates exceeds 300 000, and the software documentations recommend to use double precision when this happens.

8.3 Analysis

The analysis was done using the PMM and the DEMM on four different meshed plates. The objective was to use the same element size in the center region of the plate, as the mesh in the tensile test experiment in Chapter 7. Therefore, a quadratic shaped area was created in the contact zone that was meshed using (geometrically) quadratically shaped elements. The element sizes chosen were 2.2 mm, 4.4 mm, 8.8 mm and 17.6 mm, the same as in the tensile test in Chapter 7, matching the material input used. The different meshed models are seen in Fig. 8.4.

The analysis was performed using the dynamic explicit time integration solver, for the same reasons as in the tensile test, and was run for an analysis time of 15 seconds. This gives a total displacement of the puncher of 50 mm. All of the analysis was performed using double precision. This choice was made because the high number of increments demanded by the finer meshed models would have made the single precision accuracy too vulnerable for instability due to round off errors.

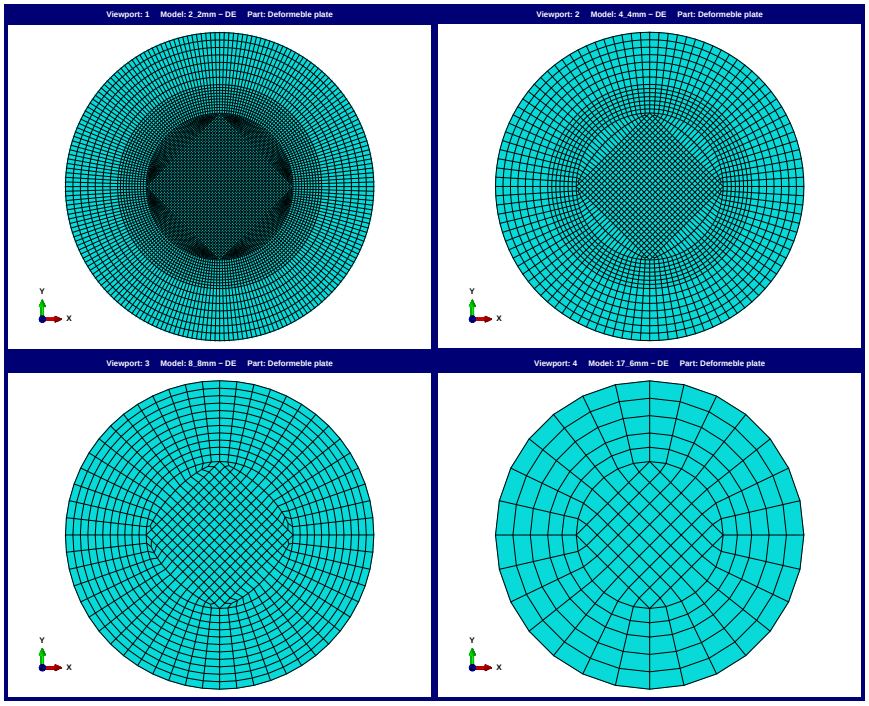

Figure 8.4: *The mesh used in the plate puncture simulation. Top left: 2.2 mm mesh, Top right: 4.4 mm mesh, Bottom left: 8.8 mm mesh and bottom right: 17.6 mm mesh.*

Output was requested for the displacement and the reaction force in the reference point of the puncher. These were used to evaluate the analysis against the force-displacement curve that was developed in the penetration tests performed by Sören Ehlers in [10]. For the deformable plate, all energy magnitudes for the whole model were outputted, while the strain measurements, stress parameters and different damage related parameters of each element were outputted as a field output.

8.4 Results and discussion

8.4.1 Introduction

The force needed to push the puncher through the plate for the different meshed FE-models varied a lot, from 120 kN to 150 kN, as seen in Fig. 8.5. The 2.2 mm and the 4.4 mm model gave about the same maximum force needed to penetrate the plate, but fracture occurred too early compared to the reference test. The 8.8 mm meshed model had a better agreement with the reference test when it came to displacement when fracturing, but the force was 30 kN too high. For the 17.6 mm meshed model, no fracture occurred using the PMM, and the DEMM gave a fracture at a force of 175 kN at a displacement of 42.5 mm.

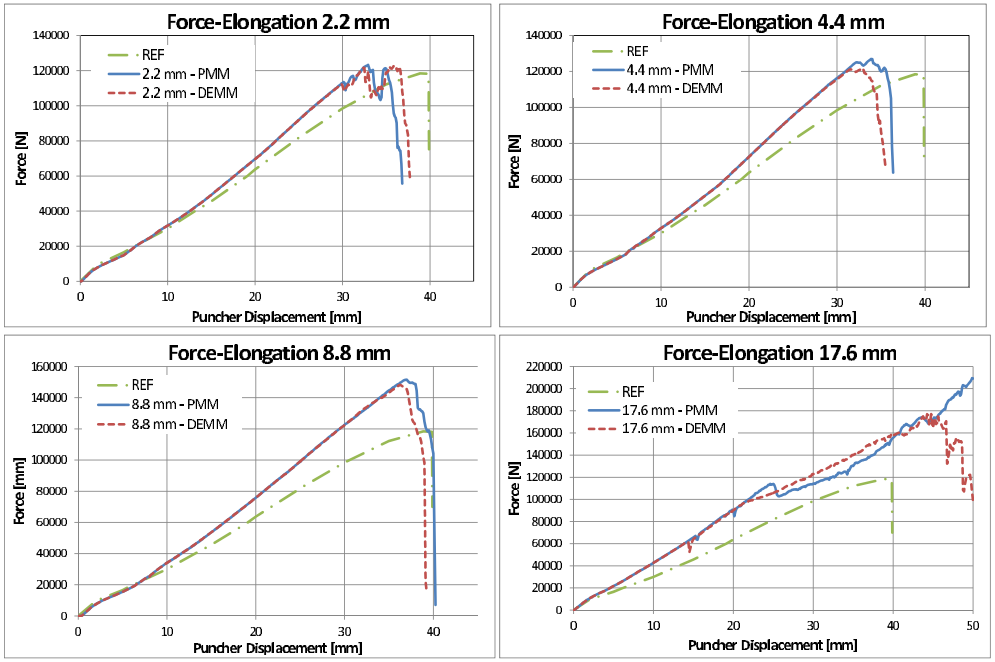

Figure 8.5: *The force-displacement diagram for the different meshed models. Top left: 2.2 mm mesh, Top right: 4.4 mm mesh, Bottom left: 8.8 mm mesh and bottom right: 17.6 mm mesh.*

As the puncher was pushed ever deeper into the plate, the energy terms were monitored to see the difference in the behavior of the meshes and the material models. It was discovered that the internal energy in the plate became higher than the external work applied at some point during the analysis. For the 2.2mm, 4.4 mm and

the 8.8 mm meshed models, this happened as the fracture happened, changing the analysis from an assumed quasi-static analysis into a dynamic analysis with large vibrations. For the 17.6 mm meshed model, this transition happened earlier than for the other mesh sizes. This is discussed in Section 8.4.2

During the whole analysis, the external work applied to the plate was defined as

$$W_{Ext} = Fu = E_{Int} + E_{KE} + E_{Fric} \tag{8.1}$$

where F is the force, u is the puncher's displacement causing the deformation of the plate, E_{Ke} is the kinetic energy in the plate, E_{Fric} is the energy lost to friction and E_{Int} is the internal energy in the plate. As long as no rupture of the plate had occurred, the analysis behaved quasi-static, without any dynamic effects present. The E_{Ke} was zero and E_{Fric} was very small. This meant that the external work was matched by the internal energy, and all the work applied to the system went into deforming the plate elastically and plastically. When the problem being solved became a dynamic case, this could be seen as a rise in the kinetic energy from vibrations occurring in the structure. This introduced viscous dampening effects and made the penalty contact work start to rise.

When this happened, the internal energy recorded by ABAQUS increased, but the external work was defined by the plate's stiffness, giving the resistance and the displacement of the puncher. The increase of internal energy was not matched by the external work. Looking at the energy balance, the external work can be calculated as [8]

$$W_{Ext} + W_{PW} = E_{Int} + E_{KE} + E_{Fric} - E_{UB} \tag{8.2}$$

where W_{ext} is the external work, W_{PW} is the penalty work, E_{Int} is the internal energy,E_{KE} is the kinetic energy, E_{Fric} is the friction energy and E_{UB} is the unbalance energy outputted by ABAQUS. The E_{UB} should always be as small as possible.

When the external work given by ABAQUS differed from the internal work, Eq. 8.2 would give the external work matching the internal energy.

8.4.2 The 17.6 mm meshed model

The 17.6 mm meshed model did not follow the force displacement curve given by [10]. Only during the elastic deformation, is it in agreement. As soon as the plastic deformation starts, the force needed to displace the puncher through the plate becomes too high. At the point of 14.12 mm displacement of the puncher, there is a wave of stress going to the plate, seen as a drop in the force for the 17.6 mm model in Fig.8.5. This happens as the center element in the plate, being the only element in the plate contacting the puncher, goes from being more or less unloaded to obtaining the same value of equivalent stress as the rest of the elements in the plate. The moment before this happens is seen in Fig. 8.6. The increase in stress is seen as the two high stress zones on each side of the contact area grow together during a short amount of time, 0.2 seconds. From symmetry, the same is also happening in stress component in the y-direction.

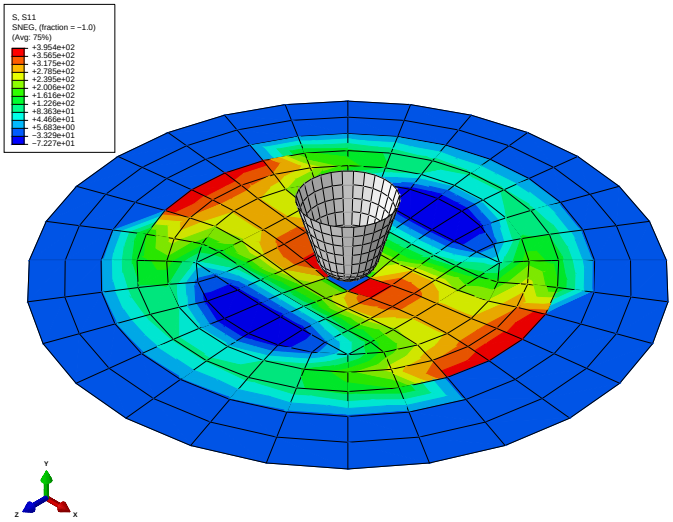

Figure 8.6: *The stress in the x-direction of the plate. Notice how the center element of the plate has a very low value of stress. Because of the symmetry, the y-direction stress and the shear stress show the same behavior. Only 0.2 seconds later the center element has obtained an equal stress state as the surrounding elements.*

As the deformation increases, the stress starts to swing back and forth from one side of the plate to the other, causing massive vibrations. At this point in time, the measured external work recorded in ABAQUS becomes smaller than the internal energy calculated. The amount of energy going into the work done by the penalty

contact definition becomes high and the solution becomes unstable. The amount of energy is in balance, the external work plus the work done by the penalty contact definition is matched by the internal energy plus the friction energy. Giving

$$W_{ext} + W_{PW} = E_{Int} + E_{KE} + E_{Fric} + E_{UB} \tag{8.3}$$

The value E_{UB} is very small, close to zero, as long as the penalty work and friction energy are small, and increasing to around 1 % as at the end of the simulation.

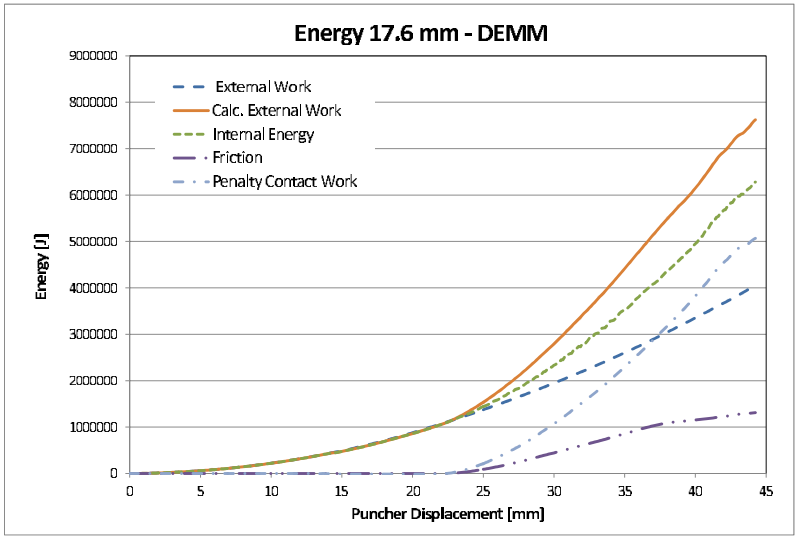

Figure 8.7: *The major energy quantities in the 17.6 mm FE-model with the DEMM. The PMM model shows the same behavior. The internal work given by ABAQUS increases beyond the external work performed on the model. This increase is given by the penalty work done by the contact simulation. By adding this penalty contact work to the external work, and comparing it to the internal energy plus the friction energy, the energy becomes balanced.*

The 17.6 mm model is clearly too coarsely meshed to be able to simulate the fracturing of a plate being punched by an object. In the tensile test the material models for PMM and DEMM showed good agreement with the reference curve, but this only took into account the uniaxial loading case for the element. When the deformation of the elements becomes more complex, this element size is not a good option for this model.

8.4.3 The 8.8 mm meshed model

The 8.8 mm model does not show any signs of unstable solution, but it overestimates the force needed to fracture the plate. The energy terms are in good balance during the deformation up to fracture. After the point of fracture, the quasi-static assumption is no longer valid, and the analysis becomes highly dynamic. This increases the kinetic energy and viscous dampening energy. As seen in Fig. 8.5 the force is overestimated, as in the 2.2 meshed and 4.4 meshed models, when the plastic deformation starts. The penetration depth when fracture occurs seems to match the reference better than in the finer meshed models, but the force is too high. This behavior, that also applies to the 17.6 mm mesh, is caused by the large sized elements being capable of describing the bending deformation of the plate that is the cause of the deformation during the first part of the test. As the puncher is pushed deeper into the plate, it forms a ring shaped zone around the contact area that is subjected to high membrane forces. The coarse meshed models behave too stiffly, and the resulting force and time of fracture becomes too high.

Also this mesh size shows signs of not being good enough for the problem that is being solved. This is visible through the amount of energy gone into removing singular modes, which is high. The viscous energy starts to rise early on, after the puncher has moved just 8 mm. The energy is very small compared to the total energy in the system, but significantly larger than the viscous energy in the finer meshed models. At the same time as the viscous effect energy start to rise, the contact penalty work also starts to increase. They are both triggered by the vibrations occurring as the loading of the plate is suddenly reduced. Both the viscous effect energy and the penalty work are shown in Fig. 8.8. The other energy components do not show any signs that would point to the quasi-static assumption not being valid.

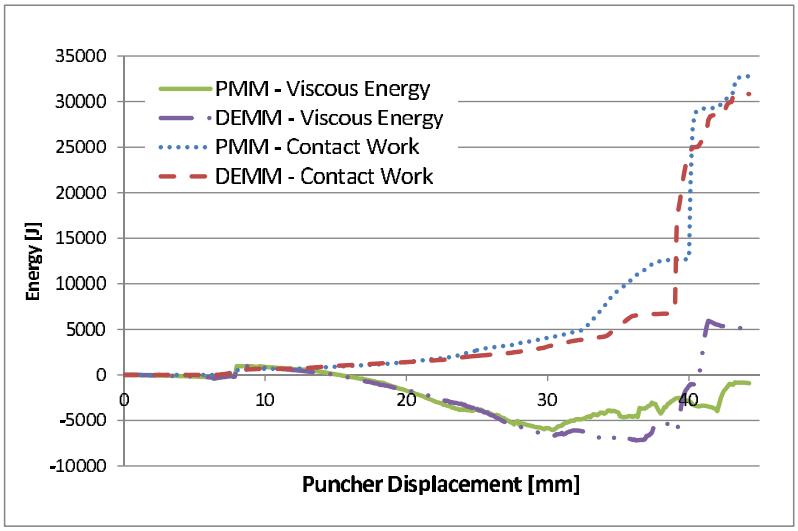

Figure 8.8: *The energy going to viscous effects and the work done by the contact definition for the 8.8 mm meshed model.*

8.4.4 The 2.2 mm and the 4.4 mm meshed model

The 2.2 mm and 4.4 mm meshed model show good agreement with the reference curve when it comes to the force needed to fracture the plate (Fig 8.5) The peak difference for the two mesh sizes is the 4.4 mm PMM model that has a deviation of 5 % from the maximum force of the reference curve. The three other deviate by around 1 % higher maximum force. The fracture happens at a lower value of penetration for the puncher. For the 4.4 mm model, the DEMM FE-model ruptures before the PMM FE-model. This is because even if the tuning of the material is done ever so thoroughly in the tensile test, there will always be a difference in the point of final fracture. The DEMM gives a higher value of penetration before the failure occurs compared to the PMM, if their tensile test tuning shows an equal elongation at the point of fracture. This happens for the 2.2 mm meshed plate. For the 4.4 mm and 8.8 mm models the DEMM model has a slightly lower elongation at fracture in the tensile test, than the PMM for the same mesh size, as indicated by the increase in damage dissipated energy in Fig. 7.15. This difference is emphasized in the plate penetration test, giving a lower penetration value at fracture for the DEMM than for the PMM. This effect is clearly enlarged when the material models are used on the plate puncture experiment. This can clearly be seen in the energy dissipated by damage for the 4.4 mm model, shown in Fig. 8.11. It

looks like the DEMM model is more sensitive to changes in the true strain in the elements at fracture, than the PMM is. For the 2.2 mm tensile test, the fracture occurs exactly at the same global elongation for both the DEMM and PMM (see Fig. 7.15 in Section 7.4.2). This is translated to the plate penetration experiment as the DEMM gives the largest penetration at fracture. (The PMM acts stiffer). In the 4.4 mm and 8.8 mm meshed FE-models, where the DEMM has a somewhat lower global elongation at the point of fracture, the plate penetration simulation shows a clearly lower penetration at fracture for the DEMM than for the PMM.

In [10], where the reference curve is taken from, the puncture experiment carried out is done on a plate that is fixed to the rigid support by being clamped to the test rig with a massive washer. Bolts are used to force the washer to clamp the rim of the specimen plate. The setup can be seen in Fig. 8.1. In the article it is argued that there is no slip between the plate and the rigid support, since there is no deformation of the bolt holes in the plate. There could be a slip even if this is true, since the deformation of the hole can be elastic, and the plate from the bolt hole to the start of the radius of the test rig could be deformed. The clamped boundary conditions in the FE-models are equal to or more rigid than the support used in the real experiment. This may help to explain some of the deviation of displacement at the time of rupture between the FE-analysis carried out in this chapter and the results from [10].

If we take a look at the shape of the fracture, this also seems to agree with the results of [10]. The fracture of the FE-analysis for the 2.2 mm and 4.4 mm meshed models is shown in Fig. 8.9. The fracture of the experiment carried out by Ehlers is shown in Fig. 8.10.

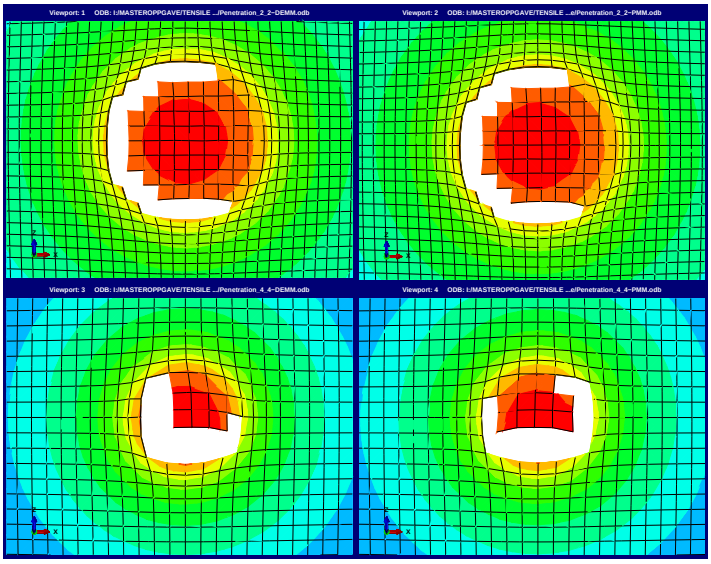

Figure 8.9: *The shape of the fracture of the plate for the 2.2 mm and 4.4 mm meshed models, with both PMM and DEMM. Top left: 2.2 mm with DEMM, Top Right: 2.2 mm model with PMM, Bottom left: 4.4 mm model with DEMM and Bottom right: 4.4 mm model with PMM.*

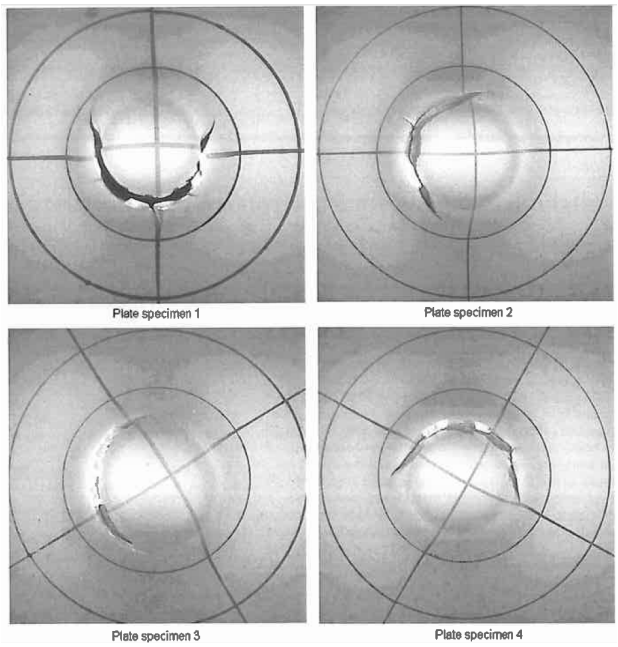

Figure 8.10: *The fracture shape of four different plate samples after the puncture test experiment. [10]*

The shape of the fracture is similar to the real fracture for the 2.2 mm model. It has

enough elements to recreate the shape seen in Fig. 8.10. The 8.8 mm model does not have enough elements in the fracture zone to display the same rupture pattern as the 2.2 mm model, but the basic shape can be seen. For both the different mesh sizes, the PMM and the DEMM gives the same shape of the fracture.

The energy outputs for the 2.2 mm and the 4.4 mm models (Fig. 8.12 to 8.15)confirm the quasi-static approach that is assumed up to the point of fracture. The external work is matched by the internal energy up to the point of fracture. From this point and further, the structures respond dynamically because the load is suddenly removed. The DEMM model gives a higher amount of penalty contact energy compared to the PMM, but this is the only major difference between the major energy outputs for the two material models. As in the tensile test, the amount of energy recorded as going into dissipating damage is different because of the different approaches in obtaining the damage. The differences are as expected after seeing the results of the tensile test, and are very small compared to the amount of energy present in the system. The energy difference in damage dissipated energy is seen in Fig. 8.11.

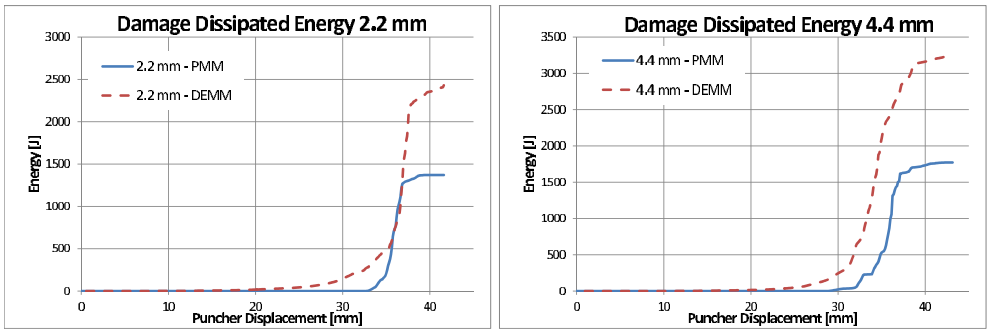

Figure 8.11: *The damage dissipated energy for the 2.2 mm mesh plate (left) and the 4.4 mm meshed plate (right).*

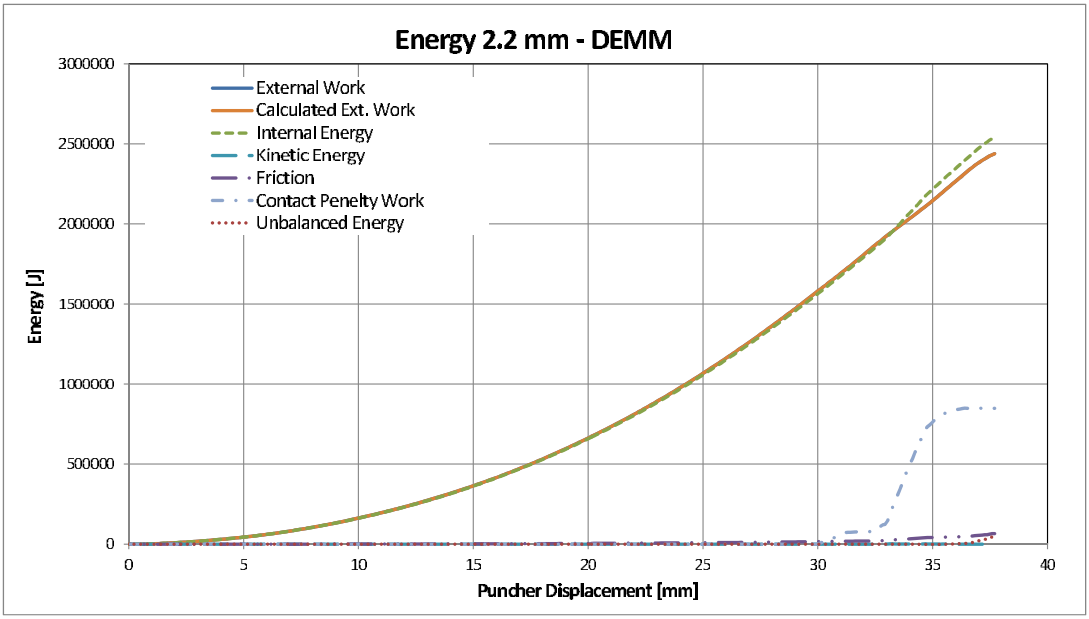

Figure 8.12: *Comparison of the energy components in the 2.2 mm meshed model using the DEMM. The internal energy is seen to become larger than the external work as the fracture develops and the plate fails. A increase in contact penalty work is seen at the same moment of time.*

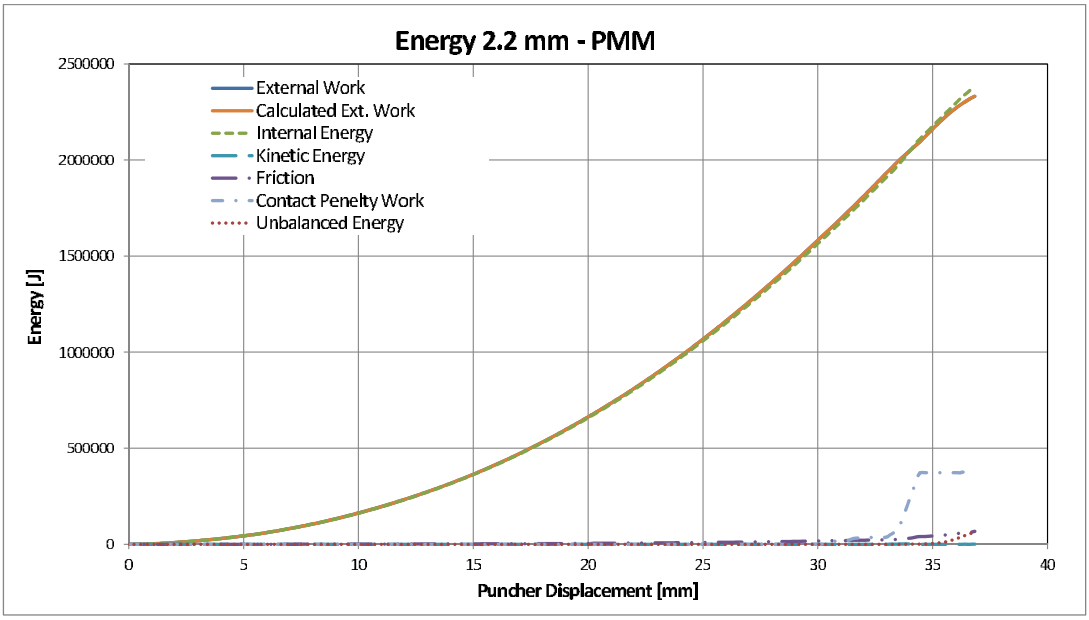

Figure 8.13: *Comparison of the energy components in the 2.2 mm meshed model using the PMM. The internal energy is seen to become larger than the external work as the fracture develops and the plate fails, like for the 2.2 mm model with the DEMM. Also here the contact penalty work increases when the failure of the plate has taken place.*

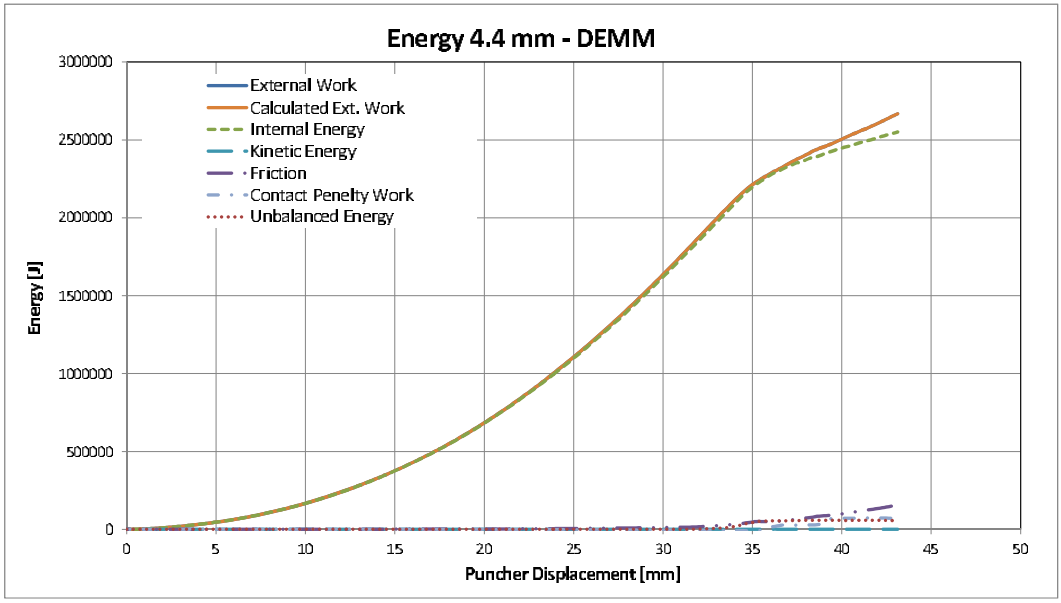

Figure 8.14: *Comparison of the energy components in the 4.4 mm meshed model using the DEMM. The internal energy is equal to or smaller than the external work, and the other energy components are small during the whole simulation.*

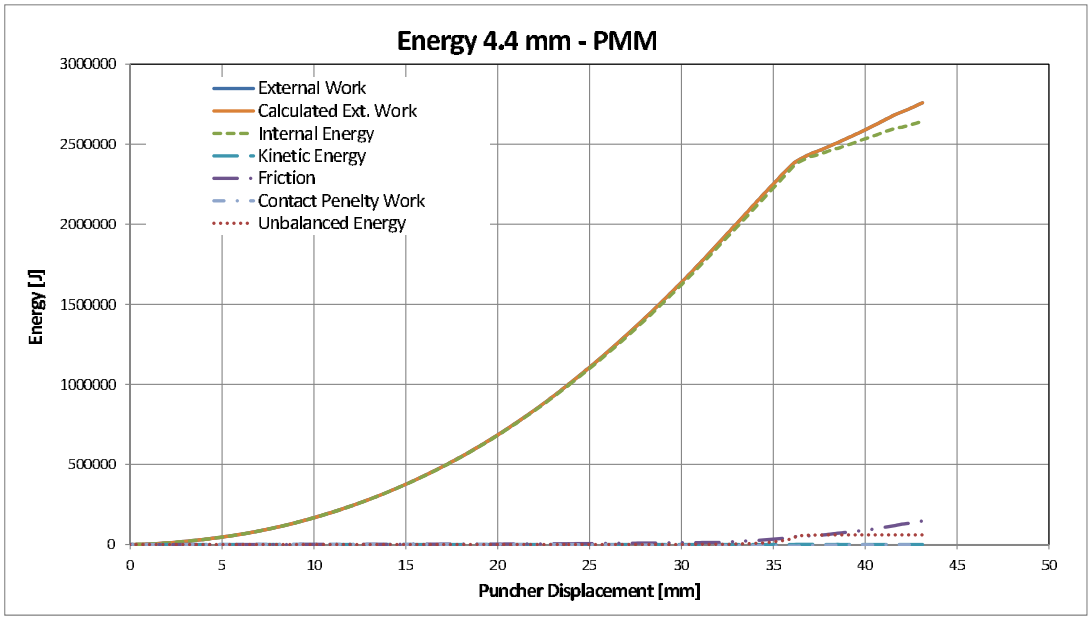

Figure 8.15: *Comparison of the energy components in the 4.4 mm meshed model using the PMM. Like for the 4.4 mm DEMM model, the internal energy is equal to or smaller than the external work, and the other energy components are small during the whole simulation.*

8.4.5 Reduction of structural strength

As expected after performing the tensile test, the remaining strength of the material involved in the fracture varies significantly between the two material models used for each mesh size. In Fig. 8.16, the difference in damage done to the elements involved in the fracture of the plate are shown for the 2.2 mm mesh. The red elements are elements that have gotten their stiffness reduced to zero, and which are deleted. The blue elements are elements that have gotten their stiffness reduced and will have a lower load-bearing capacity if the structure would have been applied a new load.

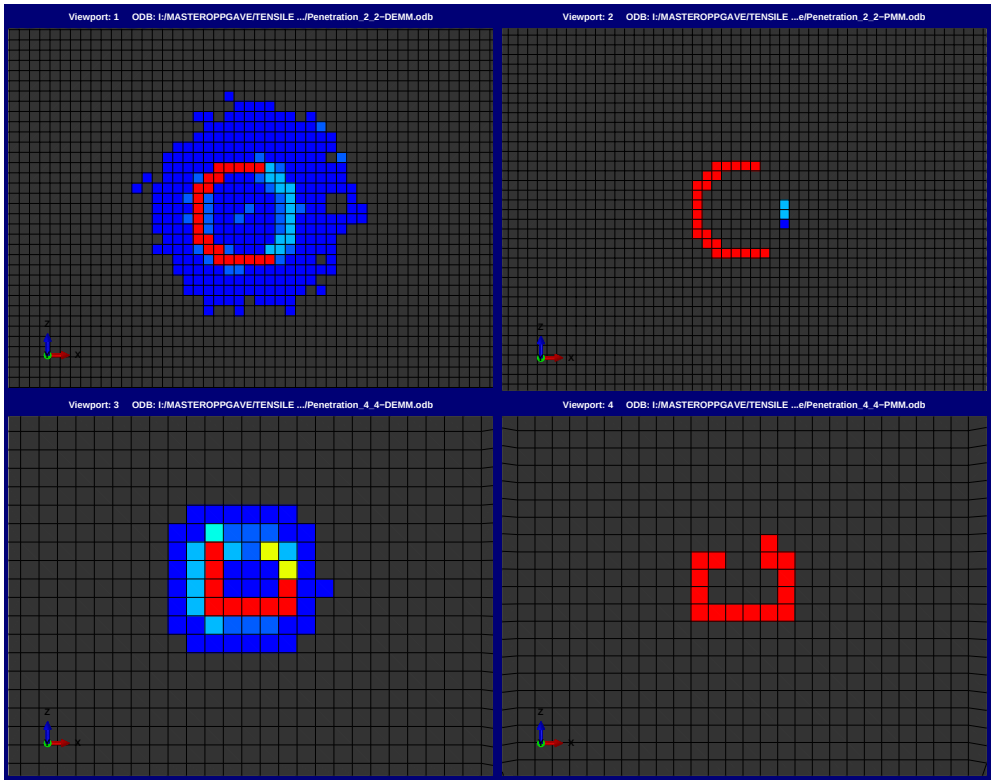

Figure 8.16: *The figure shows the elements that have gotten their elastic stiffness reduced by the fracture models. The DEMM applies damage to more elements than the PMM, and the overall strength of the material in the zone of fracture is therefore reduced more. Top left: 2.2 mm DEMM, Top right: 2.2 mm PMM, Bottom left: 4.4 mm DEMM and Bottom Right: 4.4 mm PMM.*

As explained in Section 7.4.3, this does not influence the results of these experiments, since the reduced stiffness is used to simulate the fracture directly. If, on the other hand, the plate simulated in this chapter would have to be reloaded again,

the reduced stiffness of the elements around the hole in the DEMM created by the fracture would give a weaker zone than in the PMM model. The structures using the different material models could then have behaved quite differently from each other.

Chapter 9

Summary and conclusion

In this thesis the theory of ductile fracturing of ductile materials simulated using the finite element method is studied. The material behavior during a fracture is explained on a microscopic level, and different theories on how to describe the growth and coalition of material voids is explained. This includes models describing the formations of void in a continuous homogeneous material developed by A.S. Argon et al., and models to describe the growth and coalition of voids developed by Rice and Tracey [21] and Gurson [12].

In the finite element method, the approach taken is somewhat different. A method developed by Sören Ehler and Petri Varsta [11] makes use of the material input in a FE-analysis to tune the material's plastic properties into being able to describe the localized effect of instability caused by the ductile fracture. Their method is compared to a fracture model that is already in use in the FE-analysis software package ABAQUS, developed by Hillerborg et al. [17]. This model defines the fracture of the FE-model by the energy needed to open a unit area of crack.

In the method developed by Hillerborg et al., a fracture displacement measure $\bar{u}_f^{pl}$ is used to define the elongation of the element from damage initiation to fracture. The model presented defines this as being equal to the global elongation for the model during the simulated creation of the crack. This is true only if there is just one element in the direction of elongation that is influenced by the fracture model. If more than one element in the direction of elongation is influenced by the fracture model, the resulting fracture displacement becomes larger than the value of $\bar{u}_f^{pl}$ in-

putted in the material definition. This affects the assumed mesh independence of this material model, since differently sized elements will behave differently. This behavior of multiple elements contributing to the fracture displacement can be reduced by including a more specified damage initiation criterion, involving parameters such as the stress triaxiality and the lode parameter, to better control which elements are included in the fracture model.

By using a tensile test experiment as reference, the two fracture models were tuned to give the same global response regarding the force-displacement of a tensile test piece simulated using ABAQUS. The two material models, referred to as the Plasticity-material-model (PMM) for the method given by Ehlers and Varsta, and the Damage-Evolution-model (DEMM) for the method developed by Hillerborg et al., showed good agreement with each other when simulating the tensile fracture of the tensile specimen using a quasi-static approach. The simulations were performed using as large element sizes as possible, considering the application later on. The energy terms did not differ for any of the mesh sizes used with the two material models. One difference that was found between using the two methods to describe the fracture behavior is the damaging of the material inside the unstable zone when using the DEMM. This results in a zone of weaker elements around the fracture developed, that will influence the residual strength of the FE-model. This behavior of reduced strength due to the fracturing process is not present when using the PMM.

The material models developed for the different mesh sized dog-bone tensile models were then used as the material input in a simulation of a circular steel plate being punctured by a cone-shaped puncher. The simulation was performed using a constant speed to force the puncher through the plate. The two models that used the largest element sizes of 17.6 mm and 8.8 mm in side length, showed signs of being too coarsely meshed for the problem that was being solved. The two finer meshed models gave the right value of force needed to fracture the plate, but the fracture occurred prematurely compared to the reference. This was probably caused by the boundary conditions giving a stiffer behavior compared to the reference experiment. The DEMM and PMM showed almost perfect behavior regarding the global force and displacement relationship in the tensile test.

In the tensile test experiment, the element size did not matter much, since the material models could be set to give the right global response regarding the uniaxial load case for all the models regardless of the size of the elements. When the de-

formation is more focused on the bending behavior of the element, the element size compared to the global size of the modeled plate is more critical. The coarser meshed models of 8.8 mm and 17.6 mm did show signs of having too few elements to simulate the real world behavior. As long as the problem was dominated by bending the response match the finer meshed models, but as the penetration of the puncher started to deform the plate in such a way that in-plane membrane forces began to dominate the fracture behavior, the coarser meshed models begun to behave too stiffly compared to the finer meshed 2.2 mm and 4.4 mm models.

Looking at the energy components, no significant differences between the two material models cannot be found before the final fracture occurs. Up to this point, the kinetic energy, viscous dampening energy, contact dissipated energy and "artificial" strain energy are small, if not zero. When the fracture develops and the force applied is suddenly reduced, this introduces dynamic effects that make the mentioned energy parameters rise and become different for the two models.

In the penetration experiment, the small difference in global behavior from the tensile test becomes larger, and influences the result by giving a clearly larger penetration depth for one of the material models compared to the other. The element damage effect caused by the accumulation of damage seems to give the models that utilize the DEMM a softer behavior than the model using the PMM, in the plate penetration test. This occurred if the material models gave exactly the same result in the tensile test. This effect is explained by the softening of the elements in the model using the DEMM, giving a softer transition from the unstable behavior of necking to final fracture, and resulting in a smaller applied force at the time of final failure. In a collision event simulation, where the striking object is often set to have an initial kinetic energy that is transferred to the stuck object, the difference of damage accumulation may yield some greater differences in the response of the deformable structure.

Appendix A

Appendix A

In this appendix, the model for plasticity and damage and failure for ductile metals in ABAQUS is presented as it is being used by the software program.

A.1 Material Plasticity in Abaqus

In ABAQUS, a material model for ductile materials is used for the calculations of the plastic behavior of the material. This model can be used on rate-independent and rate-dependent materials, and has simple algebraic equations with a stiffness matrix that can be explicitly developed. This makes it fast and easy to use. The input data is inputted as a true equivalent stress to true equivalent plastic strain relationship, and the first line must contain a stress-strain state with zero equivalent plastic strain. This data point is used to calculate the yielding of the material [1]. The inputted data must be arranged in increasing order depending on the equivalent stress, otherwise ABAQUS will abort the analysis and display an error message.

The plasticity of a material is assumed to be governing the deformation when the von Mises yield criterion is satisfied. This criterion is given as ([7] sec. 4.3.2.)

[1] The yielding point is the transition between a pure elastic behavior and an elasto-plastic material, according to the von Mises yield criteria.

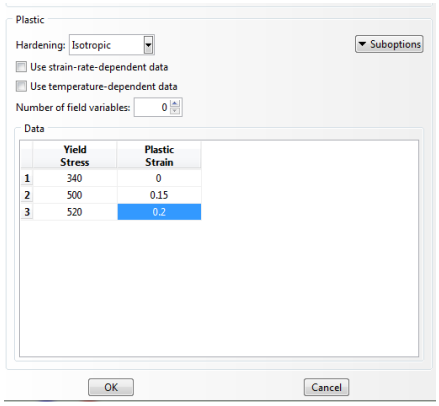

(a) The input menu for the plastic properties in a material. For a rate-independent material only the true stress and the true strain are inputted, additionally there can be added temperature- and strain rate dependent data and different field variables. Different suboptions can also be assigned.

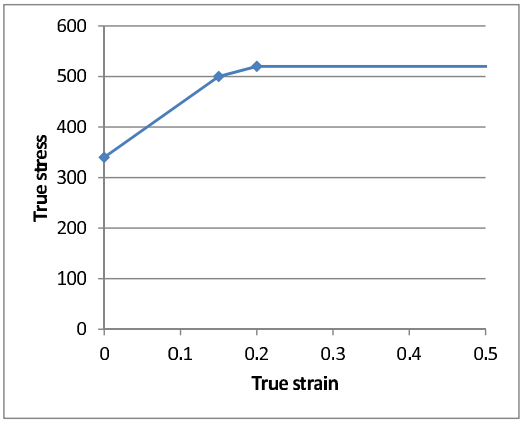

(b) The inputted data in figure A.1(a) will produce a true stress-true strain relationship as shown here. After the last point of inputted data, ABAQUS assumes that the material will behave perfectly plastically, giving the straight line.

$$q = \bar{\sigma}(\bar{\varepsilon}^{pl}) \tag{A.1}$$

For rate-independent materials $\bar{\sigma} = \sigma^0$, and for rate dependent materials, the plasticity is dependent on the temperature- and the strain rate.

At the end of each increment, the criterion is tested against the fully elastic behavior, and if the equivalent stress in the material satisfies the criterion, the plastic behavior is used in the next increment in order to calculate the stress and strain.

As the material follows the plastic behavior of the model, the incremental stress and strain relation is defined as

$$\partial\sigma = \left[Q\zeta + (K - \frac{1}{3}Q)\boldsymbol{II} - R\boldsymbol{SS}\right] : \partial\varepsilon \tag{A.2}$$

where

$$Q = \frac{2}{3}\frac{q}{\frac{2}{3}\sqrt{\hat{\boldsymbol{e}} : \hat{\boldsymbol{e}}}} \tag{A.3}$$

$$S = \frac{2\frac{E}{2(1-\nu)}}{1 + \frac{3\frac{E}{2(1-\nu)}}{q}\Delta\bar{e}^{pl}}\hat{\boldsymbol{e}} \tag{A.4}$$

$$R = \frac{1}{q\tilde{e}}\frac{1 - \Delta\bar{e}^{pl}\frac{d\bar{\sigma}}{d\bar{e}^{pl}}/q}{1 + \frac{d\bar{\sigma}}{d\bar{e}^{pl}}/\frac{3E}{2(1-\nu)}} \tag{A.5}$$

,

$\boldsymbol{I}$ is the identity matrix and ζ is the fourth-order unit tensor. This definition is valid for bodies where there are three direct strains defined by the kinematic solution. If there is a state of plane stress or uniaxial stress, the relation is somewhat simpler. For plane stress, the incremental stress and strain relation is found by imposing the condition of $\partial\sigma_{33} = 0$ into equation (A.2). For uniaxial stress the relation is simply the direct variation of $\sigma_{11} = 2/3\mathbf{S}_{11}$, that is

$$\partial\sigma_{11} = \left[\frac{3}{2}Q - R\sigma_{11}^2\right]\partial\varepsilon_{11} \tag{A.6}$$

A.2 Damage Initiation Criteria

ABAQUS offers a wide range of different models in order to define the point of failure initiation and the following damage evolution. For isotropic ductile materials, the *Damage Initiation criterion for fracture of metals* is used. This criterion uses the true stress and true strain state in the element to evaluate if the element satisfies the criterion inputted by the user. For ductile fracture, three damage initiation criteria are provided; *ductile criteria*, *shear criteria* and *Johnson-Cook criteria*. Only the two first will be presented here. They are based on the model deveoped by Hooputra et al. [18].

A.2.1 Ductile criteria

The ductile criterion is used to predict the onset of damage for a material due to nucleation, growth and coalescence of voids inside the material. The criterion is met if the equivalent true strain in the element reaches a preset value, the equivalent true plastic strain at the onset of damage $\bar{\varepsilon}_D^{pl}$. This preset value is dependent on the stress triaxiality η and the equivalent plastic strain rate $\dot{\bar{\varepsilon}}^{pl}$ in the element. ([7] sec. 20.2.2)

$$\bar{\varepsilon}_D^{pl}(\eta, \dot{\bar{\varepsilon}}^{pl}) \tag{A.7}$$

The evaluation of this criterion is done by comparing the incremental increase in equivalent plastic strain against the preset criterion for the state of stress triaxiality and strain rate the element is being deformed under. This is defined as

$$\omega_D = \int \frac{d\bar{\varepsilon}^{pl}}{\bar{\varepsilon}_D^{pl}(\eta, \dot{\bar{\varepsilon}}^{pl})} = 1 \tag{A.8}$$

For each increment, the value of ω_D will increase as

$$\Delta\omega_D = \frac{\Delta\bar{\varepsilon}^{pl}}{\bar{\varepsilon}_D^{pl}(\eta, \dot{\bar{\varepsilon}}^{pl})} \geq 0 \tag{A.9}$$

E.g. a material has defined a value for $\bar{\varepsilon}_D^{pl}$ in both tensile (positive strain rate) and in compression (negative strain rate), and $\bar{\varepsilon}_{D,Ten}^{pl} = 2\bar{\varepsilon}_{D,Comp}^{pl}$. This means that the equivalent plastic strain for damage initiation for tensile loading is twice that of compressive loading. If the material is first stretched to an equivalent plastic strain value of $\frac{1}{2}\bar{\varepsilon}_{D,Ten}^{pl}$, the accumulated value of ω_D will be 0.5. If the material is then compressed, the material will reach the point of damage initiation when the compressive strain value is $\frac{1}{2}\bar{\varepsilon}_{D,Comp}^{pl}$, since this amount of compression will also accumulate a value of $\omega_D = 0.5$. The tensile stretching of the material has weakened it so that it can only withstand a fraction of the compressive load it would have withstood without the initial stretching. This means that equation A.9

can also be written as

$$\Delta\omega_D = \sum_{i=1}^{j} \frac{\Delta\bar{\varepsilon}^{pl}}{\bar{\varepsilon}_D^{pl}, i(\eta, \dot{\bar{\varepsilon}}^{pl})} \geq 0 \tag{A.10}$$

where j is the number of damage initiation criteria for different stress triaxiality and strain rate states that is used.

A.2.2 Shear criterion

The shear fracture damage initiation criteria works exactly the same way as the ductile criterion, the only difference is that instead of stress triaxiality η, the stress state is given by a shear stress ratio θ_S. This ratio is defined as $\theta_S = (q + k_S p)/\tau_{max}$, where q is the von Mises stress, p is the hydrostatic stress, τ_{max} is the maximum shear stress and k_S is a material parameter. Following is the definition of the equivalent plastic shear stress at shear damage initiation $\bar{\varepsilon}_S^{pl}$, and the shear initiation factor ω_S.

$$\bar{\varepsilon}_S^{pl}(\theta_S, \dot{\bar{\varepsilon}}^{pl}) \tag{A.11}$$

$$\omega_S = \int \frac{d\bar{\varepsilon}^{pl}}{\bar{\varepsilon}_S^{pl}(\theta_S, \dot{\bar{\varepsilon}}^{pl})} = 1 \tag{A.12}$$

$$\Delta\omega_S = \frac{\Delta\bar{\varepsilon}^{pl}}{\bar{\varepsilon}_S^{pl}(\theta_S, \dot{\bar{\varepsilon}}^{pl})} \geq 0 \tag{A.13}$$

A.3 Damage evolution

When an element has met the damage initiation criterion (e.x. $\omega_D = 1$), a damage evolution can be found for which the true stress is reduced to zero when the true

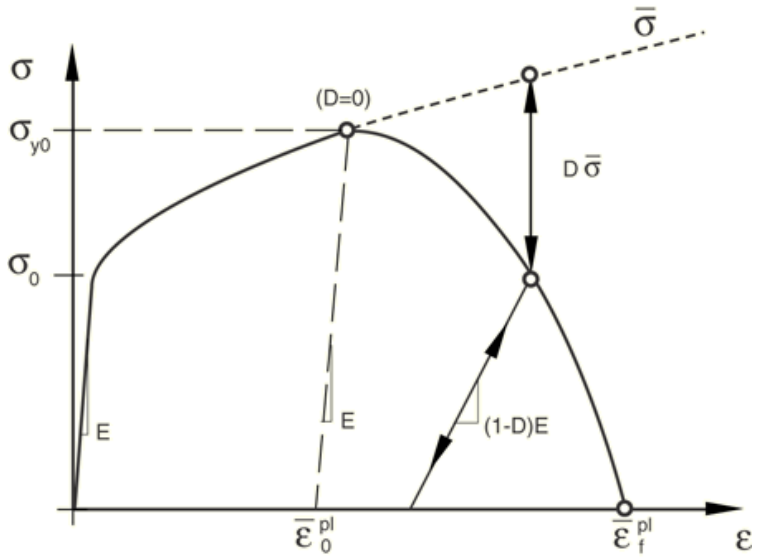

Figure A.1: *The development of true stress against true strain in an element undergoing stiffness reduction due to damage evolution. The dashed line represents the plasticity unaffected by the damage evolution, and the solid line the path of the plasticity due to damage evolution.*

strain continues to increase. The damage evolution reduces the stiffness of the element as the plastic strain continues to increase past the strain value of the damage initiation criterion, and may be set to remove the element from the mesh when the stiffness is reduced with a factor of 0.001 (99.9 % reduction of the stiffness). Nothing other than the elastic stiffness is changed by the damage evolution. The mass is preserved even when the element is removed from the mesh, but nodes may be subjected to high accelerations prior to element deletion, giving them an unnaturally high speed that may give strange results related to kinetic energy and translation.

The damage evolution described here can be triggered for materials by using the damage initiation criterion for ductile metals, as described above. It uses mesh independent measures to calculate the path of the plasticity influenced by the damage evolution.

The damage evolution is based on the energy that is to be dissipated in the element when strained from damage initiation to failure. The fracture energy is defined as

$$G_F = \int_{\bar{\varepsilon}_0^{pl}}^{\bar{\varepsilon}_f^{pl}} L\sigma d\bar{\varepsilon}^{pl} = \int_0^{\bar{u}_f^{pl}} \sigma d\bar{u}^{pl} \tag{A.14}$$

where σ is the equivalent true stress in the element.

The damage evolution is defined as mesh independent because it does not directly use any parameters that are dependent on the element size in the model. Instead of defining the deformation after damage initiation as plastic strain, it is defined as an equivalent plastic displacement $\bar{u}^{pl}$. It is defined as

$$\dot{\bar{u}}^{pl} = L\dot{\bar{\varepsilon}}^{pl} \tag{A.15}$$

where L is a *characteristic element length* calculated from the initial geometry of the element. (See section 4.4.2 for further details.)

At the point of damage initiation, the overall damage variable D is zero, as seen in Fig. A.1. As the element is deformed and the strain value increases, D will increase in value reducing the elastic stiffness of the element to $(1 - D)E$. The true stress in the element σ is also reduced from its undamaged value (the dashed line in figure A.1) to the value of $\sigma = D\bar{\sigma}$. At the point of damage initiation, the stress is σ_{y0}, the plastic strain is $\bar{\varepsilon}_0^{pl}$ and $D = 0$. At the point of failure and element deletion the stress is zero, the plastic strain is $\bar{\varepsilon}_f^{pl}$ and $D = 1$. The path between these two points can be defined by the physical deformation as a straight line, a curve defined by several points defined by a value of D and a corresponding deformation measure, or exponential. Alternatively it can be defined as the amount of energy that will be dissipated during the deformation from damage initiation to failure, either in a linear or exponential form.

For each damage initiation criterion, there may be a contribution to the overall damage of the material in the element. Therefore an overall damage variable D is calculated as

$$D = max\left\{d_{mult}, max_{j \in N_{max}}(d_j)\right\} \tag{A.16}$$

where d is an individual damage evolution damage variable and d_{mult} is a combination of two or more independent damage evolutions with different damage initiation criteria.

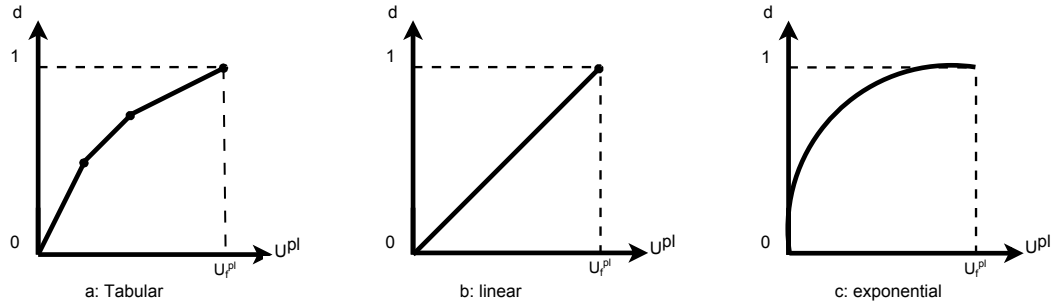

Figure A.2: *When using the $\bar{U}^{pl}$ to define the damage evolution, there path of the elements true stress/true strain relationship can be define in three difrrenet ways.The linear model follows a straight line from damage initiation to failure, while the tabular option allows the definition of points defined by the damage parameter D and the damage elongation length u^{pl}. The exponential option is defined by an endpoint as in the linear option, and a parameter regulating the amount of curvation of the path.*

$$d_{mult} = 1 - \prod_{k \in N_{mult}} (1 - d_k) \tag{A.17}$$

N_{mult} and N_{max} are the sets of active mechanisms that contribute to the overall damage in a multiplicative and a maximum sense.

If an element undergoing deformation in the damage evolution domain is unloaded, it will follow a linear unloading path defined by the current elastic stiffness in the element. Later, when a new load is applied, it will follow the same elastic path back to the path defined by the damage evolution, and continue the plastic deformation according to this.

It is worth noting that the damage initiation and damage evolution is used in each integration point in the element independently. This means that a solid element with one integration point will only be evaluated in that point altogether. A shell element with multiple integration points through the thickness of the element, will evaluate the damage initiation and damage evolution differently for each of the integrations point. For pure compression and pure tensile loading, this will not influence the behavior, but for bending, the different integration points will fail at different plastic strains because of the different loading pattern for each of them.

Bibliography

[1] Ansi/ieee std 754-2008, ieee standard for binary floating-point arithmetc. Technical Report 754-2008, IEEE, 2008.

[2] T. L. Anderson. *Fracture Mechanics - Fundamentals and Applications - Third Edition*. taylor & Francis, 2008.

[3] Yuanli Bai and Tomasz Wierzbicki. A new model of metal plasticity and fracture with pressure and lode dependence. *International Journal of Plasticity*, 24(6):1071–1096, 2008.

[4] I. Barsoum, J. Faleskog, and S. Pingle. The influence of the lode parameter on ductile failure strain in steel. *Procedia Engineering 10*, 10:69–75, 2011.

[5] Shailendra Singh Bhadauria, M.S. Hora, and K.K. Pathak. Effect pf stress triaxiality on yielding of anisotropic materials under plane stress condition. *Journal of Solid Mechanics*, 1(3):226–232, 2009.

[6] Robert D. Cook, David S. Malkus, Michael E. Plesha, and Robert J. Witt. *Concepts and Applications of Finite Element Analysis*. John Wiley & Sons, 2007.

[7] Dassault Systémes. *Abaqus Analysis User's Manual*, ver. 6.11 edition.

[8] Dassault Systémes. *Abaqus/CAE User's Manual*, ver. 6.11 edition.

[9] Dassault Systémes. *Getting started with Abaqus: Interactive Edition*, ver. 6.11 edition.

[10] Sören Elhers. Strain and stress relation until fracture for finite element simulations of a thin circular plate. *Thin-Walled Structures 48*, 48(1):1–8, 2010.

[11] Sören Elhers and Petri Varsta. Strain and stress relation for non-linear finite element simulations. *Thin-Walled Structures 47*, 47(11):1203–1217, 2009.

[12] A.L. Gurson. Continuum theory of ductile rupture by void nucleation and growth: Part i - yield criteria and flow rules of porous ductile media. *Journal of Engineering Materials and Technology*, 99:2–15, 1977.

[13] Tor Erik Hals. *Konstruksjonsmekanikk*. Tapis Forlag, 2 edition, 1999.

[14] R. Hill. *The Mathematical Theroy of Plasticity*. Oxford University Press Inc., oxford classical (published 1998) edition, 1950.

[15] A. Hillerborg. A model for fracture analysis. Technical report, Division of building materials the Lund Institute of Technology, 1978.

[16] A. Hillerborg. The theoretical basis of a method to determine the fracture energy gf of concrete. *Materials and Structures*, 18:291–296, 1985.

[17] A. Hillerborg, M. Modéer, and P.E. Petersson. Analysis of crack formation and crack growth in concrete by means of fracture mechanics and finite elements. *Cement and Concrete Research*, 6(6):773 – 781, 1976.

[18] H Hooputra, H Gese, H Dell, and H Werner. A comprehensive failure model for crashworthiness simulation of aluminium extrusions. *International Journal of Crashworthiness*, 9(5):449–464, 2004.

[19] Jay R. Lund and Joseph P. Byrne. Leonardo da vinci's tensile strength tests: Implications for the discovery of engineering mechanics. *Civil Engineering and Environmental Systems*, 18(3):243–250, 2001.

[20] J. Oliver. A consistent characteristic length for smeared cracking models. *International Journal for Numerical Methods in Engineering*, 28(2):461–474, 1989.

[21] J.R. Rice and D.M. Tracey. On the ductile enlargement of voids in triaxial stress fields. *Journal of the Mechanics and Physics of Solids*, 17(3):201–217, 1969.

[22] Viggo Tvergaard. On localization in ductile materials containing spherical voids. *International journal of fracture*, 18(4):237–252, 1982.

[23] Viggo Tvergaard. Material failure by void growth to coalescence. *Advances in Applied Mechanics*, 27:83–151, 1989.

[24] Tomasz Wierzbicki and Norman Jones. *Structural failure*. John Wiley and Sons Inc., 1989.